FORSCHUNGSZENTRUM ROSSENDORF

WISSENSCHAFTLICH-TECHNISCHE BERICHTE
FZR-314
März 2001
ISSN 1437-322X

Institute of Ion Beam Physics and Materials Research

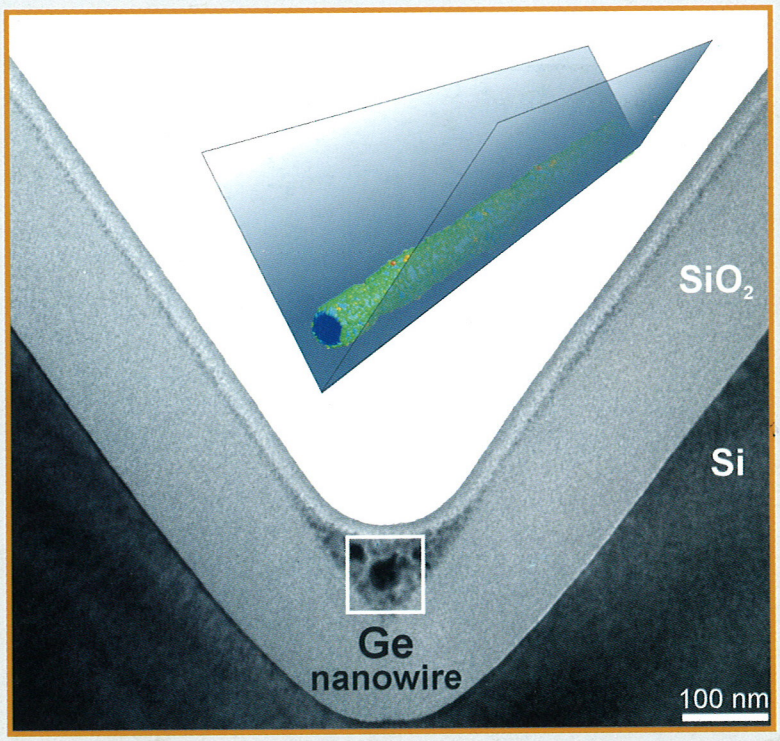

Annual Report 2000

Forschungszentrum Rossendorf e.V.
Mitglied der Wissenschaftsgemeinschaft Gottfried Wilhelm Leibniz

FORSCHUNGSZENTRUM ROSSENDORF
Mitglied der Wissenschaftsgemeinschaft Gottfried Wilhelm Leibniz

WISSENSCHAFTLICH-TECHNISCHE BERICHTE
FZR-314
März 2001

Annual Report 2000

Institut für Ionenstrahlphysik und Materialforschung

Editors:

J. von Borany, M. Helm, H.-U. Jäger,

W. Möller, E. Wieser

Contents

Statistics

Preface

The Research Center Rossendorf (Forschungszentrum Rossendorf, FZR) represents the largest governmental research institution in the "new" states of the Federal Republic of Germany. Its presently about 600 employees, organized in five institutes, study problems of basic and applied science in the fields of materials science, biomedical and environmental research, and nuclear physics. The FZR is a member of the "Gottfried Wilhelm Leibniz Society" (WGL), with the federal government and the state of Saxony each contributing 50 % of the basic funding.

The Institute of Ion Beam Physics and Materials Research (IIM) employs more than 100 scientists, engineers, technicians and PhD and diploma students. The institute combines basic research and application-oriented studies in the fields of ion beam applications to materials and semiconductor research. According to recommendations of the German Science Council, the institute constitutes a national and international ion beam center, which, in addition to its own scientific activities, offers services and transfers know-how on ion beam techniques to universities, other research institutes, and industry.

For these purposes, a broad range of ion-related equipment is available, delivering ion energies from about 10 eV (plasma treatment) to several 10 MeV (electrostatic accelerators). For the diagnostics of ion-treated surfaces, standard analytical techniques are available such as transmission electron microscopy, X-ray diffraction, Auger and photoelectron spectroscopy, and a number of chemical, optical, electrical, and mechanical diagnostics. Sample preparation is available for a large number of different materials including standard silicon processing.

The diagram on page 4 displays the main R&D activities of the institute. It is the purpose of the present Annual Report to document its scientific progress in 2000 by a few selected extended contributions, numerous short contributions, and a statistical overview on publications, conference contributions and lectures given by members of the institute. It also reports on the training of young scientists and on external and collaborative actions.

A few developments and actions deserve special comments. Most important, since February 2000 the institute is commonly managed by two directors. With the appointment of Prof. Manfred Helm and the establishment of a new division "Semiconductor Spectroscopy" the semiconductor activities of the institute have been strengthened. A main mid-term goal of the new division is to utilize the far-infrared radiation from the free-electron laser at the superconducting electron accelerator ELBE at the FZR, which is presently under construction.

In addition to the European Large Scale Facility "Center for Application of Ion Beams in Materials Research" ("AIM"), under which more than 20 different groups from all over Europe were hosted, the "Synchrotron Radiation Beamline for Radiochemistry and Materials Research (ROBL)" has also commenced routine operation as a European Large Scale Facility. The dedicated research capacity of both installations was fully booked with about 30 different user groups in materials research. At the end of 2000, the institute was also selected as "Marie-Curie Training Site" of the European Union, named "Development of Functional Layers Using Ion Beam Techniques". By its support, foreign PhD students are invited to perform part of their work at Rossendorf.

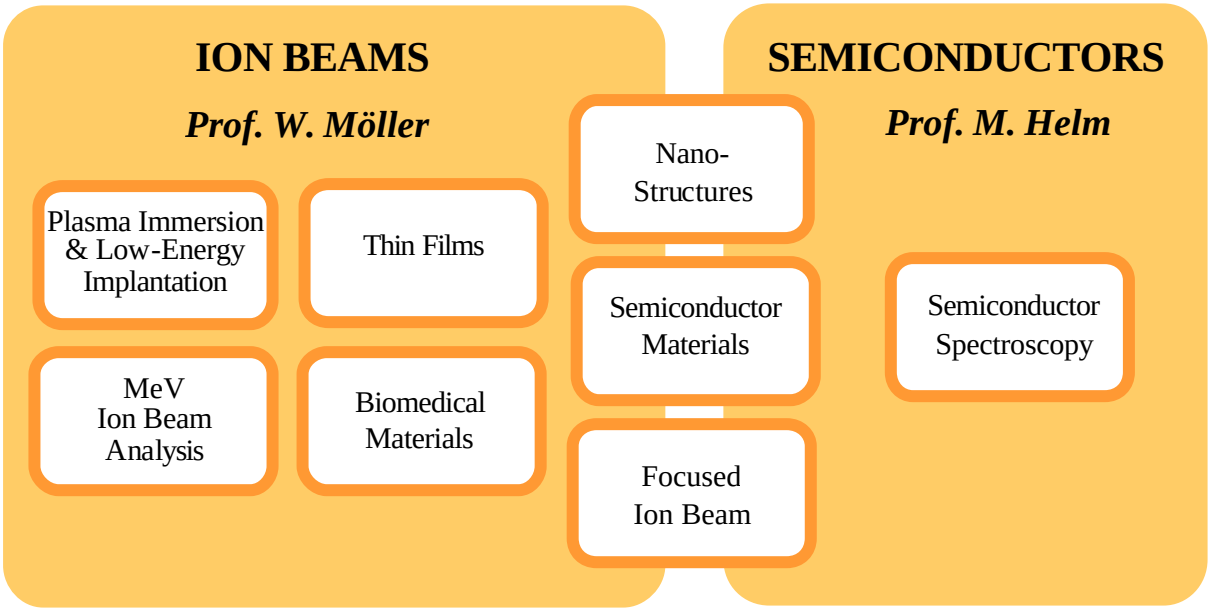

In 2000, two diploma students and two PhD students finished their theses at the institute and their examinations at the Technical University of Dresden. Young scientists collected some awards, as, e.g., the renowned Prof. Jürgen Geiger award for an outstanding thesis, and an award in a business plan competition of the Free State of Saxony.

In 2000, technology transfer and ion beam service activities of the institute have again been significantly extended. Direct contracts with industry and governmental collaborative projects cover process simulation for microelectronics, the doping of silicon carbide, the development of new non-volatile memories and of sensors operated at high temperature, the improvement of diffusion barriers for copper metallisation in microelectronics, the surface treatment of mechanical tools, and the enhancement of corrosion resistance of high-temperature metallic alloys. Services for universities, other research institutes and industry include numerous applications of ion beam analysis, the enhancement of ceramic coating adhesion on dental implants, the surface hardening of cutting, forming and engraving tools, and the ion-beam tailoring of high-power semiconductor device properties.

The institute would like to thank all partners and friends, and the organizations who supported its progress in 2000. Special thanks are due to the Executive Board of the Forschungszentrum Rossendorf, the Minister of Science and Arts of the Free State of Saxony, and the Minister of Education and Research of the Federal Government of Germany. Our partners from universities, industry and research institutes all around the world contribute essentially to the success of the institute, and play a crucial role for its further development. Last but not least, the directors would like to thank all members and guests of the institute for their active and excellent contributions in 2000.

Prof. Wolfhard Möller

Prof. Manfred Helm

Self-Assembly of Ge Nanowires by Ion Implantation into V-Grooved (001) Si Surfaces

T. Müller, K.-H. Heinig, B. Schmidt and A. Mücklich

The fabrication of more and more miniaturized electronic and photonic devices requires a spatially controlled formation of nanostructures. Examples are electronic devices based on semiconducting nanowires, and photonic devices based on chains of metallic nanoclusters that conduct light by coupling of surface plasmons.

Ion Beam Synthesis (IBS) is a successful approach for the controlled synthesis of nanostructures, e.g., quantum dots [1,2]. An interesting application of IBS to form Si nanowires has recently been demonstrated by high fluence O^+ implantation into Si V-grooves [3]. This process appears to rely strongly on sensitive self-organization phenomena during phase separation. A more direct way is achieved by implantation of Ge^+ (or other ions) into oxide covered V-grooves. The key is the tailoring of the profile of implanted Ge by the V-groove topography. Ge is enriched in the bottom and will coalesce there to a continuous wire with a diameter of few nanometers.

V-grooves aligned along the <100> direction on (001) Si wafers were prepared by photolithographic patterning of a SiO_2 mask and anisotropic etching with 30% KOH at 80 °C. This selective and self-adjusting etch process results in atomically smooth (111) crystal facets forming the sidewalls of the V-groove with an angle of 54.7° with respect to the wafer surface. V-grooves of 2 and 4 µm width were studied. After removing the SiO_2 etch mask dry thermal oxidation was performed at 1000 °C in O_2, leading to 200 nm SiO_2 on the (001) Si surface and 220 nm SiO_2 on the (111) sidewalls of the V-groove. As visible in Fig. 1(a), a sharp SiO_2 surface depression forms at the V-groove tip during oxidation. The SiO_2 covered V-grooves were implanted at room temperature with 1×10^{17} Ge^+ cm^{-2} at 70 keV. Subsequent annealing was carried out in dry N_2 (5.0 purity) at 950 °C for different times. Rapid thermal annealing (RTA) and furnace processing were used complementarily. The samples were transferred into the cold furnace in order to minimize the impact of the small amounts of moisture during furnace processing.

High–dose Ge^+ implantation erodes the SiO_2 surface on V-groove sidewalls and leads to a significant material transport (Si, O, and Ge) towards the bottom. This is shown by a comparison between XTEM images before and after ion implantation (Fig. 1(a) and 1(b)). The sharp depression of the as-oxidized surface at the V-groove tip is filled during implantation by sputtered and then redeposited material, which has been simulated recently [4]. The analytical model in Ref. [4] uses a continuum description for the surface evolution under ion irradiation, including sputtering and redeposition of sputtered atoms, and describes very well the surface shape of V-grooves found by XTEM (Fig. 1b) after high-dose ion implantation. Moreover, Ge is accumulated in the V-groove bottom as predicted by Ref. [4]. This enrichment is proven by analytical TEM (EDX) of as-implanted samples as shown in Fig. 2. The Ge concentration

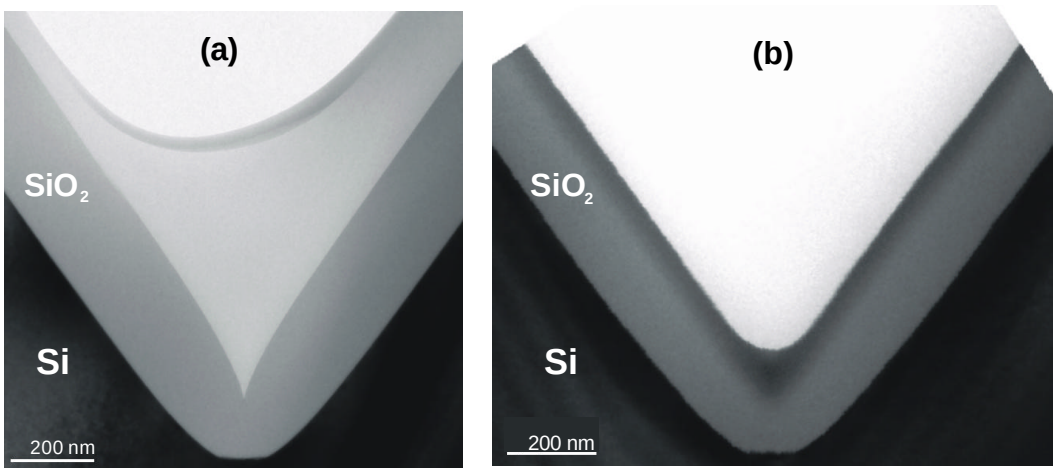

Fig. 2: XTEM images of (a) an as-oxidized and (b) an as-implanted V-groove (1×10^{17} Ge^+ cm^{-2} at 70 keV).

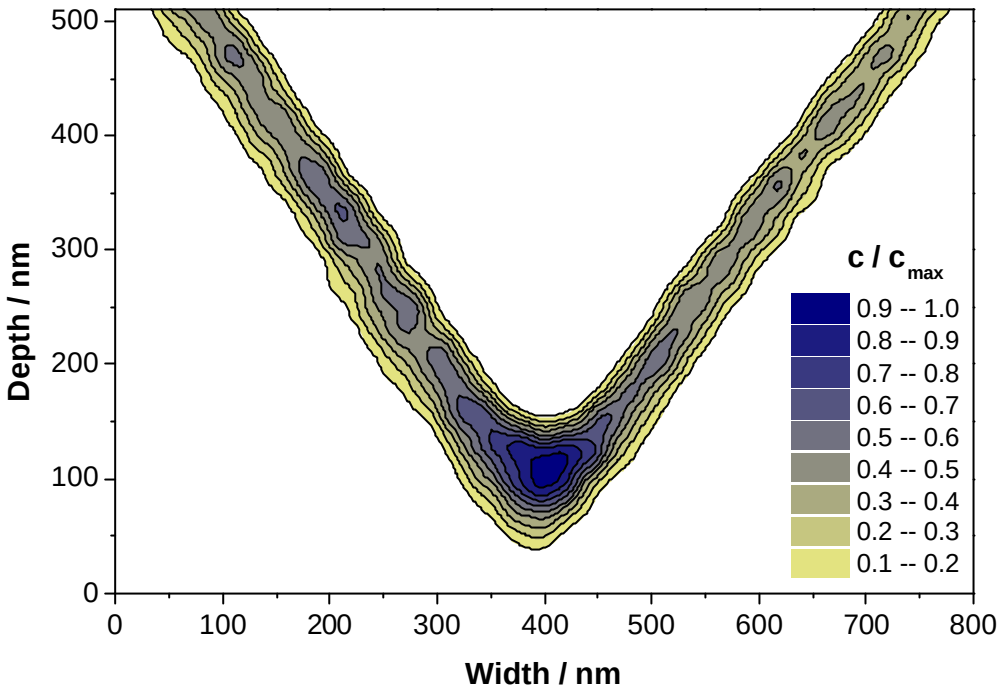

Fig. 2: Ge mapping by Energy Dispersive X-ray Analysis of a cross-section of an as-implanted V-groove (1×10^{17} Ge^+ cm^{-2} at 70 keV). The grayscale of the contour plot is normalized to the maximum Ge concentration of 30 at.% in the V-groove bottom.

in the bottom reaches with 30 at.% more than twice of the concentration in the sidewalls, which is essential for the formation of a nanowire. The Ge content in the sidewalls is constant, the asymmetry in the concentration profile originates from the thickness variation of the XTEM sample.

Ge nanoclusters form in the V-groove sidewalls and the bottom during annealing of the Ge^+ implanted V-grooves. Cross-sectional TEM (XTEM) images of annealed samples are shown after annealing for 5 min (RTA, Fig. 3(a)) and 10 min (furnace, Fig. 3(b)). Only at the bottom the density and size of the clusters is sufficient for the coalescence to a continuous wire. The large dark dots, visible at the V-groove bottoms of Fig. 3, are cross-sections of the expected Ge nanowires. With annealing time increasing from 5 min up to 10 min at 950 °C the diameter of the Ge wire grows from 18 to 35 nm. The continuity of the Ge wires remains to be proven. Nevertheless, several XTEM images taken from different cross-sections show always the large black dot with identical diameter in the V-groove bottom, which is at least a strong indication for a continuous wire. Furthermore, it can be seen (Fig. 3(b)) that especially in the case

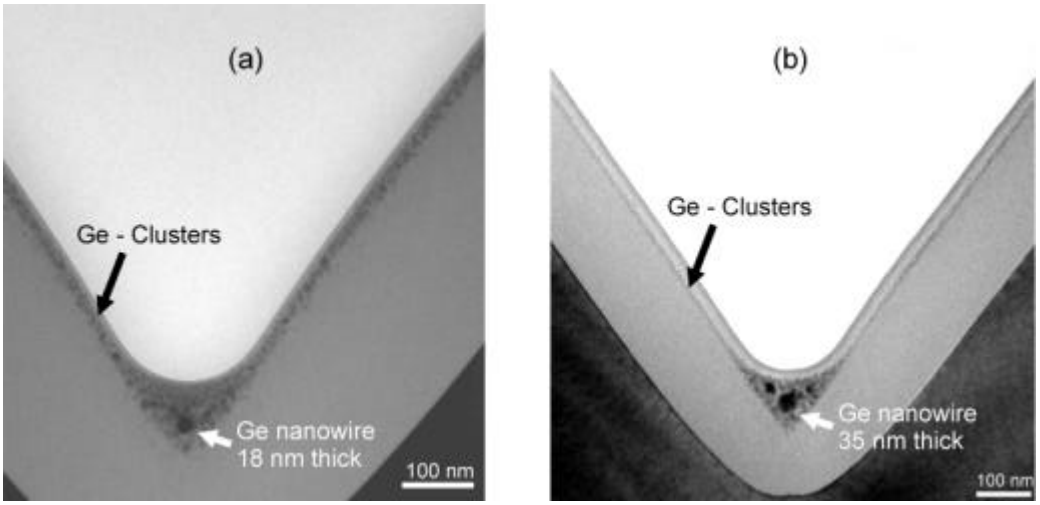

Fig. 3: XTEM images of annealed samples: (a) RTA annealing in dry N_2 for 5 min at 950 °C and (b) furnace annealing in dry N_2 for 10 min at 950 °C.

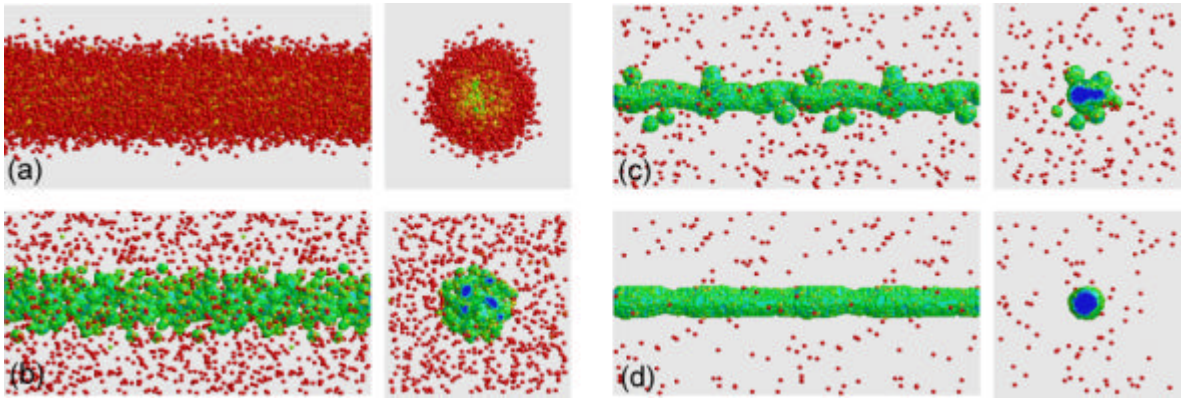

Fig. 4: Kinetic lattice Monte Carlo simulation of the nanowire formation from an initial cylindrical Gaussian profile with a peak concentration in the center of 31 at.% and a standard deviation of 4 nm. Shown are (a) the initial, (b),(c) intermediate (10000 and 102000 Monte Carlo steps), and (c) the final (490000 Monte Carlo steps) state. The final wire diameter is approximately 5 nm.

of furnace annealing the first 20 nm below the SiO_2 surface are affected by residual moisture from the annealing ambient leading to Ge oxidation and redistribution processes, which have been described in Refs. [2,5]. Obviously, the nanowire region has not been strongly affected by oxidants, since it is deeper than 20 nm in the SiO_2 and contains a much higher total amount of Ge. It should be noted that oxidation suppresses the formation of Ge nanoclusters in the sidewalls because of a more flat Ge profile there.

The optimization of IBS of nanowires requires a high experimental effort, which can be reduced by process simulations. Therefore, kinetic lattice Monte Carlo simulations have been carried out to understand the wire formation mechanism and, finally, to predict the wire geometry and growth. Fig. 4 shows an atomistic simulation of the synthesis of a Ge nanowire with a diameter of 6 nm, which grows from an initially cylindrical Gaussian profile of Ge. The assumed initial profile with a peak concentration of 31 at.% and a standard deviation of 4 nm was aligned to the <100> direction of the simulation lattice. 95 % of the implanted atoms lay in a cylinder of 16 nm diameter which resembles the Ge-rich region at the bottom of the V-groove. The wire growth process consists of different steps: (i) the nucleation stage, (ii) the competitive growth of Ge clusters (Ostwald-ripening), and finally (iii) their coalescence. The complete coalescence will only occur, if the initial profile is not too broad or the Ge concentration not too low. Otherwise, the clusters remain isolated and grow at the expense of smaller ones without coalescence.

It should be emphasized that a continuous wire is metastable since a set of large clusters has a smaller surface area and is energetically favored. Especially thin wires with $d < 5$ nm can overcome the energy barrier and break up into droplets due to thermal fluctuations. Simulations show that wires aligned to the <110> direction having (111) facets would be more stable than <100>-aligned wires with (100) surfaces due to different surface energies. However, nanowires synthesized within an amorphous SiO_2 layer are expected to be polycrystalline or, for annealing above the melting temperature, liquid. For the wire evolution in the solid state, grain boundaries may provide another source of instabilities for a breakup.

It has been demonstrated that IBS can be used to fabricate (poly)crystalline Ge nanowires embedded in amorphous SiO_2. Ge nanowires of 18 nm and 35 nm diameter were synthesized by Ge^+ implantation into oxidized Si V-grooves and subsequent annealing. Kinetic lattice Monte Carlo simulations were performed allowing for a more detailed understanding of the wire formation.

References

[1] C.W. White, J.D. Budai, P. Withrow, J.G. Zhu, S.J. Pennycook, R.A. Zuhr, D.M. Hembree Jr, D.O. Henderson, R.H. Magruder, M.J. Yacaman, G. Mondragon, S. Prawer, Nucl. Instr. Meth. B **127/128** (1997) 545

[2] K.H. Heinig, B. Schmidt, A. Markwitz, R. Grötzschel, M. Strobel, S. Oswald, Nucl. Instr. Meth. B **148** (1999) 969

[3] Y. Ishikawa, N. Shibata, F. Fukatsu, Nucl. Instr. Meth. B **147** (1999) 304

[4] T. Müller, K.H. Heinig, B. Schmidt, Nucl. Instr. Meth. B, in press

[5] S. Oswald, B. Schmidt, K.H. Heinig, Surf. Interface Anal. **29** (2000) 249

Efficient Blue Light Emission from Silicon: The First Integrated Si-Based Optocoupler

L. Rebohle, J. von Borany, D. Borchert*, H. Fröb**, T. Gebel, M. Helm and W. Skorupa

*Fraunhofer-Institut für Solare Energiesysteme, 79100 Freiburg, Germany

**Institut für Angewandte Photophysik, Technische Universität Dresden, 01062 Dresden, Germany

The enormous development of information technology has created an ever increasing demand for optoelectronic devices able to generate, modulate and process optical signals [1]. The standard material for present-day electronics, silicon, is unfortunately badly suited to operate as a light emitter due to its indirect band gap of about 1.1 eV. To date, mostly compound semiconductors are used as discrete devices in optoelectronics, rendering impossible complete Si-based optoelectronic integrated circuits. Various Si-based materials for light emission have been studied so far, among them Er-doped Si/SiO_2 and porous Si being the prime examples with emission in the near-infrared and red spectral region, respectively.

In this paper we present the first integrated optocoupler whose fabrication, using ion implantation into SiO_2, is completely compatible with standard Si technology. It is based on Ge-implanted SiO_2 layers as light emitter exhibiting bright blue-violet electroluminescence (EL) light with a record wall-plug efficiency of 0.5%. The advantages of ion-implanted SiO_2 layers are based on the excellent mechanical, chemical and electrical properties of SiO_2 and the good reproducibility of ion implantation and its compatibility to standard Si technology. Red EL has been observed in Si- and Ge-implanted SiO_2 layers [2-4], but the power efficiency was either not given or below10^{-4}. Recent investigations revealed the possibility to extract violet EL from Ge-implanted SiO_2 films and blue EL from Si-implanted SiO_2 films with a power efficiency of about 5 x 10^{-4} and ≤ 10^{-4}, respectively [5-7]. For Si these results were confirmed in Refs. [8,9]. Finally we would like to mention, that – in the case of red PL - even a net optical gain has very recently been achieved in Si-implanted SiO_2 layers [10].

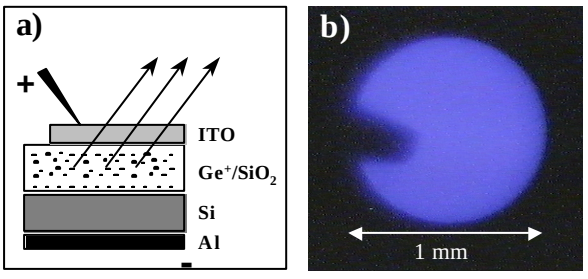

Fig. 1: Structure of the luminescent MOS devices (a). On the right side (b) a photograph of a luminescent device is given. The shadow of the contact needle can be seen on the left.

SiO_2 films with a thickness between 130 and 500 nm on [100]-oriented, n-type Si substrates were thermally grown at 1000 °C. The oxide films were implanted with Ge ions resulting in a Gaussian implant profile with a peak Ge concentration ranging between 0.3 and 3 %. After implantation, rapid thermal annealing (RTA) at 1000 °C was applied with annealing times between 1 s and 30 s. In some cases, a furnace annealing at 500 °C for 30 min followed by a RTA anneal at 1000 °C for 1 s was performed. Metal-oxide-semiconductor (MOS) device structures for EL studies were prepared using sputtered 80 nm thick layers of indium tin oxide (ITO) and Al as top and bottom electrodes, respectively. The transmission of the ITO layer is higher than 80 % in the relevant wavelength region. An array of devices with a diameter of 0.5 mm was made by photolithographic patterning. The cross section of the structure is shown schematically in Fig. 1(a). By application of a positive voltage to the top electrode (ITO) the devices exhibit strong violet EL, which is well visible with the naked eye (Fig. 1(b)). EL and photoluminescence (PL) measurements were performed at room temperature in a Spex Fluoromax spectrometer with a R298 Hamamatsu photomultiplier. The setup was calibrated with a reference source and a power meter, and the resulting uncertainty of the measured efficiency is estimated to be a factor of 2.

Fig. 2(a) displays the normalized EL and PL spectrum of a 200 nm thick Ge-implanted SiO_2-layer containing 3 % Ge after RTA at 1000 °C for 30 s. Whereas the PL was recorded using an excitation wavelength of 240 nm (5.17 eV), the EL was observed by applying an external electric field of 7.15 $MVcm^{-1}$. Both spectra are peaked in the violet spectral region at 3.18 eV (390 nm) and, apart from a marginally broader width of the EL

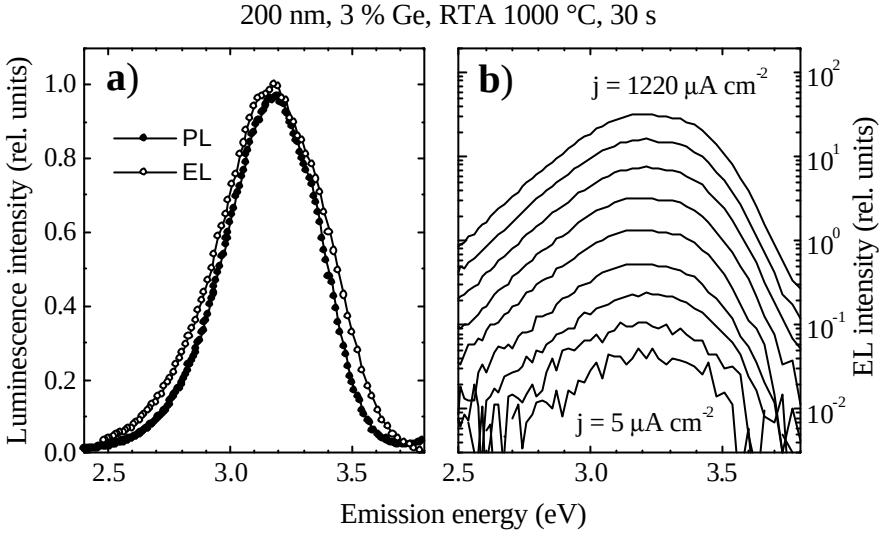

Fig. 2: The PL and EL spectra of a Ge-implanted oxide layer (a). Both spectra are nearly identical. The oxide layer is 200 nm thick, contains 3 % Ge, and was annealed at 1000 °C for 30 s. Whereas the shape of the EL spectrum does not change with the injection current density (b), the EL intensity shows a linear dependence on it.

peak, the spectra are almost identical. This implies that the luminescence for both, PL and EL, is caused by the same type of luminescence center, and that the emission mechanism is identical. Fig. 2(b) shows the EL of the same device for different injection current densities on a logarithmic scale. Obviously the shape of the spectrum does not change at all with the injection current. Furthermore, the EL intensity exhibits a linear dependence on the injection current over 3 orders of magnitude.

In a previous investigation [7] we found that the violet PL of Ge-implanted layers is caused by an oxygen deficiency center. The energy level scheme of such a center is shown in Fig. 3 and consists of a singlet ground state S_0, a singlet first excited state S_1, and a triplet first excited state T_1. The blue-violet PL can be understood as a radiative excitation from the ground state to S_1, followed by intersystem crossing to T_1 and a radiative transition back to S_0. The radiative transition $T_1 \rightarrow S_0$ (which is actually forbidden to first order) is also the origin of the observed EL, but in the case of EL there are several possibilities to populate the T_1 state.

In the following the more complex situation of electrical excitation (Fig. 4) is considered. If a sufficiently high electric field is applied, electrons from the Si can enter the oxide layer via tunnel injection. In case of a pure oxide layer the electrons have to tunnel through the whole barrier (process 1). If there are traps (process 2) or nanoclusters (process 3) located close to the Si-SiO_2-interface the injection can be assisted considerably by reducing the effective tunnel distance. In the case of equilibrium the electrons moving in the

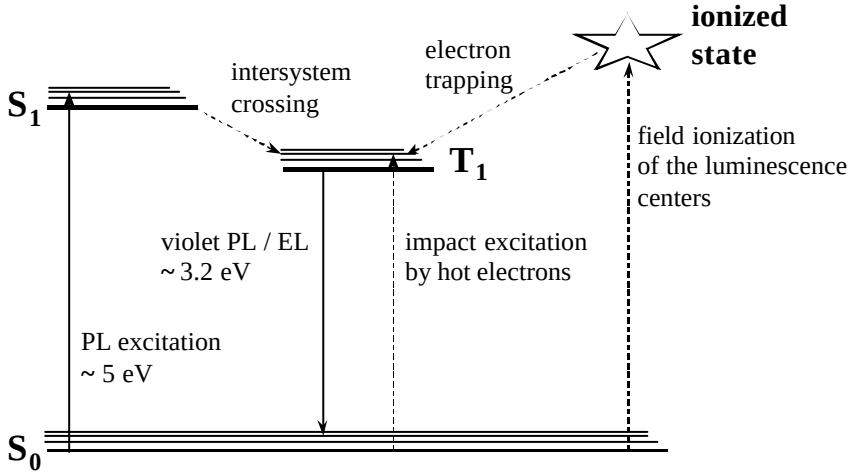

Fig. 3: Energy level scheme of an oxygen deficiency center consisting of a ground singlet state S_0, a first excited singlet state S_1 and a first excited triplet state T_1. Radiative transitions are marked by solid, non-radiative by dashed arrows.

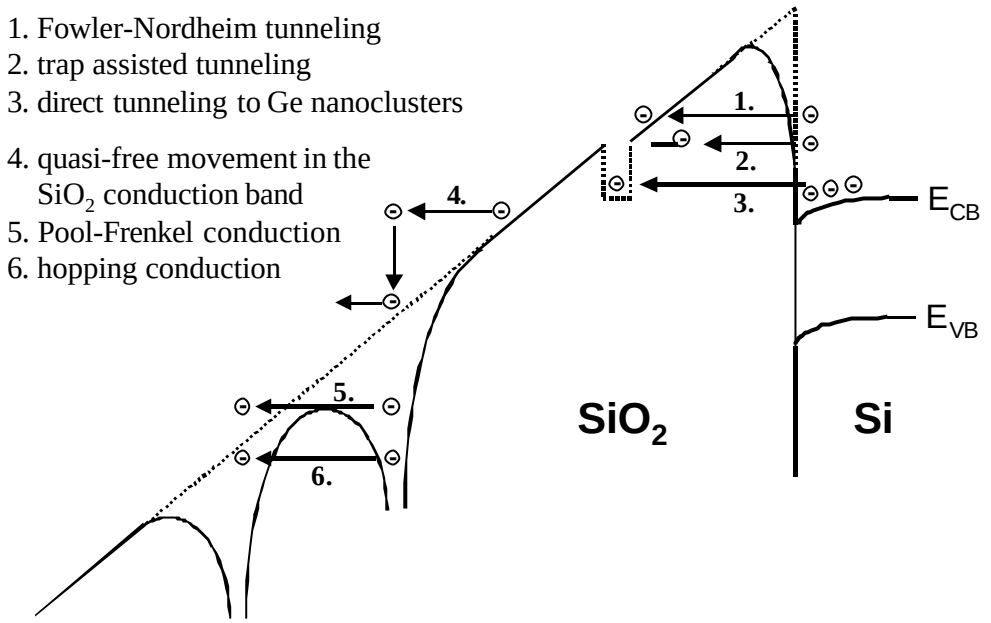

Fig. 4: Charge carrier injection and transport in an ideal MOS structure under forward bias.

conduction band of SiO_2 are characterized by a distinct energy distribution, which varies over the position in the oxide layer. The majority of the electrons will have low energies not high enough to excite a luminescence center. However, hot electrons from the high-energy tail of this distribution can be scattered at luminescence centers being in the ground state S_0, and the transferred energy can be used to excite the luminescence centers (process 4). For impact excitation by hot electrons, neither the $S_0 \rightarrow S_1$ nor the $S_0 \rightarrow T_1$ transition is restricted by optical selection rules, but, due to its lower energy, the $S_0 \rightarrow T_1$ transition appears to be more probable. On the other hand, at high electric fields the luminescence centers can be ionized (process 5 and 6), which can be regarded as the excitation from the ground state S_0 to an "ionized state". The released electrons move towards the metal electrode and leave the luminescence centers positively charged. If these centers trap an electron they can relax – in most cases – back to the ground state. However, with a certain probability the centers can relax to the T_1 state, too. Both excitation modes are inserted in the energy level scheme of Fig. 3.

Let us now briefly discuss the potential of Ge-implanted SiO_2 layers for applications in optoelectronic devices. One crucial feature is of course the luminescence efficiency. The investi-gations show, that the power efficiency, defined as the ratio between the optical output and the electrical input power, increases with decreasing oxide thickness and reaches a record value of 0.5 % for 130 nm. This value is very remarkable for an optically forbidden transition and is among the best in the field of Si-based light emission. Nevertheless, there are further critical issues important for large-scale optoelectronic applications: a good integrability with common Si technology, and a short luminescence decay constant. As far as technology goes, the three main fabrication steps, namely thermal oxidation, ion implantation and annealing below 1000 °C, are well established procedures in microelectronic device fabrication. Due to its excellent mechanical, chemical and electrical properties, SiO_2 itself is an attractive material, which is already widely employed in microelectronics. Moreover, the EL efficiency has proven relatively insensitive to the exact processing conditions, which should permit straightforward adaptation of the process to industry requirements. Thus the compatibility with the current Si technology is one of the main advantages of the Ge-implanted SiO_2 films as luminescent devices. Regarding the luminescence decay constant, operation at several GHz is of course desired for optical data communication. This requires decay times in the sub-ns range and has not been achieved for any Si-based emitters. For other applications, operation frequencies in the kHz range will suffice. For the present devices, a PL decay time of the order of 100 µs has been measured [7], which excludes high-frequency applications at present. Thus, probable applications will be in the low-frequency domain, e.g. for display and sensor technology.

To demonstrate the suitability of Ge-implanted SiO_2 layers for optoelectronic applications, we have manufactured an all-silicon-technology based integrated optocoupler [11] whose structure is drawn in Fig. 5. An optocoupler

galvanically separates the circuit of a light emitter (transmitter) from the detection circuit (receiver),

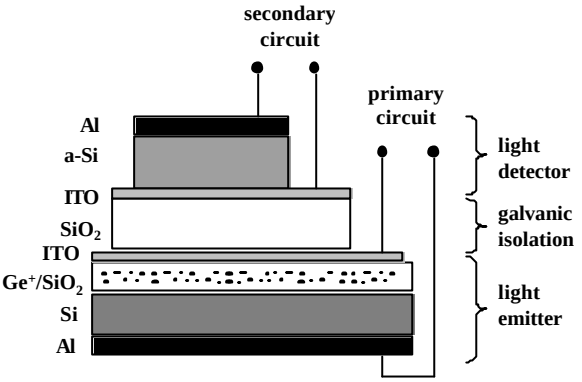

Fig. 5: Schematic structure of the integrated optocoupler consisting of a light emitter based on Ge-implanted SiO_2 layers and a light detector made of amorphous Si. Emitter and detector are galvanically isolated by a thick and transparent oxide layer.

and information is transmitted between them via light pulses. The emitter circuit is almost identical with the structure of Fig. 1(a) and is isolated from the receiver circuit by a thick and transparent oxide layer. The receiver consists of a pin-diode made of amorphous silicon, which was deposited using a cluster tool for CVD processes. The sensitivity of the pin-diode is about 0.2 A/W at a wavelength of 400 nm. Whereas a high voltage determined by the thickness of the Ge-implanted SiO_2 film (e.g. 100 V for 130 nm) is applied to the primary circuit, the pin-diode operates below 5 V. The receiver signal current exhibits a linear dependence on the emitter current over more than two orders of magnitude. The integrated optocoupler can be used as a sensor in microsystems. Moreover, the relatively short emission wavelength could be advantageous for applications in biotechnology. If arranged in an array, the emitter devices could trigger a biochemical reaction in locally defined areas of the array.

In summary, we have demonstrated a bright blue-violet electroluminescent device fabricated using Ge-implanted SiO_2 layers with different oxide thicknesses. The EL efficiency increases with decreasing oxide thickness and reaches a record value of 0.5 % for a thickness of 130 nm. The high potential of this device for optoelectronic application is demonstrated with the first-ever all-silicon optocoupler.

Acknowledgements

We would like to thank T. Dekorsy for helpful discussions and for critically reading the manuscript.

References

[1] Mel-Ari Optoelectronic Road Map, http://www.cordis.lu/esprit/src/melop-rm.htm

[2] L.S. Liao, X.M. Bao, N.S. Li, X.Q. Zheng, N.B. Min, Solid State Comm. **97** (1996) 1039

[3] J.Y. Zhang, X.L. Wu, X.M. Bao, Appl. Phys. Lett. **71** (1997) 2505

[4] K.V. Shcheglov, C.M. Yang, K.J. Vahala, H.A. Atwater, Appl. Phys. Lett. **66** (1995) 745

[5] L. Rebohle, J. von Borany, R.A. Yankov, W. Skorupa, I.E. Tyschenko, H. Fröb, K. Leo, Appl. Phys. Lett. **71** (1997) 2809

[6] L. Rebohle, J. von Borany, W. Skorupa, I.E. Tyschenko, H. Fröb, J. Luminesc. **80** (1999) 275

[7] L. Rebohle, J. von Borany, H. Fröb, W. Skorupa, Appl. Phys. B **71** (2000) 131

[8] F. Kozlowski, H.E. Porteanu, V. Petrova-Koch, F. Koch, Mat. Res. Soc. Symp. Proc. **452** (1997) 657

[9] P. Knàpek, B. Rezek, D. Muller, J.J. Grob, R. Lévy, K. Luterovà, J. Kocka, L. Pelant, phys. stat. sol. (a) **167** (1998) R5

[10] L. Pavesi, L. Dal Negro, C. Mazzoleni, G. Franzò, F. Priolo, Nature **408** (2000) 440

[11] T. Gebel, W. Skorupa, J. von Borany, L. Rebohle, D. Borchert, W. Fahrner, German Patent pending, reference number 100 11 258.7

Nonvolatile Memory Based on Si Implanted Gate Oxides

J. von Borany, T. Gebel, M. Klimenkov, K.-H. Stegemann* and M. Wittmaack*
** Zentrum Mikroelektronik Dresden, Grenzstraße 28, D-01109 Dresden, Germany*

The concept of a nanocrystal memory [1,2] has several attractive features. First, it overcomes limitations of current (Flash)-EEPROM technologies: higher endurance and lower voltages become possible enabling further scaling and memories of higher density. Second, the retention characteristics can be possibly tailored from DRAM-like to EEPROM-like memories by adjusting the cluster size and their distance to the Si/SiO_2 interface. Third, the simple transistor structure and the full CMOS compatible process integration ability makes the nanocrystal memory to be an ideal candidate for an embedded memory designed for system-on-chip applications.

This contribution summarizes electrical properties of MOS or transistor structures with nanocluster containing SiO_2 films of 20-30 nm thickness. Previous investigations show, that in Ge or Si implanted SiO_2 films with an impurity concentration of about 5 at% small, spherical nanoclusters are formed after annealing at 900-1100 °C [3,4]. The clusters with a typical size below 5 nm and a density between (0.5-1) x 10^{12} cm^{-2} primarily exist around the peak of the implantation profile. Moreover, in Ge implanted SiO_2 films two separated nanocluster regions can be obtained, which are formed by the bulk nanoclusters mentioned before and an additional δ-like nanocluster band located at a distance of only 2-3 nm from the Si/SiO_2 interface [5].

Applying a programming pulse of typically 10 V, 10...100 ms at the gate of a MOS structure with Ge or Si implanted SiO_2 one obtains a reproducible and stable shift of the flatband voltage which is attributed to the storage of electrons at cluster related centers. With a pulse of the opposite polarity the charge can be removed from the clusters and the flatband shift is reversed.

Considering the application for a nonvolatile memory the charge storage has to fulfill the condition of 10 years retention. A comparison of Ge and Si implanted SiO_2 films has shown a larger programming window but a worse retention behavior for the case of Ge implanted SiO_2 layers [6]. As the implantation conditions have been normalized to an uniform damage of about 1 displacements per atom (dpa) at the Si/SiO_2 interface, the difference should not caused by damage effects. We assume, that for the case of existing near interface nanoclusters (as valid for Ge) direct tunneling effects contribute to cluster discharging.

This report restricts to the case of Si, in particular with the background that for the first time a 256k nvSRAM (**n**on-**v**olatile **s**tatic **r**andom **a**ccess **m**emory) has been successfully prepared by Zentrum Mikroelektronik Dresden based on gate oxides containing Si nanoclusters. Si implanted SiO_2 films have been investigated at MOS structures, single n-enhancement transistors, and at complete non-volatile memories. For all cases the fabrication is based on a standard CMOS process with the only difference of additional Si implantation and annealing after gate oxide growth.

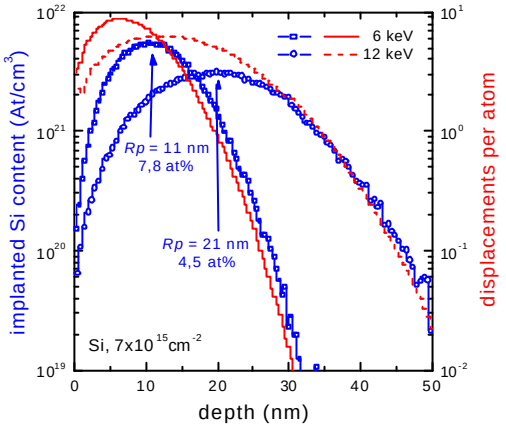

Fig. 1: Results of TRIM calculations of low energy Si implantation into thin gate oxides, using 6 keV for 20 nm and 12 keV for 30 nm oxide thickness, respectively. The implantation fluence is 7 x 10^{15} cm^{-2}. The symbols represent the implantation profiles (left axis), the lines the damage distribution (right axis).

(100) wafers of n-type (for MOS structures) or p-type (for single transistors or memories) have been used. The thermally grown gate oxides of 20 or 30 nm (typical for high voltage devices in mixed signal BiCMOS or CMOS processes) were implanted with $^{28}Si^+$ ions of 6 or 12 keV, respectively, to a fluence ranging from 5 to 9 x 10^{15} cm^{-2}. Afterwards the implanted gate oxide was annealed at 950 or 1050 °C for 30 s followed by the deposition of a 300 nm poly-Si film, which is doped by phosphorous ion implantation and photolithographically patterned to form the gate electrode. For MOS capacitors a number of different annealing

steps with appropriate T-t profiles and atmospheres as characteristic for the full CMOS process are applied to simulate the real thermal budget during the memory fabrication with respect to different isolation (TEOS/BPSG) and metallization levels.

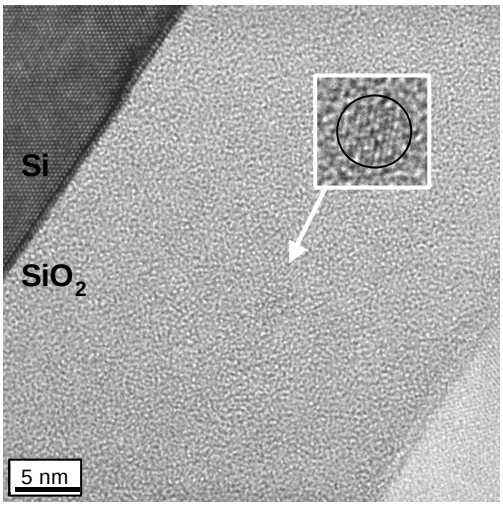

Fig. 2: High resolution TEM micrograph of a Si implanted (12 keV, 1×10^{16} cm^{-2}) SiO_2 film after rapid thermal annealing at 1050 °C, 30 s in dry nitrogen. The inset shows the [111] lattice planes (distance: 0,317 nm) of a single Si nanocrystal of 3.8 nm size. The measured lattice plane distance corresponds very well with the Si bulk value (0.313 nm).

The implantation profiles in the SiO_2 layer (Fig. 1) are characterized by a peak impurity content of 5-8 at% and a projected range located at a distance of about 10 nm from the Si/SiO_2 interface. Contrary to other studies of Si nanoclusters in SiO_2 films realized by ion beam synthesis (IBS), the implanted Si content in the SiO_2 film is quite low (e.g. [7]: 20-50 at%). Our implantation parameters were chosen with respect to a damage rate of about 1 dpa at the Si/SiO_2 interface to minimize the amorphization of the Si substrate. But due to the lower Si content and the corresponding small cluster size they are very hardly to detect in the transmission electron microscope (TEM). As a Z contrast technique cannot be used, the only chance is to image the lattice planes of the nanocrystals. As shown in the TEM micrograph of Fig. 2 single nanocrystals have been obtained with a size between 3-4 nm. The nanocrystals are randomly oriented in the SiO_2 matrix. Therefore, only a few clusters with suitable alignment to the electron beam can be obtained and a determination of the cluster density is not possible.

Fig. 3 shows the IV-characteristics of a 30 nm gate oxide implanted with 12 keV Si^+ ions for different fluences as measured at MOS structures in accumulation. In comparison to the unimplanted reference one can clearly observe an enhanced conductivity of the oxide film for electric fields between 4 - 8 MV/cm.

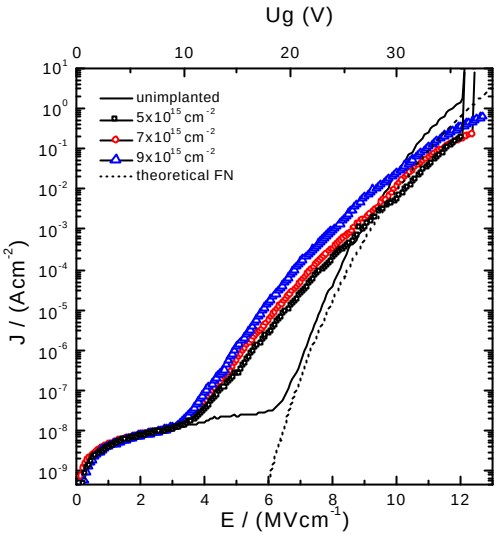

Fig. 3: IV-characteristics of MOS structures with Si implanted (12 keV, $5 - 9 \times 10^{15}$ cm^{-2}) SiO_2 films (d = 30 nm) compared with an unimplanted reference and the theoretical Fowler-Nordheim plot (m = 0.5 mo; Φ = 2.95 eV).

The current slightly increases with increasing fluence. A similar behavior is well known from stress induced leakage current (SILC) after exposing thin SiO_2 films to high electric fields [8]. For that case, energetic electrons cause structural defects, which are related to energy levels in the SiO_2 bandgap, enabling trap assisted tunneling. At ion implanted SiO_2 films traps may be generated as a result of nanocluster formation (e.g. from a specific atomic arrangement at the Si cluster surface). For a field strength > 8 MV/cm the IV-characteristics is determined by the Fowler-Nordheim tunneling current for both the implanted sample and the unimplanted reference. In agreement to the results of Ref. [9] the breakdown is above 10 MV/cm for all fluences, which indicates no significant loss of the oxide quality by the ion beam treatment. This is confirmed by the very smooth Si/SiO_2 interface as observed in the TEM image (Fig. 2). A detailed study concerning the interpretation of the IV characteristics - especially for the "mid-field" region - is in progress.

Programming of the MOS structures has been performed applying positive (write) or negative (erase) voltage pulses to the gate electrode. Relatively long pulse times (~ ms) had to be used in order to reach inversion. The programming window size was obtained by measuring the shift of the CV-curve under flatband conditions (Fig. 4). The programming window increases with raising implantation fluence. For an implantation fluence

of 7 x 10^{15} cm^{-2} the programming window always exceeds 0.5 V, which is of practical relevance.

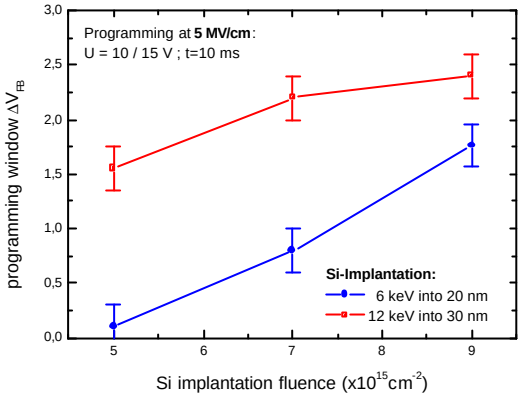

Fig. 4: Programming window measured at MOS capacitors with Si implanted gate oxides for different implantation fluences. The programming window DV_{FB} represents the difference of the flatband voltage measured after wirting (+V) and erasing (-V) with pulses of opposite polarity.

So far, the nature of the charge storage center is not completely elucidated. In most papers the charge storage due to the quantum confinement of the clusters is discussed [10]. However, there are also some arguments, which indicate other reasons like trap assisted charge storage at cluster related centers [11] similar to the well-known mechanism in overstoichiometric Si_3N_4, which is applied in the SNOS memory technology [12,13].

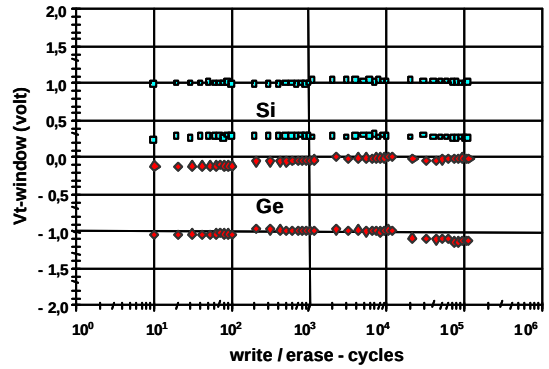

Fig. 5: Endurance characteristics measured at MOS capacitors for Si-implanted (6 keV, 5x 10^{15} cm^{-2}) or Ge-implanted (12 keV, 3.5 x 10^{15} cm^{-2}) gate oxides of 20 nm thickness. The programming pulse for both, writing and erasing, is kept constant to 10 V / 10 ms.

The endurance characteristics was measured on selected wafers. As shown in Fig. 5 the programming window did not degrade up to 10^5 cycles, which is the current limitation for Flash-EEPROM technologies. This result indicates, that the electron transport in the cluster containing SiO_2 film is not dominated by Fowler-Nordheim-tunneling for programming voltages, which corresponds to a field strength of 5 MV/cm.

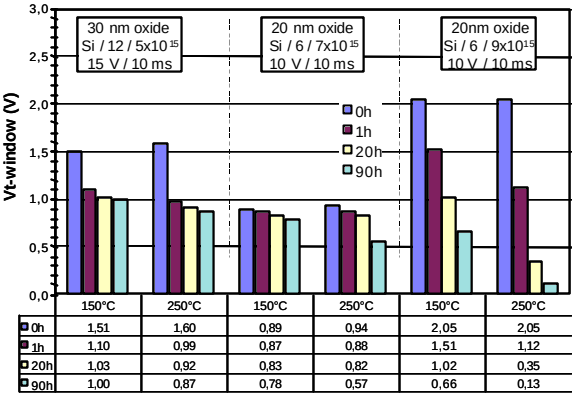

	150°C	250°C	150°C	250°C	150°C	250°C
0h	1,51	1,60	0,89	0,94	2,05	2,05
1h	1,10	0,99	0,87	0,88	1,51	1,12
20h	1,03	0,92	0,83	0,82	1,02	0,35
90h	1,00	0,87	0,78	0,57	0,66	0,13

Fig. 6: Results of data retention measurements after storage at 150 °C or 250 °C for MOS capacitors with Si implanted gate oxides. The values below the figure represent the remaining programming window after different storage durations.

For nonvolatile memory applications the data retention is one of the most important parameters. In Fig. 6 the retention characteristics measured for Si implanted SiO_2 gate oxides is shown. Charging was performed by applying 10 ms pulses of 10 / 15 V for 20 / 30 nm thick SiO_2 films, respectively (=5 MV/cm). Afterwards the wafers were stored at 150 °C or 250 °C up to 90 h without any electrical potential at the gate. According to microelectronics reliability specification the storage of 250 °C, 20 h corresponds to data retention of 10 years at room temperature. Except for the highest investigated fluence the DV_{FB} window remains nearly constant above 0.5 V even after an annealing treatment of 250 °C, 90 h .

In a 0.8 µm CMOS process on p-type silicon, n-channel enhancement transistors were fabricated. The threshold voltage V_t for transistors located at wafer areas with unimplanted gate oxide is ~ 0.6 V (w/L = 20 / 0.8 µm). The transistors with Si implanted gate oxide show a stable programming window of DV_t ~ 4 V (Fig. 7). The I_{DS}-V_{GS} curves are going from the off-state to the on-state and back through the zero point. A current sensing window over nine decades is possible at room temperature, which is a very comfortable window for the memory application. The sub-threshold leakage current is low, which is an additional indication for a good quality of the implanted gate oxide and the Si/SiO_2 interface. The programming window is independent of the width/length ratio of the transistor. Details concerning the measurement of the EEPROM properties for various transistor geometries (w/L-ratio) or different programming parameters described elsewhere [5].

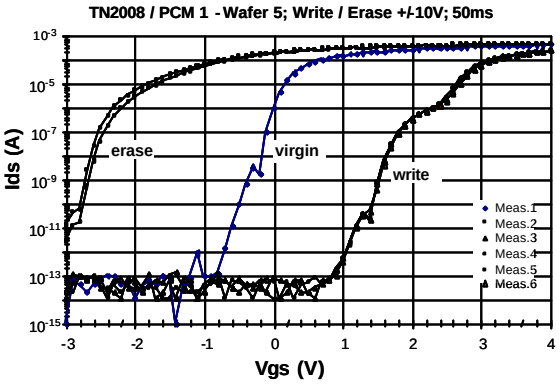

Fig. 7: Drain-source current vs. gate-source voltage for a n-channel transistor with implanted gate oxide (Si, 6 keV; 5 x 10^{15} cm^{-2}) of 20 nm. The programming was performed with write/erase pulses of +/- 10 V for 50 ms.

Due to the promising results from the single transistor elements a full 256k-nvSRAM demonstrator has been prepared and tested. A nvSRAM has two separate modes of operation - a SRAM mode and a nonvolatile mode. In SRAM mode, the memory operates as an ordinary static RAM. In nonvolatile operation, data are transferred in parallel from SRAM to EEPROM or visa verse. Two EEPROM-cells are incorporated in each static memory cell. The SRAM can be read and written an unlimited number of times, while independent non-volatile data resides in the EEPROM. Data transfer from the SRAM to the EEPROM cells ("STORE") or back ("RECALL") takes place automatically upon power down or power up, respectively.

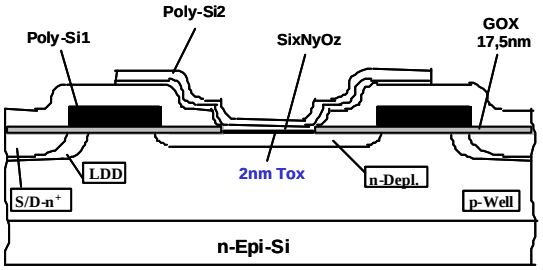

Fig. 8: Cross section of the SNOS cell. For the nanocluster memory the $SiO_2/Si_xN_yO_z$ stack is replaced by a Si implanted SiO_2 film.

As a reference EEPROM configuration the SNOS-transistor-cell (**s**ilicon-**n**itride-**o**xide-**s**ilicon), made by a 24 nm nitride on 2 nm tunnel oxide with a poly-Si gate has been used [13,14]. In the modified technology we replaced the oxide-nitride stack by a Si-implanted oxide (^{28}Si, 6 keV, 5-9 x 10^{15} cm^{-2}) followed by rapid thermal annealing (950 °C, 30 s, N_2) and the deposition of 100 nm poly-Si used as gate electrode material (Fig. 8). After the integration of this "nanocluster module" the standard process flow is continued. Measurements with the standard wafer test program prove the full functionality of the 256k-nvSRAM. The DV_t window is > 1 V for programming pulses of 12 V / 8 ms is comparable to that of the SNOS-cell. Data retention and endurance measurements on device level are in progress.

Acknowledgements

The work is supported by the Freistaat Sachsen (Project: SMWK 4-7531.50-03-844-98/4 and SMWA 4785), which is gratefully acknowledged. The authors want to thank H.J. Thees (Infineon Technologies) and K.H. Heinig (FZR) for their valuable contribution to this work.

References

[1] S. Tiwari, F. Rana, K. Chan, L. Shi, H. Hanafi, Appl. Phys. Lett. **69** (1996) 1232

[2] C. Wasshuber, H. Kosina, S. Selberherr, IEEE Trans. on Electr. Dev. **45** (1998) 2365

[3] J. von Borany, K.H. Heinig, W. Skorupa, in Adv. in Solid State Physics **39** (1999) 171, ed. by B. Kramer, Vieweg-Verlag, 1999

[4] A. Markwitz, B. Schmidt, W. Matz, R. Grötzschel, A. Mücklich, Nucl. Instr. and Meth. **B142** (1998) 338

[5] J. von Borany, K.H. Heinig, R. Grötzschel, M. Klimenkov, M. Strobel, K.H. Stegemann, H.J. Thees, Microelectronic Engineering **48** (1999) 231

[6] K.H. Stegemann, H.J. Thees, M. Wittmaack, J. von Borany, K.H. Heinig, T. Gebel, Int. Conf. on Ion Implant. Technology (IIT'2000)

[7] P. Normand, D. Tsoukalas, E. Kapetanakis, J.A. van den Berg, D.G. Armour, J. Stoemenos, Microelectronic Engineering **16** (1997) 79

[8] B. Ricco, G. Gozzi, M. Lanzoni, IEEE Trans. on Electr. Dev. **45** (1998) 1554

[9] H.J. Thees, M. Wittmaack, K.H. Stegemann, J. von Borany, K.H. Heinig, T. Gebel, Microelectronics Reliability **40** (2000) 867

[10] S. Tiwari, J.A. Wahl, H. Silva, F. Rana, J.J. Welser, Appl. Phys. A **71** (2000) 403

[11] Y. Shi, K. Saito, H. Ishikuro, T. Hiramoto, J. Appl. Phys. **84** (1998) 2358

[12] S. Minami, Y. Kamigaki, IEEE Trans. on Electr. Dev. **40** (1993) 2011

[13] K.-H. Stegemann, A. Bemmann, A. Freigofas, B. Gerth, C. Beyer, ITG-Fachtagung 03/98 (1998), 95

Ion Beam Synthesis of Graphite and Diamond in Silicon Carbide

V. Heera, W. Skorupa, B. Pécz* and L. Dobos*
*Research Institute for Technical Physics and Materials Science,
H-1525, Budapest, P.O.B. 49, Hungary

High dose ion implantation in combination with thermal annealing is a promising technique to produce precipitates or complete layers of new phases with desired properties below the surface of solid materials. This process - also called ion beam synthesis (IBS) - was mainly employed to modify the electronic properties of silicon substrates [1]. One prominent example is the SIMOX process [2] where a buried insulating SiO_2 layer in Si is formed by O implantation. Further interesting applications of IBS are the formation of metal silicides [3] or SiC layers in Si [4,5].

In recent years the semiconductor related materials research has been focused more and more on wide band gap semiconductors like SiC, diamond and GaN because of their outstanding properties for electronic applications [6,7]. Among the wide band gap semiconductors SiC is the one with the most mature device technology. However, little is known about the IBS of new phases in SiC. Only few attempts have been made to produce insulating [8,9] or conductive [10] layers in SiC by IBS. There are some special problems of IBS in SiC. SiC is an extremely dense material with very tight bonds. Therefore it is difficult to eliminate the implantation damage or to redistribute the implanted ions by thermal annealing [11]. In addition the implanted ions produce a huge strain in the lattice. One way to overcome this problem is to perform the implantation at temperatures high enough for dynamic annealing and strain relaxation. Recently, it has been shown that crystalline precipitates of Al_4C_3 in perfect epitaxial orientation with the surrounding SiC lattice can be synthesized by high dose Al implantation into 6H-SiC at 500 °C [12]. However, the implanted Al ions react only with the C atoms leaving remainders of crystalline Si in the SiC substrate.

In view of the recent results it is an interesting question which phase is formed by excess carbon in the SiC lattice under the nonequilibrium conditions of IBS. Several carbon phases are known: Cubic and hexagonal diamond, graphite and amorphous carbon [13].

Pieces of n-type 6H-SiC wafers were implanted with 60 keV, 1×10^{18} C^+/cm^2 at temperatures of 300 °C, 600 °C and 900 °C. The atomic and damage energy distributions of the implanted carbon in SiC calculated by SRIM [14] are shown in Fig. 1. This is only a rough estimation of the expected profiles because high dose effects like sputtering and dynamic changes of target composition and density are neglected. The amount of implanted carbon corresponds to a deposited graphitic layer of 81 nm. According to the calculation, the composition of the compound is about $Si_{0.20}C_{0.80}$ in the carbon maximum at the depth of 130 nm. The sputtered depth is estimated to be about 20 nm. Therefore the ion energy should be high enough to produce a buried layer of a carbon phase completely covered by SiC. The investigated temperature range was chosen because 300 °C is the critical temperature necessary to avoid amorphization of SiC [11], whereas 900 °C is well above the temperature where graphitization of diamond is obtained by ion implantation [15]

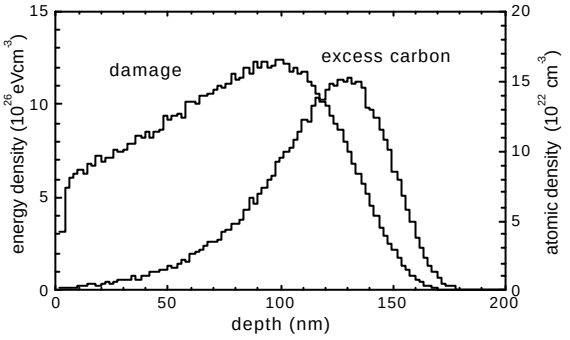

Fig. 1: Calculated profiles of damage and excess carbon.

The surface of the implanted SiC pieces was inspected with an optical microscope. Neither surface cracks nor inhomogeneities were observed. The phase formation was investigated by cross-section transmission electron microscopy (XTEM) in a Philips CM20 electron microscope. Cross sectional specimens for TEM were prepared by ion milling.

Fig. 2 shows the XTEM micrograph of the sample implanted with 1×10^{18} C^+/cm^2 at 300 °C. Although the damage energy in the near-surface surface region is more than 200 times higher than

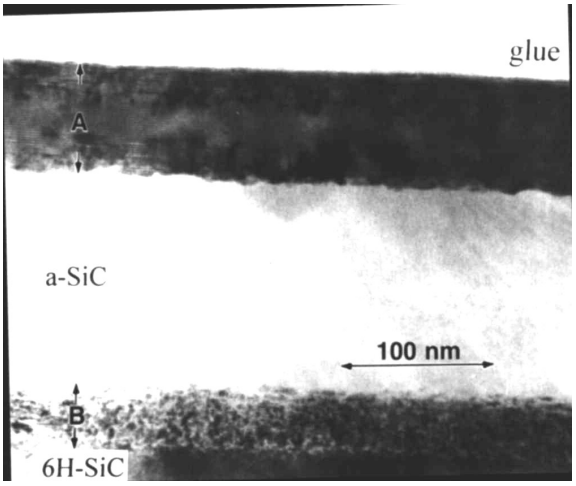

Fig. 2: XTEM micrograph of the sample implanted at 300 °C.

the amorphization energy of SiC at room temperature [11], a crystalline 6H-SiC layer of about 75 nm is left as indicated by the visible lattice fringes marked as region A in Fig. 2. Selected area diffraction (SAD) confirmed this result. This means that an effective self-annealing of radiation damage takes place in SiC at 300 °C. The TEM analysis reveals that an amorphous phase (a-SiC) is produced in the depth region between 75 and 210 nm, which is followed by a small zone B of highly defective crystalline 6H-SiC of about 45 nm width. Because the damage energy in the amorphized zone is not substantially higher than in the near-surface region it can be concluded that the amorphous phase is stabilized by the excess carbon atoms in this region. The center of the amorphous region corresponds well with the calculated maximum of the implanted carbon profile. However, the amorphous zone is a little broader than expected from the calculated carbon distribution. This can be explained by swelling due to the carbon deposition inside the layer.

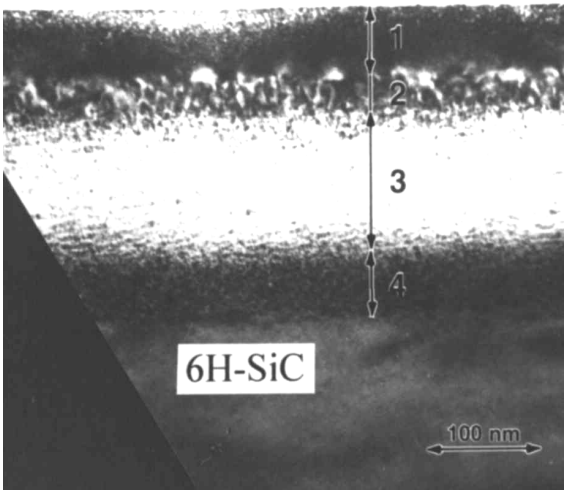

Fig. 3: Cross section of the sample implanted at 600 °C.

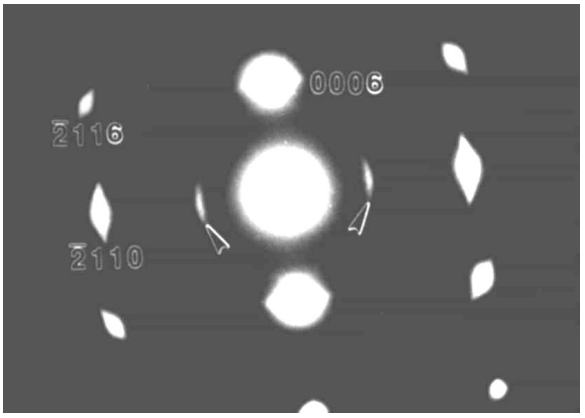

Fig. 4: SAD pattern taken from the zone (3) of the sample shown Fig. 3.

Amorphization is completely prevented for implantation at 600 °C as shown in Fig. 3. In the cross-section four crystalline zones can be distinguished. The top surface region (1), 55-60 nm thick, is almost defect-free 6H-SiC. The adjacent 6H-SiC layer (2) with a width of about 30 nm contains several lattice defects. The main zone (3) is a 100 nm thick layer with crystalline precipitates generating a bright contrast in the micrograph. This zone is followed by a stripe of damaged SiC (4). The SAD pattern taken from zone (3) is shown in Fig. 4. It consists of SiC reflections, which are elongated due to lattice defects. Beside the SiC reflections two arrowheads mark reflections which can be identified as (0002) graphite reflections. Obviously, the graphite has a texture. The formation of graphite precipitates by the excess carbon inside the SiC crystal is not surprising because all Si-C bonds are saturated and graphite is the only equilibrium phase of carbon.

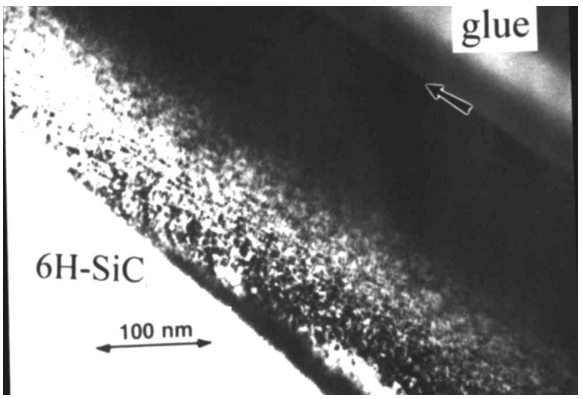

Fig. 5: XTEM micrograph of the sample implanted at 900 °C. The original surface is marked by an arrow.

Unexpected results were obtained for the carbon implantation at 900 °C. An overview of the specimen is shown in Fig. 5. Around the depth of 150 nm a buried zone with precipitates is found in

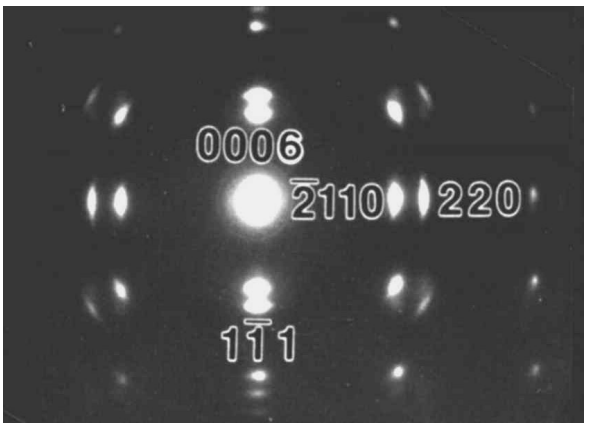

Fig. 6: SAD pattern taken from the implanted region of the sample shown in Fig. 5. Diamond spots (cubic indices) are superimposed on the 6H-SiC diffraction pattern.

the weakly damaged 6H-SiC matrix. The SAD pattern (Fig. 6) reveals the coexistence of hexagonal SiC and cubic diamond grains, which are in perfect epitaxial relation. The size of the diamond grains is between 2 and 5 nm as determined by dark field imaging with the (220) reflection of diamond (Fig. 7). The width of the diamond zone is about 100 nm. No graphitic inclusions were detected by the TEM analysis in the implanted layer.

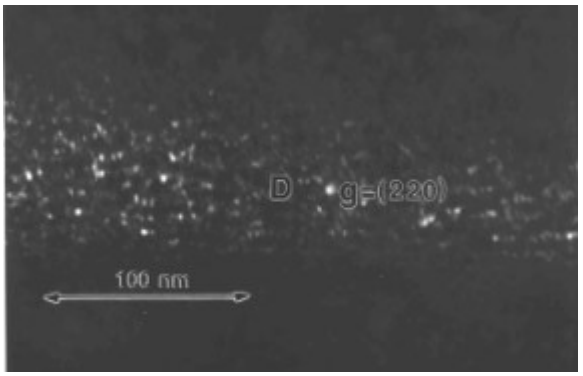

Fig. 7: Dark field image of the sample implanted at 900 °C taken with the (220) diamond spot.

The mechanism of the diamond formation by IBS in SiC is not quite clear. It can be assumed that the tetrahedrally coordinated SiC lattice, which is preserved during the high temperature implantation, acts as a template for the growth of diamond. In addition, local nonequilibrium conditions in the ion cascades (thermal spikes, shock waves) [1] or temporary stress on interstitially incorporated carbon atoms by the surrounding SiC lattice could contribute to the diamond nucleation. Weselowski et al. [16] demonstrated the transformation of graphitic carbon onions to diamond by ion irradiation in the temperature range between 700 °C and 1100 °C. They explained the transformation process by a compression of the carbon onions induced by knock-on displacements. Obviously, the target temperature plays a crucial role for the diamond formation. Occasionally formed diamond nuclei are destroyed by the implantation damage below temperatures of 700 °C resulting in growing graphite or amorphous carbon at temperatures of 600 °C or 300 °C, respectively.

References

[1] J.F. Ziegler (ed.), Handbook of Ion Implantation Technnology, Elsevier, New York, 1992

[2] W. Skorupa, in: J.P. Colinge et al. (Eds.), Physical and Technical Problems of SOI Structures and Devices, Kluwer Academic, Dordrecht, 1995, pp. 39-54

[3] D. Panknin, E. Wieser, W. Skorupa, W. Henrion, H. Lange, Appl. Phys. **A 62** (1996) 155

[4] C. Serre, L. Calvo-Barrio, A. Perez-Rodriguez, A. Romano-Rodriguez, J.R. Morante, Y. Pacaud, R. Kögler, V. Heera, W. Skorupa, J. Appl. Phys. **79** (1996) 6907

[5] J.K.N. Lindner, B. Stritzker, Nucl. Instr. Meth. B **148** (1999) 528

[6] H. Morkoc, S. Strite, G.B. Gao, M.E. Lin, B. Sverdlov, M. Burns, J. Appl. Phys. **76** (1994) 1363

[7] P.R. Chalker, Thin Solid Films **343-344** (1999) 616

[8] W. Wesch, A. Heft, H. Hobert, G. Peiter, E. Wendler, T. Bachmann, Nucl. Instr. Meth. B **141** (1998) 160

[9] M. Ishimaru, R.M. Dickerson, K. Sickafus, Appl. Phys. Lett. **75** (1999) 352

[10] W. Skorupa, V. Heera, Y. Pacaud, H. Weishart, Nucl. Instr. Meth. B **120** (1996) 114

[11] V. Heera, W. Skorupa, Mater. Res. Soc. Symp. Proc. **438** (1997) 241

[12] V. Heera, H. Reuther, J. Stoemenos, B. Pécz, J. Appl. Phys. **87** (2000) 78

[13] H.O. Pierson, Handbook of carbon, graphite, diamond and fullerenes, Noyes, Park Ridge, 1993

[14] J.F. Ziegler, J.P. Biersack, U. Littmark, The Stopping and Range of Ions in Solid, Pergamon, New York, 1985, Vol. 1

[15] R. Kalish, Appl. Surf. Sci. **117/118** (1997) 558

[16] P. Wesolowski, Y. Lyutovich, F. Banhart, H.D. Carstanjen, H. Kronmüller, Appl. Phys. Lett. **71** (1997) 1948

Retention of the Potential Energy of Multiply Charged Argon Ions Incident on Copper

U. Kentsch*, H. Tyrroff, G. Zschornack* and W. Möller

** Technical University of Dresden, Institute of Nuclear and Particle Physics*
Mommsenstr. 13, 01069 Dresden, Germany

The potential energy of highly charged ions, which is defined by the sum of the binding energies of all electrons removed from the atom, may exceed the kinetic energy significantly, giving rise to new phenomena of ion-surface interaction. Correspondingly, an active research field has developed during the past years covering aspects of atomic physics and ion-beam surface modification [1,2]. In the latter field, enhanced sputtering was demonstrated for a number of materials such as thin carbon films [3], GaAs [4] and SiO_2 [5]. Corresponding applications to ion beam lithography have been proposed [6] with the clear advantage that the potential energy is deposited within a depth of a few nm only [7], so that any deep damage can be avoided at sufficiently low kinetic energy. With this respect, a crucial quantity is the fraction of the potential energy which is being retained in the surface, thus being available for surface modification. High yields of photons [1,8] and electrons [2,9,10] have been observed which might carry away a substantial fraction of the potential energy, even if quantitative estimates, which are subject to high uncertainty, only yield an energy reemission coefficient in the order of 10% [11].

To the knowledge of the authors, only one measurement of the retained fraction of the potential energy of highly charged ions has been described previously [11]. For single impacts of Au^{69+} and Xe^{52+} as obtained from an electron beam ion trap (EBIT) ion source, the authors measured the electronic energy deposition in a silicon detector. It was found that 35% to 40% of the potential energy is converted into electron-hole pairs at a depth of more than 50 nm, i.e. below the insensitive contact layer of the detector. These numbers may represent a lower limit for the actual amount of retained potential energy since low-energy electrons do not contribute to the signal, and due to a possible influence of the contact layer which is difficult to quantify. The present paper reports on a novel measurement using stationary calorimetry with ions of medium charge from an ECR ion source (Ar with $q \leq 9$ where q denotes the charge state). This technique is more direct since all excitations which remain in the solid after ion impact are finally turned into heat. The present investigation is complementary to Ref. [11] with respect to the experimental technique and the species of highly charged ions. Nevertheless, similar numbers of the retained fraction of the potential energy are obtained.

The experiments have been performed at the Rossendorf 7.5 GHz ECR ion source which is equipped with sector field magnetic separation and a beam deceleration system [12-14]. The ions are accelerated with a voltage of 5 kV and, after beam transport including magnetic separation, decelerated to a final energy between 75 and 240 eV*q at the target. A calorimetric set-up similar to devices used at laser beam facilities [15] was constructed to measure the temperature raise during irradiation. A copper foil of 0.1 mm thickness and 10 mm diameter was connected to an LN_2 cooled heat sink by four copper wires of 100 µm diameter. Simultaneously, the wires form the electric leads to a platinum temperature sensor and a small resistive heater for power calibration, both glued to the rear side of the target. The target is housed in a LN_2 cooled environment and insulated from ground to enable ion current measurement during irradiation. Alternatively, a Faraday cup can be moved into the target position before and after irradiation for ion beam positioning and ion current calibration.

After starting the ion irradiation, the target temperature approaches equilibrium with a time constant of 64 s, with the equilibrium temperature being proportional to the deposited power delivered by the ion beam. A temperature stability of the heat sink of 1 mK during at least 8 hours was provided by LN_2 cooling and a LakeShore temperature controller. The power calibration by the resistive heater resulted in a sensitivity of the setup of s = 1.335 mK/µW at a target temperature of 146 K. The temperature sensor was powered by a constant current supply and the voltage reading across the sensor was performed by a Keithley 2182 nanovoltmeter. The experiment was computerized using AD converters and IEEE interfaces. The sensitivity and stability of the setup are sufficient

to run experiments down to an ion beam power of about P_t = 150 nA * 50 V = 7.5 μW.

The total energy of an incident ion is given by the sum of its kinetic energy and its potential energy,

$$E_{tot} = E_{kin} + E_{pot} = qe\left(U_{acc} - U_{dec} + U_{pl}\right) + E_{pot} \quad (1)$$

where U_{acc} and U_{dec} denote the acceleration and deceleration voltages, respectively, U_{pl} the ECR plasma potential, and e the elementary charge. With the chosen plasma parameters, the plasma potential has been measured to U_{pl} = 40±2 V by comparing the settings of the analysing magnetic field for different charge states. If fractions DE_{kin} and DE_{pot} of the kinetic and the potential energy, respectively, are retained in the target, the power input P_t to the target reads with the ion current I_t

$$P_t = \frac{\Delta E_{kin} + \Delta E_{pot}}{qe} I_t \quad (2)$$

Each set of experiments has been performed at constant target current. This was achieved by defocusing the stronger components of the q/m spectrum, where m denotes the ion mass, after magnetic separation but keeping constant all plasma parameters of the discharge.

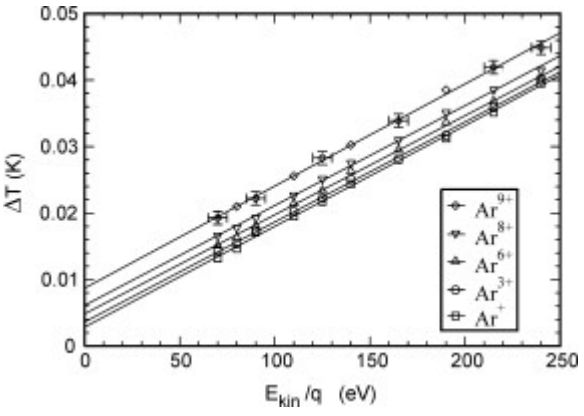

Fig. 1: Rise of the target temperature *DT* measured during irradiation of copper with argon ions, for different charge states Ar^{q+} as function of the kinetic energy of the impinging ions per charge number, at a beam current of 150 nA and target temperature of 146 K.

Fig. 1 illustrates the experimental procedure and represents a typical result taken for argon ions. The stationary rise of the target temperature is shown in dependence on the charge state of the impinging argon ions at a beam current of 150 nA. The error bars, which are given for Ar^{9+} ions, are similar for the other charge states. The different results corresponding to different ion charges can clearly be distinguished, indicating an increasing energy deposition at increasing charge number. The data have been fitted by linear regression for each charge state, yielding identical slopes within the error bars. This justifies the assumption that the relative retained fraction of the kinetic energy, DE_{kin}/E_{kin}, is independent of the kinetic energy. Then, data of the retained fraction of the potential energy, $DE_{pot}(q)$, can be obtained by extrapolating to zero kinetic energy. The results are shown in Fig. 2 (top) for different charge states, together with the corresponding theoretical prediction of the total potential energy of the ions which has been calculated using the GRASP1 code [16]. (The experimental value for q = 5 is not recorded due to an interference with impurity ions.) The experimental results and the theoretical prediction are related to obtain the retained fraction of the potential energy as shown in Fig. 2 (bottom). In view of the large error bars in particular for the lower charge states, the retained fraction of the potential energy is found to depend, if at all, weakly on the incident charge, with an average value of approximately 30% to 40%.

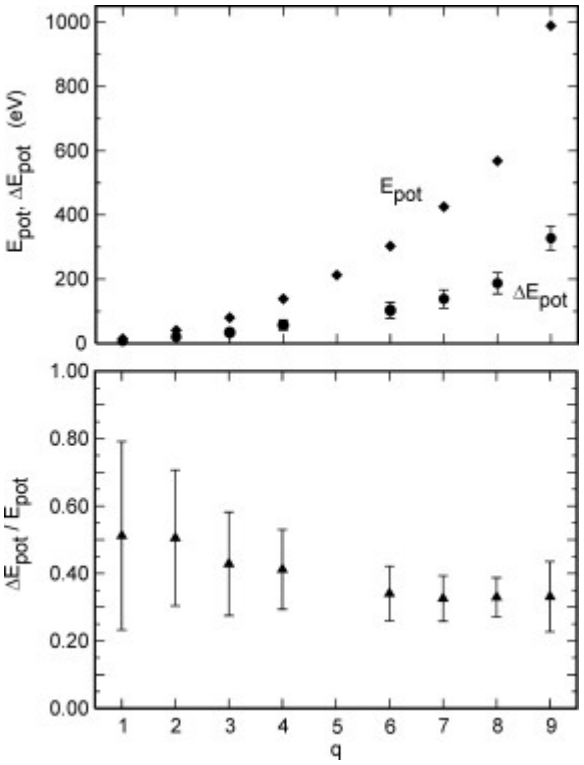

Fig. 2: Measured retained potential energy (dots) and calculated total potential energy (diamonds) (top), and relative retained fraction of the potential energy (bottom), for different charge states q of argon ions incident on copper, measured at an ion beam current of 400 nA.

Any dependence of the retained fraction of the potential energy on the charge number might also be obscured by an implicit energy dependence, since the data points at each abscissa in Fig.

1 have been obtained at constant voltage, so that data sets for higher charge numbers correspond to higher average kinetic energies. However, any significant deviation from linearity is not observed in Fig. 1. Nevertheless, higher kinetic energies might cause the potential energy to be deposited in larger depths, which might reduce the fraction which escapes, in qualitative agreement with the trend of Fig. 2.

Surprisingly, the present result is in perfect agreement with the finding by Schenkel et al. [11] for Xe^{52+} and Au^{69+} in silicon. This, however, might be fortuitous. As mentioned above, the different experimental technique employed in their work does not necessarily provide the full retained amount of potential energy. Moreover, their work is related to very heavy ions with very high charge, corresponding to a potential energy between about 10 keV and 200 keV, compared to between 10 eV and 1 keV in the present work. Also, the kinetic energies employed in their experiments were considerable higher (several 100 keV) than for the present study. Thus, different mechanisms of energy transfer and relaxation might govern the interaction of the highly charged ions with the surface, including the energy relaxation and the fraction which is lost into photon and electron emission. Moreover, it appears improbable that the retained fraction of potential energy would be independent of the target material.

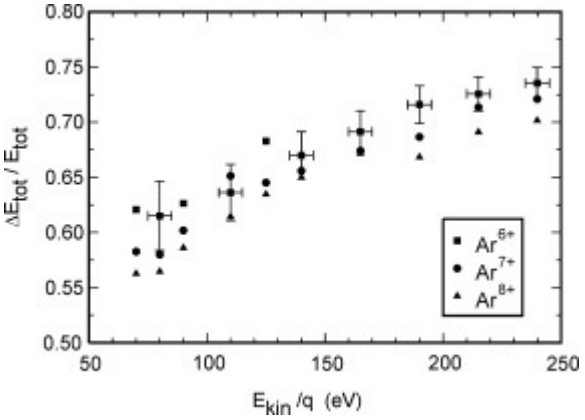

Fig. 3: Relative retained fraction of the total energy versus the kinetic energy of Ar ions incident on copper, at different charge states as measured with a beam current of 400 nA.

From both studies, it can be concluded that a substantial fraction of the potential energy is retained in the target. At sufficiently low kinetic energy, the potential energy contributes significantly to the total energy, so that its retained fraction affects the total energy deposition. This is also evident from Fig. 3 which relates the total amount of retained energy to the kinetic energy for different charge states. At higher charge states, the total deposited energy decreases since a higher fraction of potential energy is lost. The dependence of the energy retention on the kinetic energy is clearly nonlinear, which can partly be attributed to collisional losses due to ion reflection and sputtering. For, e.g., Ar^{7+}, at its lowest kinetic energy under investigation of about 500 eV, about 20 eV and 40 eV are lost by reflected ions and sputtered Cu atoms, respectively, according to TRIM computer simulation [17], whereas the above data indicate a loss of about 140 eV of the potential energy of 400 eV. From this, a total energy retention of about 75% would result. A similar calculation for the highest kinetic energy yields about 85%, in qualitative agreement with the trend of Fig. 3. However, the experimental data are lower than these predictions by 10...15%. A similar difference had been found by Coufal et al. [18] for the case of singly charged ions, being attributed to kinetic excitation and ionisation, and the corresponding emission of secondary electrons as well as ions and excited neutrals. This part of the energy balance is not described by binary collision computer simulation. However, if these processes are significant, the above separation of kinetic and potential energy retention may not hold down to a 10% level.

The fact that a substantial fraction of the potential energy of highly charged ions is retained also for medium charge states, may have important consequences for applications in material science. In contrast to the production of ions with the highest charge states, which requires consumptive equipment even for very low ion currents, medium charge states can be obtained at ion fluxes which are becoming comparable to those employed in conventional, i.e. low-charge ion implantation.

It has been demonstrated in the present paper that the dissipation of potential energy of argon ions with medium charge states can be measured by stationary calorimetry at a temperature of about 150 K. For argon ions in copper at kinetic energies between 75 eV and 2.2 keV, an average retained fraction of potential energy of 30% to 40% is found for charge numbers up to 9. The retention of the total energy, i.e. including the kinetic energy, ranges from about 60% to 75% and can largely be accounted for by the retained fraction of the potential energy and collisional energy lost by reflected ions and sputtered target atoms. A deficit of 10% to 15% remains which is probably due to kinetic excitations and emissions.

Work is in progress to extend the database with different ion species, target materials and charge states.

Acknowledgements

The authors would like to thank D. Rabus of the Physikalisch-Technische Bundesanstalt Berlin for useful discussions and comments.

References

[1] A. Arnau, F. Aumayr, P.M. Echenique, M. Grether, W. Heiland, J. Limburg, R. Limburg, R. Morgenstern, P. Roncin, S. Schippers, R. Schuch, N. Stolterfoth, P. Varga, T.M.J. Zouros, H.P. Winter, Surf. Sci. Rep. **27** (1997) 113, and references therein

[2] D.Schneider, M.A.Briere, Phys. Scr. **53** (1996) 228, and references therein

[3] T. Schenkel, M.A. Briere, H. Schmidt-Böcking, K. Bethge, D.H. Schneider, Phys. Rev. Lett. **78** (1997) 2481

[4] T. Schenkel, A.V. Hamza, A.V. Barnes, D.H. Schneider, J.C. Banks, B.L. Doyle, Phys. Rev. Lett. **81** (1998) 2590

[5] M. Sporn, G. Libiseller, T. Neidhart, M. Schmid, F. Aumayr, H.P. Winter, P. Varga, Phys. Rev. Lett. **79** (1997) 945

[6] J.D. Gillaspy, D.C. Parks, L.P. Ratliff, J. Vac. Sci. Technol. B **16** (1998) 3294

[7] T. Schenkel, M.A. Briere, A.V. Barnes, A.V. Hamza, K. Bethge, H. Schmidt-Böcking, D.H. Schneider, Phys. Rev. Lett. **79** (1997) 2030

[8] R. Schuch, D. Schneider, D.A. Knapp, D. DeWitt, J. McDonald, M.H. Chen, M.W. Clark, R.E. Marrs, Phys. Rev. Lett. **70** (1993) 1073

[9] J.W. McDonald, D. Schneider, M.W. Clark, D. Dewitt, Phys. Rev. Lett. **68** (1992) 2297

[10] D. Niemann, M. Grether, M. Rösler, N. Stolterfoht, Phys. Rev. Lett. **80** (1998) 3328

[11] T. Schenkel, A.V. Barnes, T.R. Niedermayr, M. Hattass, M.W. Newman, G.A. Machicoane, J.W. McDonald, A.V. Hamza, D.H. Schneider, Phys. Rev.Lett. **83** (1999) 4273

[12] D. Henke, H. Tyrroff, R. Grötzschel, H. Wirth, Nucl. Instrum. Meth. B **98** (1995) 528

[13] D. Henke, H. Tyrroff, Rev. Sci. Instrum. **67** (1996) 1070

[14] D. Henke, H. Tyrroff, H. Wirth, G. Zschornack, Report FZR-131, Research Center Rossendorf, 1996

[15] H. Rabus, V. Persch, G. Ulm, Appl. Optics **36** (1997) 5421

[16] I.P. Grant, B.J. McKenzie, P.H. Norrington, D.F .Mayers, N.C. Pyper, Comp. Phys. Commun. **21** (1980) 207

[17] J.F. Ziegler, J.P. Biersack, Stopping and Ranges in Matter, SRIM vs. 2000.39, http://www.research.IBM.com/ionbeams

[18] H. Coufal, H.F.Winters, H.L. Bay, W. Eckstein, Phys. Rev. B **44** (1991) 4747

Charge State Distributions of Heavy Ions after Scattering at Surface Atoms

C. Klein, R. Grötzschel, M. Mäder and F. Herrmann

During the last years high resolution Rutherford Backscattering Spectrometry (HRBS) has proven to be a promising tool for the analysis of shallow depth profiles [1]. In HRBS swift ions are scattered at the sample and subsequently energy-analysed with a magnetic or electrostatic spectrometer. The interpretation of HRBS spectra is however hampered by the charge state dependent separation of the scattered ions caused by the presence of magnetic or electrostatic fields. In general the charge state of the incoming ion is well defined, whereas the outgoing charge state can be altered by the interaction with the target. This interaction can be divided into three steps: (i) The incoming ion can lose or capture electrons to or from the material it passes through, (ii) the resulting charge state distribution (CSD) is redistributed during the scattering collision, and (iii) eventually a third change of the CSD takes place on the exit path of the ion. When the ions have passed a certain amount of material, a statistical equilibrium CSD develops. Such equilibrium CSDs are tabulated for a large number of ions and are only weakly dependent on the target material [2,3]. The equilibration length is typically in the order of a few or a few tens of nm for ions in the MeV range [4]. Tabulated stopping power and straggling data refer to the equilibrium case. When the desired depth resolution becomes smaller than the equilibration length, the applicability of these data for converting energy to depth is no longer obvious. A better knowledge of non-equilibrium CSDs is necessary. Additionally, there is little information about the CSDs caused by the binary collision itself [5,6]. Due to the multibody interactions involved in such a collision and the complex and correlated loss and capture mechanisms it is almost impossible to calculate CSDs for this case [5]. The situation thus suggests an experimental approach to determine the CSD of the collision process. Recently, Boerma et al. investigated 3 MeV C^{2+} ions incident on sub-monolayers of Au and Ag at scattering angles of 40° and 60°. They found that an equilibrium-like CSD already develops after a single collision [6]. It depends neither on the scattering partner nor on the scattering angle. These findings agree with experiments performed on dilute gas targets showing the same behaviour for a large number of projectile-target combinations at scattering angles below 10° [5]. On the other hand, both results are in contrast to the work of Jamecsny [7], who investigated 1.2 MeV Ar^{+}-ions scattering from a clean Au single crystal as well as from Au vapor. Using an electrostatic spectrometer with monolayer depth resolution he found a marked difference between the CSDs of ions emerging from the topmost layer and those obtained for ions coming from larger depths, where the CSDs are expected to be in equilibrium. One aim of the present work was therefore to find out the conditions under that the CSD is equilibrium-like or not. To this end we have investigated CSDs for various ion species after a single collision with Au and Ta atoms. To make sure that no interaction other than a single binary collision influences the charge state of the outgoing ion, we prepared Si samples covered with less than a monolayer of Au and Ta, respectively. Care has to be taken regarding the role of the surface, because at small angles of incidence or at small angles of emergence, the surface can influence the charge state too [8].

The experimental setup is shown in Fig. 1. For HRBS a magnetic spectrometer of Browne-Buechner type [9] was installed. It consists of a uniform magnetic field with circular field boundaries of a radius of 650 mm. The maximum field is 0.89 T corresponding to a mass-energy product of 16 MeV×amu. A Si detector of 50 mm × 10 mm with a resistive front electrode serves as one-dimensional position sensitive detector. The spectrometer is connected to a UHV chamber (base pressure 5×10^{-10} Torr) housing a 5-axis goniometer with a DC heating stage, two UHV evaporators, a sputter gun, a RHEED system, and a residual gas analyser. The spectrometer can be operated both in forward and in backward scattering geometries, the scattering angles being 144.5° and 35.5°, respectively (denoted by (5) and (6) in Fig. 1). The ion beam is supplied from the Rossendorf Tandetron and monitored by measuring the backscattering yield from an Al beam chopper covered with a thin Au film. A silicon detector in the UHV chamber serves for normalising the CSD measurements. Fig. 2 shows an example of the spectrometer resolution, that was determined by measuring an HRBS spectrum using 2 MeV Li^{+} as primary ion and a clean Si (111) surface as target.

The oxide was removed by flashing the sample several times to 1150 °C at a pressure below 4×10^{-9} Torr. After this treatment the well known 7×7 reconstruction could be observed on the RHEED screen. The width of the high energy edge amounts to 3.8 keV corresponding to a depth resolution of 2.4 Å. Due to the lack of other data, we used tabulated stopping power data for converting the energy spread to a depth resolution. Since the distance between adjacent planes in the case of Si (111) is 3 Å, the achieved depth resolution is in the order of one monolayer.

Samples with a submonolayer of Au were prepared by in-situ evaporation onto a Si (111) surface cleaned in the way described above. After Au deposition of 0.8 monolayers at 400 °C and subsequent annealing at the same temperature for 5 min the RHEED pattern changes to a

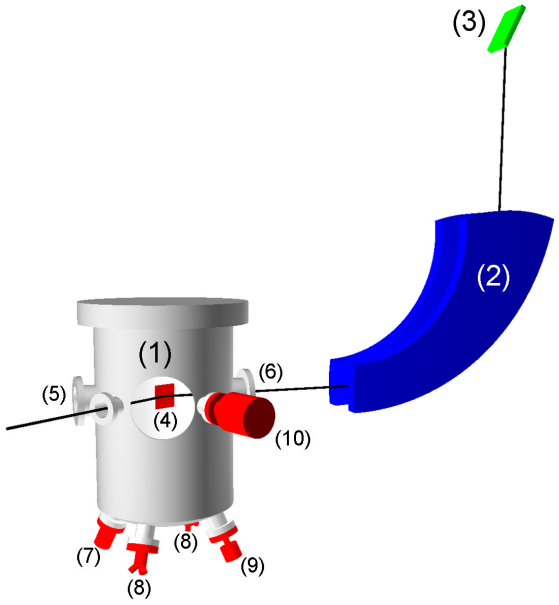

Fig. 1: Schematic experimental setup showing (1) UHV scattering chamber housing the 5-axes goniometer (AML, not shown) with 35.5°-port (6) and 144.5°-port (5), (2) Browne-Buechner spectrometer (Danfysik), (3) position sensitive detector (Canberra), (4) view on target inside the chamber, (7) residual gas analyser (Leybold Inficon), (8) evaporators (EFM3, Omicron), (9) sputter gun (IG5, Oxford Applied Research), and (10) RHEED gun (EK-35-R, Staib Instruments).

$\sqrt{3}\times\sqrt{3}$R30 reconstruction. Under these conditions the Au atoms are believed to form a layer on top of the Si bulk [10]. The Ta samples were prepared by *in situ* evaporation at room temperature onto a Si sample etched in HF before insertion into the UHV chamber. The coverage was held below 0.1 monolayer to prevent island formation.

The CSDs obtained for Li, C, and Cl ions are shown in Figs. 3 and 4. All CSDs were taken at a scattering angle of 35.5°. As a first step we examined in which way the presence of the surface influences the CSD. Fig 3 shows results for the case

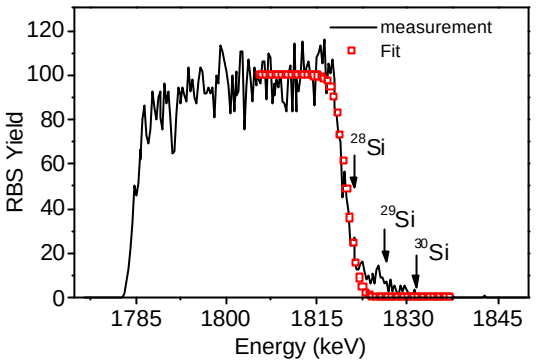

Fig. 2: Spectrometer resolution as obtained by scattering of 2 MeV Li^+ ions off a clean Si (111) surface. Scattering angle $\theta = 35.5°$, exit angle $\alpha_2 = 2°$, energy width DE = 3.8 keV, resulting depth resolution 2.4 Å. The arrows mark the position of the high energy edges of ^{28}Si (1821 keV), ^{29}Si (1827 keV), and ^{30}Si (1832 keV).

of 3 MeV Li^{2+} ions scattered from Au surface atoms. In equilibrium there are no Li^+ ions at this energy and the ratio $\gamma = Y(Li^{2+})/Y(Li^{3+})$, where $Y(Li^{2+})$ and $Y(Li^{3+})$ denote the yield of Li^{2+} and Li^{3+} ions, respectively, is about 0.5 [11]. The charge state ratio is displayed in Fig. 3(a) as obtained after a single collision for different angles of incidence. Here the angle of incidence is defined with respect to the surface. In the region of small angles of incidence γ remains almost constant at a value of 1.1, whereas for small angles of emergence it approaches the equilibrium value. The most obvious interpretation for this behavior is an interaction of the emerging ions with surface electrons. This observation is corroborated by the angular dependence of the energy of the emerging Li^{2+} ions shown in Fig. 3(b). For intermediate angles α_1 around the symmetric scattering condition, the energy is nearly constant within an accuracy of 1 keV. However, at small angles of incidence as well as at small angles of emergence the energy decreases by up to 6 keV. Assuming this energy loss to be caused by a thin layer of electrons, the curve was fitted by the function $\Delta E = E_0 - a/\sin(\alpha_1) - b/\sin(35.5°-\alpha_1)$. The result is shown by the thin curve in Fig. 3(b). Within the experimental errors the agreement of fitted and measured data points is reasonable. For the fit parameters a = 0.17 keV and b = 0.11 keV are obtained. Comparing these values to the stopping power of Li ions in Au, which is about 1.1 keV/nm, the observed energy loss corresponds to an 'electron layer' thickness of 1-1.5 Å. As the latter is below the typical thickness of a monolayer, it is concluded that both the energy loss and

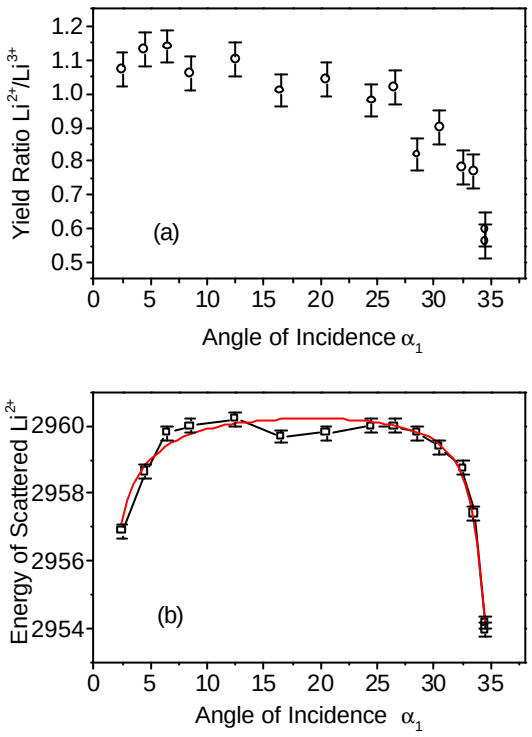

Fig. 3: (a) Yield ratio γ of Li^{2+}/Li^{3+}, and (b) energy of 3 MeV Li^{2+} ions, scattered to 35.5° from a monolayer of Au, as function of the angle of incidence α_1. The angle of incidence is defined with respect to the surface.

the decrease of the fraction of Li^{2+} ions as compared to Li^{3+} ions is due to surface electrons that extend to about 1 Å outside the bulk. As a consequence the CSDs of single collision processes can only be expected to show up at larger angles of emergence.

As a second step the CSDs for C and Cl ions are compared at velocities (in Bohr units) of 1.42 (0.6 MeV), 2.59 (2 MeV), and 3.67 (4 MeV) for C and 1.15 (1.221 MeV) for Cl, respectively. All ions were scattered at sub-monolayers of Ta. Fig. 4 shows the corresponding equilibrium as well as single collision CSDs. In most cases the CSD for a single collision is shifted to higher charge states as compared to the equilibrium CSD. The difference is most prominent for Cl, while it is only a few tens of a charge unit for C at 2 MeV and 0.6 MeV. For C at 4 MeV there is no observable difference. In all cases the incoming ion has lost a considerable amount of its electrons during the collision. The findings show similar trends as Refs. [6,7]. In [7] the highest observed charge state for Ar was $q = 9+$, which is consistent with the highest charge state of $q = 8+$ for Cl that carries one electron less than Ar. In the same way the similarity of equilibrium and single-collision CSDs in the case of C is consistent with the results of Boerma et al. [6]. However, as the examples of Cl and of Ref. [7] show, this similarity might be only fortuitous. Comparing C and Cl moving at comparable velocities, it is found that C shows a trend to produce higher charge states in a single collision than in equilibrium as well. The observed difference is however much smaller than in the case of Cl. Thus the assumption that charge state equilibrium is attained in a single collision is not general. It is still open, if there is a general trend that the difference in equlibrium and single-collision CSDs increases with increasing nuclear charge *Z*.

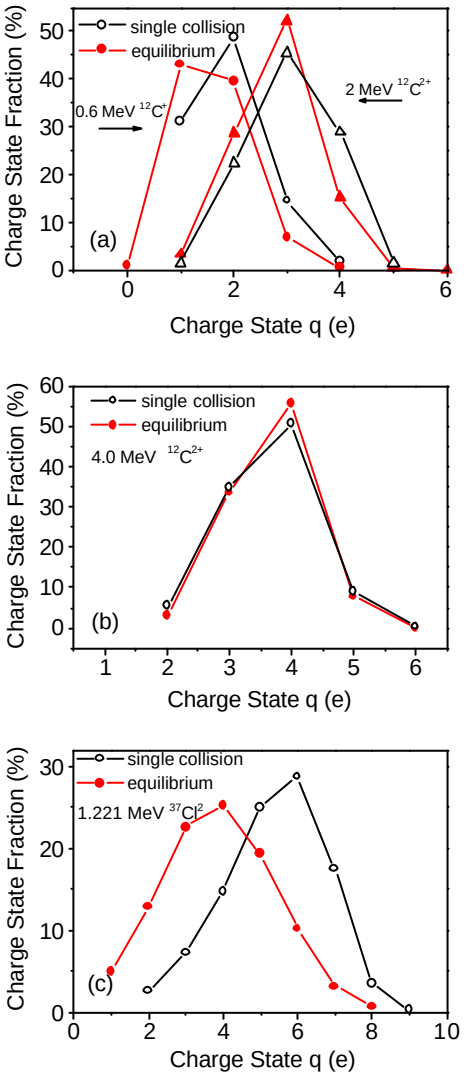

Fig. 4: CSD for (a), (b) C and (c) Cl ions after a single collision (open symbols) with Ta atoms and in equilibrium (full symbols). Indicated energies refer to the energy of the incoming ion. The equilibrium data were taken from [4,5].

In conclusion a magnetic spectrometer with a depth resolution of a monolayer was employed to study the charge state distribution after surface scattering. The observed charge state distributions

are in contradiction with the assumption that an equilibrium is obtained in a single collision.

Acknowledgements

The authors thank Dr. O. Kruse for his valuable contributions to the present work.

References

[1] W.M. Arnoldbik, Z.X. Jiang, P.F.A. Alkemade, D.O. Boerma, Nucl. Instr. Meth. B **136-138** (1998) 540

[2] K. Shima et al., Atomic Data and Nuclear Data Tables, Vol. **51**, No. 2 (1992) 174

[3] K. Shima, T. Mikumo, H.Tawara, Atomic Data and Nuclear Data Tables, Vol. **34**, No. 3 (1986) 358

[4] F. Sols, F. Flores, Phys. Rev. B **30** (1984) 4878

[5] M. Meron, B. Rosner, Phys. Rev. A **30** (1984) 132

[6] D.O. Boerma, W.M. Arnoldbik, N.M. Kabachnik, V.A. Khodyrev, Nucl. Instr. Meth. B **122** (1997) 181

[7] S. Jamecsny, PhD Thesis, Max-Planck-Institut für Metallforschung, Stuttgart, 1998

[8] K. Kimura, H. Ohtsuka, M. Mannami, Phys. Rev. Lett. **68** (1992) 3797

[9] C.P. Browne, W.W. Buechner, Rev. Sci. Instr. **27** (1956) 899

[10] R. Plass, L.D. Marks, Surf. Sci. **380** (1997) 497, and references therein

[11] W. Jiang, R. Grötzschel, W. Pilz, B. Schmidt, W. Möller, Phys. Rev. B **59** (1999) 226

Growth of Low Stress Cubic Boron Nitride Films by Simultaneous Medium Energy Implantation

C. Fitz, A. Kolitsch and W. Fukarek

Cubic boron nitride (cBN) has a hardness of 60 GPa and is next to diamond the hardest material known. In contrast to diamond it does not react with metals and is chemically stable against oxidation even at elevated temperatures. Thus, cBN is a very promising material for tribological applications. The reason that cBN films are not commercially used is the high intrinsic stress S_{cBN} (typical 10-20 GPa) developed in standard growth processes. It causes the films to crack and to peel off from the substrate if a critical thickness of some 100 nm is exceeded. Ion irradiation (Ar^+, Kr^+, and Xe^+) performed at room temperature with energies E_{ion} = 35 keV to 1.1 MeV can be employed to relax the stress in cBN films [1-3]. However, one has to be aware that the cBN film is damaged during the ion irradiation. Thus, the fluence, or more specifically the displacements per atom (dpa), must be limited, in order to find the best compromise between stress relaxation and cBN destruction. Recently, using a complex process of sputter cleaning, sequential growth, ion induced stress relaxation, and annealing, the deposition of thick (1.3 µm), low stress (0.5 GPa) cBN films has been demonstrated [4]. It has been shown that also argon post implantations performed at 340 °C can be utilized to reduce stress [5]. Compared to implantations at room temperature, less disorder and damage are created for the same stress relaxation. Consequently, it should be possible to deposit stress relieved, thick cBN films in a single process by simultaneous medium energy (35-70 keV) implantation of argon ions during growth. Such a technique of growth and simultaneous medium ion energy irradiation has been proposed by Ullmann [6], but to our knowledge it has not been realized up to now.

The aim of this work is to demonstrate the growth of low stress cBN films under simultaneous medium energy irradiation. Argon as well as nitrogen ions have been used for implantation, to study if the process of stress relief depends on the ion mass. The evolution of stress has been controlled by means of *in-situ* cantilever curvature measurements during deposition. The BN phases present in the film have been characterised *ex-situ* by polarised infrared reflection spectroscopy (PIRR). The stoichiometry was investigated by elastic recoil detection analysis (ERDA).

The films studied in this work were prepared at 340 °C by ion beam assisted deposition (IBAD) on silicon cantilevers. Elemental boron was deposited from an electron beam evaporator and irradiated with a mixture of argon and nitrogen ions, at an ion energy of 500 eV and an ion (argon plus nitrogen) to neutral (boron) arrival ratio of I/N = 1.8. The base and the working pressure were 1 x 10^{-5} mbar and 2 x 10^{-4} mbar, respectively. The simultaneous medium energy implantations were performed with single charged argon (Ar^+) or nitrogen (N^+) ions provided by a commercial high current ion implanter DANFYSIK 1090 [7], at an angle of incidence of 34°, with respect to the surface normal. In order to compare the implantations and their effects on stress, the ion energies ($E(Ar^+)$ = 70 keV, $E(N^+)$ = 35 keV) and the ion current densities ($J(Ar^+)$ = 5.32 x 10^{13} ions/cm^{2}min, $J(N^+)$ = 1.49 x 10^{14} ions/cm^{2}min), were chosen to create identical displacement rates in comparable depth regions.

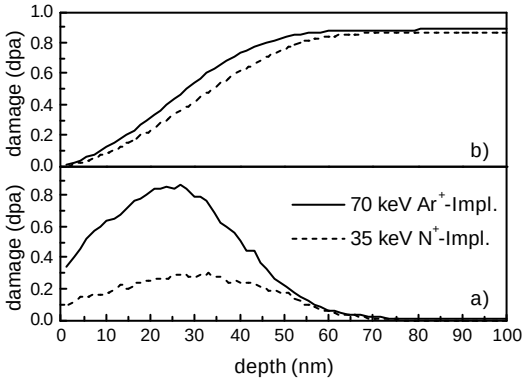

Fig. 1: Calculated damage depth profiles: a) Displacements created by a 1 x 10^{15} ions/cm^2 post implantation into a cBN film, b) Damage depth profiles in the growing film created by simultaneous growth and medium energy implantation; for details, see text.

Fig. 1(a) shows the damage depth profiles calculated with the program SRIM-2000.39 [8] for a fluence of 1 x 10^{15} ions/cm^2 in cBN (ρ = 3.5 g/cm^3). The displacements are produced for both ion species in the same depth region. In Fig. 1(b) the resulting damage profile (stationary state) created during growth and simultaneous implantation is plotted versus the film thickness. For both implantations a final number of 0.88 dpa is created during growth and simultaneous implantation. For

the calculation of the damage profiles the ion current densities and the film growth rates obtained during the experiments were used. The growth rates were derived from reflectivity data recorded during film growth and are 1.9 nm/min in the case of argon and 2.1 nm/min for nitrogen implantations, respectively. From the results obtained for Ar^+ postimplantations performed at 340 °C [5] and taking into account the displacement depth profile, it is expected that the stress in the simultaneously irradiated films is reduced to ≈ -1.5 GPa, whereas cBN should be not transformed into sp^2-bonded boron nitride.

An optical method [9] based on the cantilever bending principle has been used to derive the force per unit width (FPUW) of the film *in-situ*. The characteristic FPUW profile, which builds up during growth [10], has been used to detect the critical time (t_{crit}) till the nucleation of cBN is completed by coalescence of cBN grains and a pure cBN layer begins to grow. Information on the evolution of the averaged stress S in cBN has been derived as well. The averaged (global) stress *S* in a film of the thickness d_f is calculated by

$$S = \frac{FPUW}{d_f}.$$

Fig. 2 shows the FPUW recorded during growth and argon irradiation. A compressive stress of -8 GPa is derived for the cBN film grown between t_{crit} = 20 min and the start of the argon implantation at 25 min. The implantation is started when the coalescence of cBN is completed, thus the nucleation process is not disturbed. Because the implantation profile does not approach the film/substrate interface, no damage in the silicon substrate is created which could disturb the cantilever curvature measurement by plastic flow. In a first step the film is irradiated with an ion current density of $J(Ar^+)$ = 1.99 x 10^{13} ions/cm^{2}min. The FPUW decreases immediately. However, during further growth the stress is only reduced from -8 to -6.2 GPa (see the slope up to 30 min). After 30 min the ion current density is increased to $J(Ar^+)$ = 5.32 x 10^{13} ions/cm^{2}min. Subsequently the film grows till the end of deposition with an reduced stress of only -1.4 GPa. This is one of the lowest values ever reported for a cBN film. The growth of nearly pure cBN phase is confirmed in the PIRR spectra recorded *ex-situ* and shown in Fig. 3.

The stoichiometry of the cBN film irradiated with argon ions was analyzed with ERDA. A B/N ratio of 1.13 was measured (51 at% B, 45.3 at% N, 2 at% H, 1.7 at% O). This B/N ratio is significantly higher than the values obtained from cBN films made with the same deposition parameters but without additional argon ion implantation (typical B/N = 1.02 ± 0.02), indicating some ion induced release of nitrogen due to the medium-energy ion implantation.

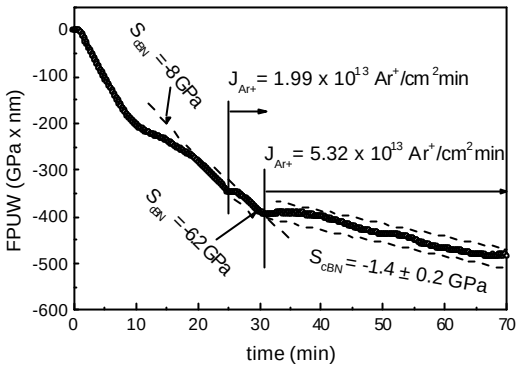

Fig. 2: FPUW recorded during the growth of a cBN film. The averaged compressive stress in cBN is reduced from -8 GPa to -1.4 GPa by simultaneous argon implantation.

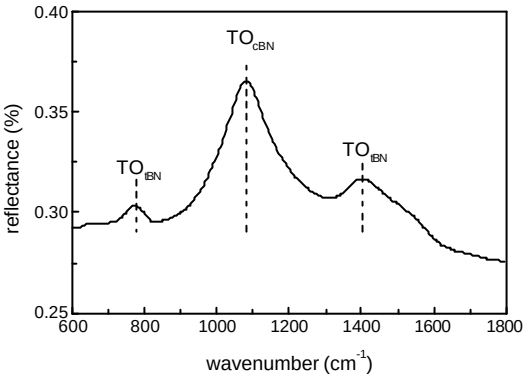

Fig. 3: PIRR-spectra of the cBN film shown in Fig. 2. The main peak at 1074 cm^{-1} is the transversal optical (TO) cBN phonon. The phonons at 780 cm^{-1} and 1400 cm^{-1} are the bending and stretching mode of turbostratic boron nitride (tBN), which grows next to the substrate till cBN grains start to nucleate and to coalescence.

The FPUW recorded during cBN growth and simultaneous N^+ irradiation is shown in Fig. 4. The film is grown without additional N^+ irradiation until the coalescence of cBN is completed. As expected, the evolution of the FPUW corresponds in this period to the argon experiment. The stress in the film prior to the implantation is also –8 GPa. After 28 min the N^+ implantation is started with the maximum ion current density $J(N^+)$ = 1.49 x 10^{14} ions/cm^{2}min. The FPUW changes immediately due to the stress relaxation within the ion collision cascades. The change in the beginning is larger compared to the argon implantation because the nitrogen implantation was started with the maximum ion current density. However, during further growth an equilibrium builds up between

the FPUW relieved by the collision cascades and the FPUW added from the growing film (see Fig. 4 between 28 and 40 min). Then the cBN film grows with a significantly relieved stress of -1.3 GPa only.

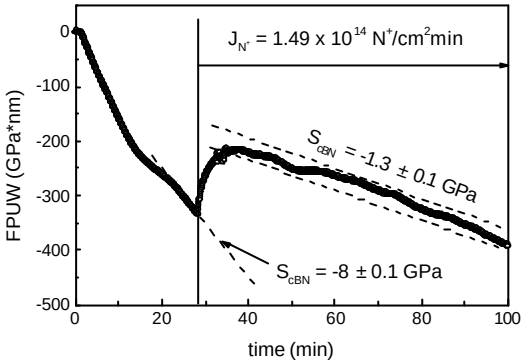

Fig. 4: FPUW recorded during the growth of a cBN film. The averaged compressive stress in cBN is reduced from -8 GPa to -1.3 GPa by simultaneous nitrogen implantation.

Comparing both experiments it must be emphasized that the stress in the cBN films is relieved by the same amount (≈6.6 GPa) for argon and nitrogen implantation, both resulting in the same number of displacements within the film (0.88 dpa). cBN is not transformed to tBN under this implantation conditions.

Fig. 5 shows the elemental depth profiles obtained by ERDA for the film irradiated with nitrogen. As can be seen the film is perfectly stoichiometric (B/N = 1.02) in contrast with the film obtained with additional argon implantation. This suggests that during nitrogen implantation boron atoms with open bonds can react with nitrogen ions supplied during the irradiation. Energetically favorable BN bonds are formed instead of BB bonds.

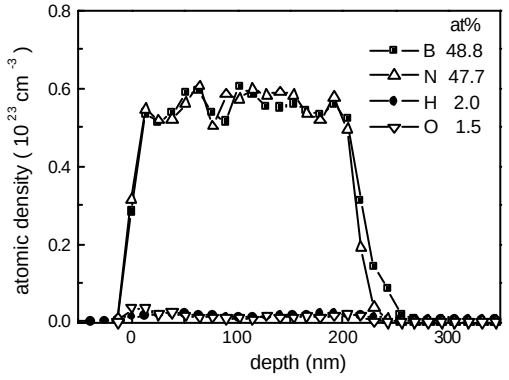

Fig. 5: Elemental depth profiles obtained by ERDA in the cBN film irradiated with nitrogen.

Summarizing the experimental results, the growth of low stress (≈ -1.4 GPa) cBN films has been achieved under simultaneous medium-energy ion irradiation, with a stationary damage level of 0.88 dpa. It has been shown that the stress relieved during argon and nitrogen implantation is similar, provided that the same number of displacements are created during the irradiation. ERDA shows that the cBN film becomes boron rich under argon irradiation. It is not clear how the excess boron atoms are bond after the outdiffusion of nitrogen. Boron precipitates, e.g. at grain boundaries, may be partly responsible for the observed stress relief similar to carbon in cBN films [11]. The stoichiometry, however, is not changed (B/N = 1.02) by the nitrogen implantation. Because the stress relief is the same during the argon and nitrogen implantations which create 0.88 dpa in the film, the major reason for the stress relief should be atomic displacements, rather than grain boundary effects.

The advantage of the present technique is that the depositions can be done under optimum deposition parameters, what causes usually a high stress, but guarantees reproducible film depositions. No extreme conditions, like very high temperatures (T ≈ 1000 °C) [12], are needed to grow low stress cBN films. Therefore the growth of thick cBN films on materials which are sensitive to high temperature (like various hard metals) should be possible. The maximum cBN film thickness is not limited by the stress. For the experimental system used here, the boron evaporation rate becomes unstable after some hours deposition time, when too much boron is lost from the boron crucible. Therefore only several 100 nm thick films have been grown up to now, but the growth of µm thick cBN films should be only a technical task.

Acknowledgements

The authors gratefully acknowledge U. Kreissig for ERDA measurements and G. Winkler for operating the implanter. The financial support of this work by the Deutsche Forschungsgemeinschaft (No. MO 297/6-1) under the auspices of the tri-national D-A-CH cooperation in the synthesis of superhard materials is gratefully acknowledged.

References

[1] J. Ullmann, E.E. Baglin, A.J. Kellock, J. Appl. Phys. **83** (1998) 2980

[2] P. Widmayer, P. Ziemann, S. Ulrich, H. Ehrhardt, Diam. Relat. Mater. **6** (1997) 621

[3] C. Fitz, W. Fukarek, A. Kolitsch, W. Möller, Surf. Coat. Technol. **128-129** (2000) 292

[4] H.-G. Boyen, P. Widmayer, D. Schwertberger, N. Deyneka, P. Ziemann, Appl. Phys. Lett. **76** (2000) 709

[5] C. Fitz, W. Fukarek, submitted to Appl. Phys. Lett.

[6] J. Ullmann, Thin Solid Films **328** (1998) 43

[7] High current ion implanter series-1090, DANFYSIK A/S, Mollehaven 31, DK-4040 Jyllinge, Denmark

[8] J.F. Ziegler, J.P. Biersack, U. Littmark, The Stopping and Range of Ions in Solids, Pergamon Press, New York, 1985

[9] C. Fitz, W. Fukarek, A. Kolitsch, W. Möller, Surf. Coat. Technol. **128-129** (2000) 474

[10] W. Fukarek, Proc. 7 th Int. Symp. Trends and Applications of Thin Films (TATF´2000), Nancy, France, 2000, 1

[11] S. Ulrich, H. Ehrhardt, T. Theel, J. Schwan, S. Westermeyer, M. Scheib, P. Becker, H. Oechsner, G. Dollinger, A. Bergmaier, Diam. Relat. Mater. **7** (1998) 839

[12] S. Matsumoto, W. Zhang, Jpn. J. Appl. Phys. **39** (2000) L442

Atomic-Scale Calculations for Steady-State Growth and Elastic Properties of Ion-Deposited Tetrahedral Amorphous Carbon Films

A.Yu. Belov, H.U. Jäger and K. Albe*

** Technische Universität Darmstadt, Fachbereich Material- und Geowissenschaften, Petersenstr. 23, D-64287 Darmstadt*

There is presently a considerable research interest in the formation of diamondlike tetrahedral amorphous carbon (ta-C) films because of their smoothness, transparency, hardness, low friction and low electron affinity. The material has a mass density close to diamond and a high fraction of tetrahedrally coordinated carbon atoms (80%-90%). Experimentally, such films have been successfully deposited by mass selected ion beams, filtered vacuum arc or laser ablation of graphite.

It is an attractive goal to understand the growth of ta-C from an atomistic perspective. The atomistic simulations reported in the past deal mostly with structural properties of ta-C, but only a few papers have focused on the deposition process itself. Three-dimensional molecular dynamics simulations of the deposition of unhydrogenated carbon films were performed by Kaukonen and Nieminen [1], and Uhlmann *et al.* [2]. We performed such investigations too, but contrary to Refs. [1,2] more than 10^3 carbon atom impacts on {111} diamond were simulated, so that steady-state film properties could be computed and analyzed [3,4].

The computationally efficient analytical C-C potentials of Tersoff [5] and Brenner [6] were used. For the Tersoff potential, film growth is computed with sp^3 fractions of approximately half of the experimentally observed values (~34%). For the more refined hydrocarbon potentials of Brenner the fraction of tetrahedrally coordinated atoms in the film is much too low, even if a density close to diamond is obtained. It can be shown that the sp^3 contents calculated with Tersoff's potential are an artifact related to the overbinding of specific bonding configurations between three- and four-fold coordinated sites. On the other hand, the range for the binding orbitals, represented by the cutoff-function, proves to be too short in Brenner's parametrization. If increased C-C interaction cutoff values are chosen, a distinct improvement is achieved in modeling the sp^3 content of deposited ta-C films.

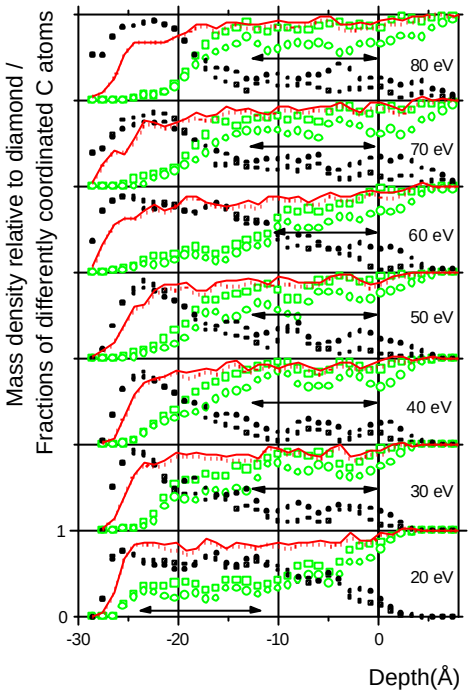

Fig. 1: Mass densities relative to diamond (solid and dashed lines) and fractions of sp^3 (? , ?) and sp^2 (¦ , ?) bonded C atoms in films simulated for C^+ ion beam depositions with different energies. Two depth profiles are given for each quantity. They differ in inclusion (solid lines, ? , ¦) or neglect (dashed lines, ? , ?) of the fivefold coordinated atoms occuring also in the computed atomic network. The horizontal arrows mark the inner film regions which were used to calculate the average film properties and their root mean square deviations plotted in Fig. 2.

Using Brenner's hydrocarbon potential (parameter set I of Ref. [6]) and such increased C-C interaction cutoffs [3], the results presented in Fig. 1 were obtained. The Fig. shows depth profiles for the mass density normalized to diamond, and for the fractions of the sp^3 and sp^2 hybridized carbon atoms. In every simulated film, a depth region with a width of about 11 Å exists where not only the density but also the other film properties are nearly

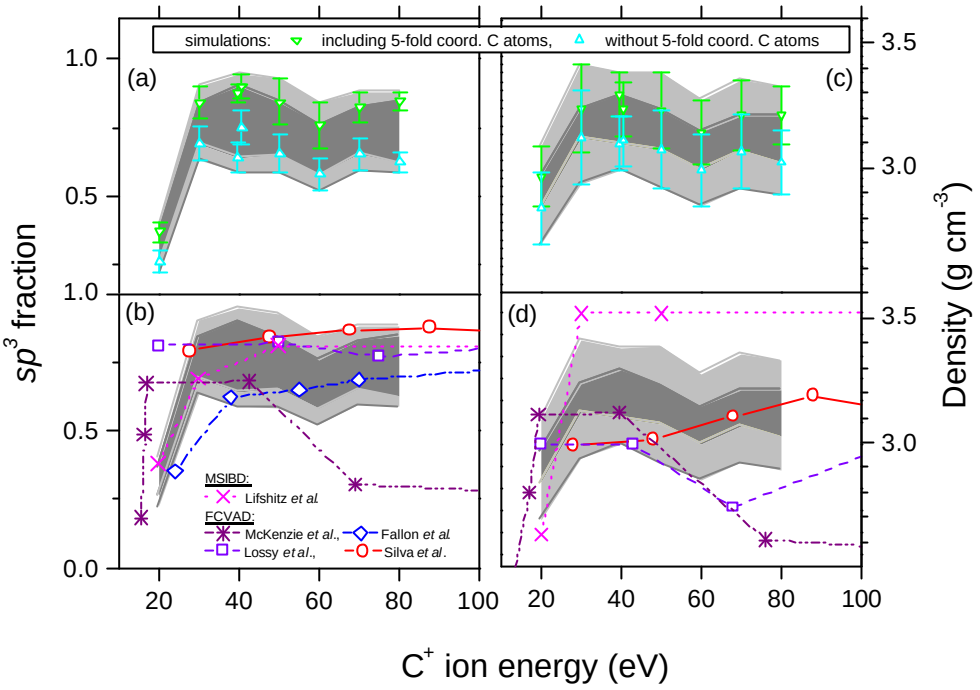

Fig. 2: The variation of (a), (b) the C sp^3 bonding and (c), (d) density in ta-C films as a function of C^+ ion energy. The parts (a) and (b) of the Fig. present the upper and lower limits, together with their standard deviations, as concluded from the simulated depth profiles shown in Fig. 1. The shadowed areas visualize these model predictions, they are compared to experimental results in parts (c) and (d) of the Fig. The data from the literature refer to mass selected ion beam deposition (MSIBD) and filtered cathodic vacuum arc deposition (FCVAD). Practically all the other E = 20 – 80 eV data which were reported in the literature, but not not included in part (b) of this Fig., would ly within our shadowed area.

constant. These depth regions are marked in Fig. 1 by horizontal arrows, and are thought to have the properties achieved in the case of steady-state film growth. For the beam energies E= 30 eV, ta-C structures with a dominant sp^3 content are formed close to the diamond {111} seed. In qualitative agreement with experimental data, our ta-C films simulated for E = 30 eV are characterized by a deep sp^3-rich dense layer below a porous sp^2-rich surface layer of lower density. The thickness of the surface layer increases with ion energy. For E = 20 eV, however, rather different film properties are found. The steady-state film region has a graphitic, sp^2-rich structure which extends up to the immediate vicinity of the surface. Consequently a broader transition region is seen in Fig. 1 between the diamond substrate and this amorphous carbon phase. The depth profiles in the inner film regions, as shown in Fig. 1, were used to calculate average values and standard deviations for the film properties. In Fig. 2, the resulting upper and lower limits for the sp^3 content and the mass density are plotted versus C^+ ion energy. The sp^3 content of the ta-C films deposited with energies E = 30-80 eV is calculated to vary between 52% and 95% (light-gray shadowed area of Fig. 2(a)). Although our predictions are still somewhat inprecise, they are in line with all recently measured sp^3 fractions (Fig. 2(b)). Only the early filtered-arc deposition investigations published by McKenzie *et al.* in 1991 yielded contradictory sp^3 data.

Atomic-scale calculations allow not only to understand the growth mechanisms of ta-C. One can also investigate its properties, using structural models of the films grown by a realistic computer simulation. This primarily concerns mechanical properties, related to interatomic interactions in amorphous C. An advantage of the molecular dynamics method is in its ability to generate models of nonequilibrium *as-deposited* ta-C films, rather than annealed minimum energy structures. A general problem with ta-C is that the as-deposited ta-C films with highest sp^3 content possess a high internal stress which limits the maximum thickness that can be deposited. This bulk stress is an intrinsic part of the growth mechanism: the penetration of C^+ ions beneath the exposed surface of the substrate during ion-beam deposition induces the lateral compression σ, promoting the formation of ta-C. The internal stress accompanies the growth of the ta-C film, increasing its elastic energy and resulting in delamination at the film/substrate interface.

Elastic properties of ta-C also correlate with the sp^3 content and thereby reflect the energetics of ta-C growth. We computed both bulk stress and elastic constants, using slices from the region of

steady-state growth, where structural properties are nearly uniform. Repeating a slice along the film growth direction, one creates a 3D periodic structure with a large *elementary cell* consisting of 500-2000 atoms. To reproduce the state of plane stress inherent to thin films, the normal dimension of the cell is optimised to eliminate the normal stress, whereas the lateral dimensions remain fixed to model amorphous film bonding to a crystalline substrate and thereby the lateral bulk stress. The calculations of elastic constants and bulk stress are based on the method of homogeneous deformations, modified in Ref. [7] to account for the inhomogeneous, or inner, displacements of atoms, which happen in complex lattices upon application of uniform strains.

The bulk stress in the simulated amorphous carbon films is found to be compressive for the whole set of investigated ion energies (E = 20-80 eV). For the two potentials of Brenner the stress behavior versus ion energy is shown in Fig. 3, displaying an average $\sigma = (\sigma_1 + \sigma_2)/2$ of two lateral stress components. The following important conclusions can be drawn from Fig. 3. First, in the graphitic structure with 65% of sp^2 content (E = 20 eV), the bulk stress is compressive rather than tensile. The transition from the graphitic-like carbon to ta-C occurs at a compressive stress of about 12 GPa for Brenner potential I and 17 GPa for Brenner potential II, if one uses an average of the bulk stresses at E = 20 eV and E = 30 eV as an estimate for the threshold stress. These values are in agreement with an experimental stress threshold of 13 GPa, above which a strong increase in the density of amorphous carbon films was observed [8].

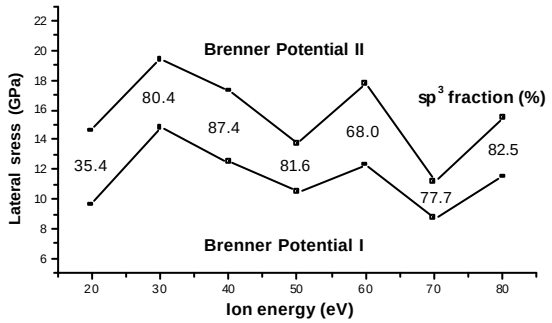

Fig. 3: Dependence of the bulk compressive stress in amorphous carbon films on ion energy. The stress was computed using the two potential functions of Brenner with increased cut-offs.

Secondly, for E = 30 eV the stress mostly follows variations of the sp^3 fraction (see Fig.2), rather than the ion energy itself. Except for the E = 60 eV results, related to the small size of the steady-state region and large fluctuations of the sp^3 content [4], it decreases as sp^3 decreases. In order to estimate the influence of structural fluctuations on the stress, computations were performed for a set of slices from one film deposited at E = 40 eV.

Table 1

Bulk stress variations with sp^3 content in a ta-C film (E = 40 eV, Brenner potential I with increased cut-offs)

Slice	1	2	3	4
σ(Gpa)	-12.5	-11.5	-11.5	-15.2
Sp^3	87.4	84.0	82.4	76.6

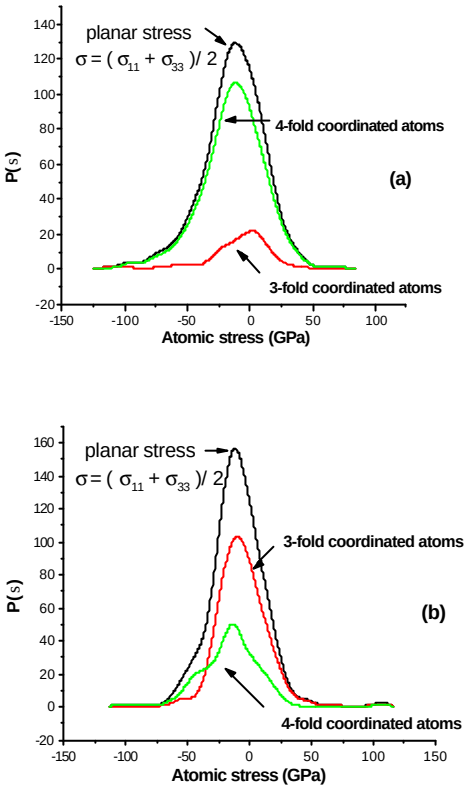

Fig. 4: Distribution of lateral atomic stresses in a ta-C film (a) and in a graphitic film (b). The ta-C film was deposited with ion energy 40 eV, the graphitic film with ion energy 20 eV. The stresses were computed for the Brenner potential I with increased cut-offs.

The slices differ in the sp^3 content. The results of Table I demonstrate a considerable influence of structural inhomogeneities on the bulk stress, which can be essentially nonuniform in ta-C films. The local variations of the bulk stress from the average value considerably increase as the local content of sp^2 bonded atoms increases.

The atomic-level stress σ_I (i) = $dE(i)/V_i d\eta_I$, representing individual contributions of atoms to

the average macroscopic stress and indicating a response of atomic energies to the strain η_l, is the next important characteristic of the nonequilibrium amorphous C structures. The distributions of lateral local stresses in a ta-C film (with average stress -12.5 GPa) as well in a graphitic film (with average stress -9.6 GPa) are shown in Fig. 4. In both cases the distribution function has a peak at higher compressive stresses than the average values, namely at -15 GPa in the ta-C film and at -13 GPa in the graphitic film. The distribution of atomic stresses in the compressed ta-C film agrees with the result [9] for stress-free minimum energy structures: the sp^2 atoms are mostly under local tensile stresses, while sp^3 atoms are under local compression. However, the behavior of atomic stresses in the stressed graphitic film is very different from that found in [9] for the stress-free case, where the tensile character of local stresses at sp^2 sites was found to be independent on sp^3 content. According to Fig. 4(b), this is not the case for an as-grown graphitic structure, where both sp^2 and sp^3 atoms are under local compression.

Elastic constants in the as-deposited ta-C films were calculated using the Tersoff potential [5], since it reproduces the elastic constants of diamond better than the potentials of Brenner. Fig. 5 displays the Lagrangian elastic constants, which depend on the average stress in the amorphous films. Both the Young's modulus and the bulk modulus follow the sp^3 content variation and increase as the sp^3 fraction increases, but they are still lower than diamond values. The results of Fig. 5 agree quite reasonably with experimentally established rules relating the Young's modulus of ta-C films with the sp^3 fraction [10].

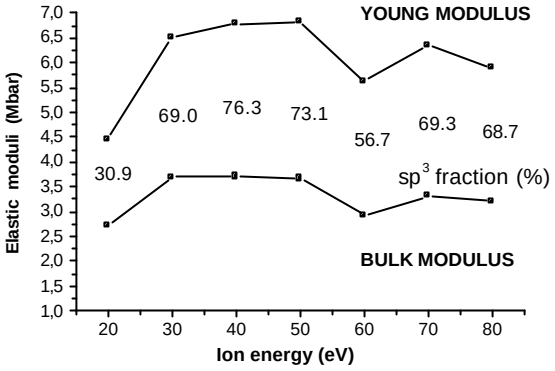

Fig. 5: Dependence of elastic constants in stressed amorphous carbon films on the ion energy and sp^3 content (Tersoff potential [5]).

Acknowledgements

One of the authors (A.Yu. B.) would like to acknowledge the financial support by Deutsche Forschungsgemeinschaft (Contract No. MO 297/9-2).

References

[1] H. P. Kaukonen, R. M. Nieminen, Phys. Rev. Lett. **68** (1992) 620; Phys. Rev. B **61** (2000) 2806

[2] S. Uhlmann, Th. Frauenheim, Y. Lifshitz, Phys. Rev. Lett. **81** (1998) 641

[3] H.U. Jäger, K. Albe, J. Appl. Phys. **88** (2000) 1129

[4] A. Yu. Belov, H.U. Jäger, to be published in Mat. Res. Soc. Symp. Proc. **648**

[5] J. Tersoff, Phys. Rev. B **39** (1989) 5566; **41** (1990) 3248

[6] D. W. Brenner, Phys. Rev. B **42** (1990) 9458; **46** (1992) 1948

[7] J. W. Martin, J. Phys. C: Solid State Phys. **8** (1975) 2858

[8] J. Schwan, S. Ulrich, T. Theel, H. Roth, H. Ehrhardt, P.Becker, S.P.R. Silva, J. Appl. Phys. **82** (1997) 6024

[9] P.C. Kelires, Phys. Rev. Lett. **73** (1994) 2460

[10] D. Schneider, T. Schwarz, H.J. Scheibe, M. Panzner, Thin Solid Films **295** (1997) 107

Cell Culture Investigation of Implant Materials

M.F. Maitz and M.T. Pham

Foreign materials are widely used in medicine as implants and devices. For the contact with the body they must fulfil the requirements of biocompatibility and biofunctionality. "Biocompatibility" has a very broad definition as the acceptance of an artificial implant by the surrounding tissue and the body as a whole. The "biofunctionality" of a material is related to its application and its function in the body.

Biomaterials testing therefore must go beyond traditional testing procedures of materials research, such as elasticity, surface hardness, roughness, surface chemistry, etc. The interaction of a material with vital cells has to be investigated. Special models have to be set up that resemble the *in situ* situation as closely as necessary to obtain the relevant information about cell growth, metabolism and differentiation. In general as a first step this is done by cell culture investigations with cells specific for the site of implantation. *In vivo* animal experiments are done in a very late state of biomaterials testing.

Hydroxyapatite (HA; formula: $3\ Ca_3[PO_4]_2 \cdot Ca[OH]_2$) is the main inorganic component of the bone. Acceptance and integration of synthetic HA in the bone has been proven to be very high. A firmly adherent coating of osseointegrated implants with this mineral therefore is desired for a stable integration of the implant into the bone. Deposition of HA out of a simulated body fluid onto surfaces of titanium has been shown to be possible after activation of the substrate by the implantation of sodium ions [1]. Deposition of HA after Na implantation is stimulated by the same mechanism as after etching with NaOH (10 M) at high temperature [2].

Deposition of calcium phosphate out of a solution may be in form of amorphous tricalciumphosphate, crystalline hydroxyapatite or a mixture of both with different biological activity and stability in the body. Direct growth of cells on a Na implanted, activated surface, without previous deposition of hydroxyapatite can be seen as an alternative, as it should enhance the cell-induced deposition. Implantation of sodium ions also causes a drastic shift of the pH at the surface, what may have impact on adjacent cells. Biological investigation of this surface treatment is therefore necessary.

Commercially pure titanium was cut into small samples and polished to 1 – 3 µm roughness. One set of samples was implanted with sodium ions (3.2×10^{17} cm^{-2}). As reference unimplanted samples were used and samples after NaOH etching [2]. Prior to use samples were steam sterilized (121 °C, 2 bar, 20 min) and pH was equilibrated for 30 min in phosphate buffered saline (PBS, pH 7.4).

For cell culture the human osteogenic sarcoma cell line SAOS-2 was chosen. This is a highly differentiated, stable and non transfected cell line, that can behave like osteoblasts. In presence of ascorbic acid (50 µg/mL) and β-glycerophosphate (β-GP, 3 mM), it produces a calcified extracellular matrix [3].

SAOS-2 cells were seeded out at a density of 10^5 cells/cm^2 in Alpha Modified Minimal Essential Medium (α-MEM) with 15% fetal bovine serum and kept in humidified air with 5% CO_2 at 37 °C. From day three the medium was supplemented with ascorbic acid and β-GP. The medium was exchanged every second or third day. Samples were taken for investigation after one day, 2 weeks and 4 weeks.

The cells in α-MEM medium after two weeks form a confluent cell layer on every sample, but the growth pattern of the individual cell and the culture as a whole is different. There is a very homogenous covering of the surface of untreated titanium, cells have a uniform shape without any special orientation. On implanted titanium growth is in a trabecular pattern with highly covered streets and less covered areas. The cell shape is highly polarized and oriented. On NaOH etched titanium cells grow very irregularly with uncovered areas and cracks in the cell layer. Cells are high and do not spread well on the surface (Fig 1). This pattern for the three types of samples is also persistent after 4 weeks.

There is no spontaneous deposition of calcium phosphate out of α-MEM medium on untreated or Na implanted titanium during the 4 weeks, whereas on NaOH etched titanium there is a thin, discontinuous deposition (Fig. 2). Energy dispersive X-ray (EDX) spectra of this layer on NaOH etched titanium show Ca and P with Ca : P > 2 : 1, indicating that it is mainly amor-

phous tricalciumphosphate instead of hydroxyapatite.

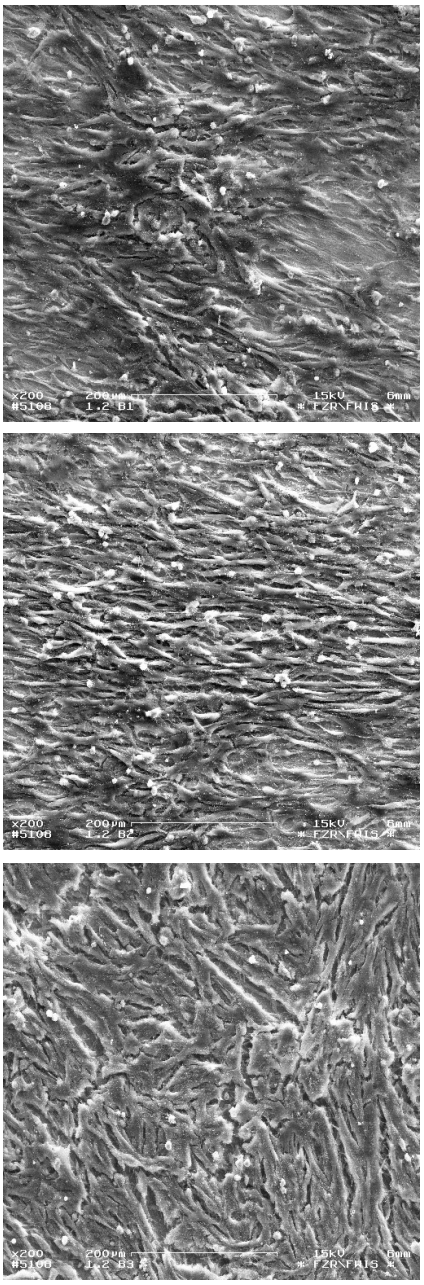

Fig. 1: Scanning electron microscopy images of SAOS-2 cell culture on Ti samples after 14 days. Top – untreated titanium, middle – Ti Na-implanted, bottom – Ti NaOH-etched.

In cell cultures grown on non treated titanium and on Na implanted titanium EDX spectra mainly show organic phosphates and only traces of calciumphosphates (Ca : P < 1), whereas in cell cultures on NaOH etched titanium calcium and phosphate could be detected in the relation Ca : P = 1.4, suggesting the presence of HA (Ca : P = 1.67).

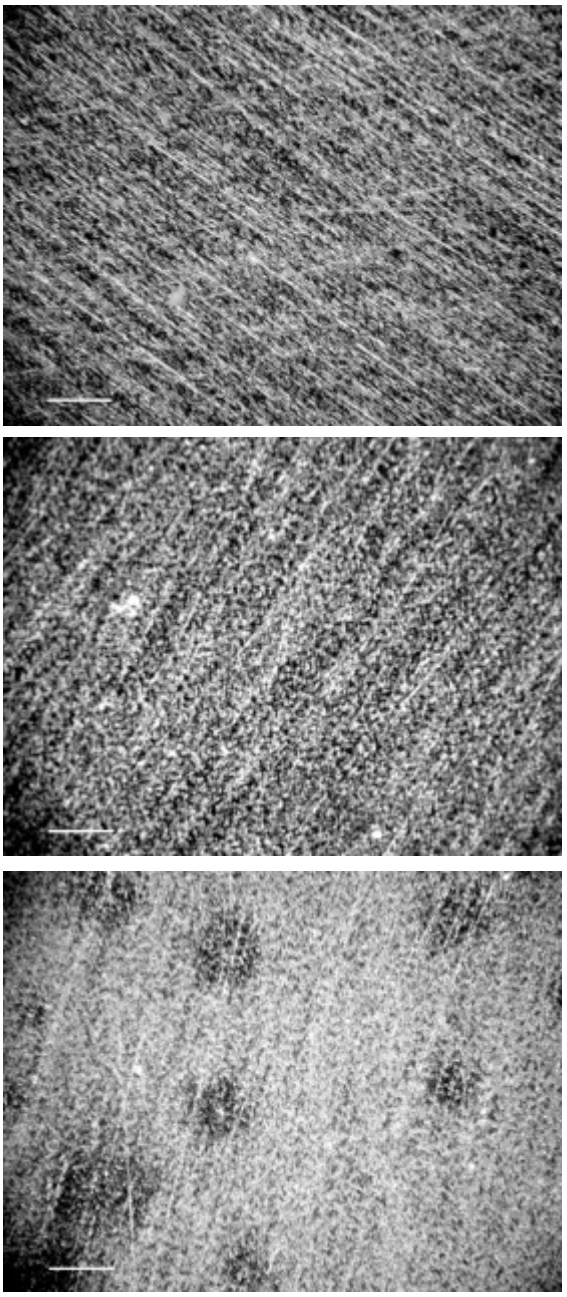

Fig. 2: Dark field microscopy of pure titanium (top), Na implanted titanium (middle) and NaOH etched titanium (bottom) after 14 days in α-MEM with 15% fetal bovine serum. As also proven by EDX, only on NaOH etched titanium an inorganic, non continuous calciumphosphate layer is formed. Bar indicating 200 µm.

Alkaline phosphatase is a key enzyme in the mineralization process of bone [4]. Its expression is a marker for differentiation and activity of the cell. It makes phosphate locally available for crystallisation with calcium and the formation of hydroxyapatite. *In vitro* the activity of this enzyme usually is quantified by dephosphorylation of paranitrophenylphosphate (pNPP). The product of this reaction has a maximum of absorbance at λ = 405 nm, which is used for measurement [5].

For investigation of alkaline phosphatase cells were removed from the samples by trypsinisation, counted under a light microscope in a Neubauer chamber and lysed by freezing at -20 °C. For each sample the extinction of 100 µL of this lysate and 20 µL of a prepared pNPP solution (Sigma, St Louis) was measured in a microplate reader at 405 nm after an incubation of 4 minutes. Values were corrected for a blank and divided by the cell count in the sample.

Results are presented in Fig. 3. At day 1 as a trend there is a higher activity of alkaline phosphatase with the treated samples compared to the untreated titanium. This trend is not observed after 2 and 4 weeks of cell culture and is even reversed, indicating equal or lower bone forming activity of the cells on ion implanted or etched samples.

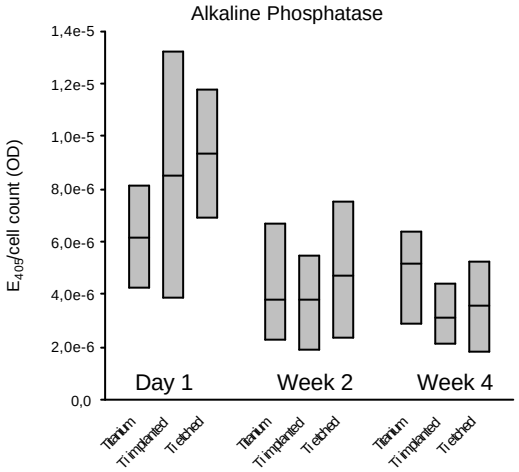

Fig. 3: Alkaline phosphatase activity per cell in the cell culture on the samples. As a measure for the enzyme activity, extinction of a pNPP reaction is reported. Bars indicate median and quartiles of the values. There are no significant differences, only as a trend there was a higher activity with the treated samples at day 1.

The results from morphology studies, calcium phosphate deposition and biochemistry indicate that the Na implanted surface and the NaOH etched surface are highly active. They influence cell growth but do not support calcification. Cell culture experiments show that deposition of calciumphosphate out of simulated body fluid is necessary prior to application in vital systems.

References

[1] M.T. Pham, M.F. Maitz, W. Matz, H. Reuther, E. Richter, G. Steiner, Thin Solid Films **379** (2000) 50

[2] H.M. Kim, F. Miyaji, T. Kokubo, T. Nakamura, J. Biomed. Mater. Res. **32** (1996) 409

[3] M. Ahmad, M.B. McCarthy, G. Gronowicz, Biomaterials **20** (1999) 211

[4] G. Harrison, I.M. Shapiro, E.E. Golub, J. Bone Miner. Res. **10** (1995) 568

[5] A. Sabokbar, P.J. Millett, B. Myer, N. Rushton, Bone Miner. **27** (1994) 57

Thin Films

*S. Y. Chun**
A. Chayahara
*Y. Horino**
M. Posselt
W. Möller

Cathodic arc deposition of nanoscale multilayers: experiments and computer simulations

Nanoscale Fe/C multilayers were fabricated by pulsed double-cathodic arc deposition with varying Fe and C ion flux and examined by XTEM. Computer simulations using the dynamic binary collision code TRIDYN were performed to get a better understanding of the multilayer deposition process. The simulation results were compared with the experimental data. For an ion fluence above 10^{16} cm^{-2} both experiment and simulation show that the production of a periodic multilayer structure with a bilayer thickness above 3 nm is possible. The investigations reveal that for a lower ion fluence the deposited Fe and C atoms are strongly intermixed so that the formation of individual bilayers is suppressed.

Collaboration: *Department of Materials Physics, Osaka National Research Institute, Osaka, Japan

J. Jagielski
*A. Piatkowska**
W. Matz
E. Richter
*G. Gawlik**
*A. Turos**

Structural and micromechanical properties of ion-beam mixed tungsten-on-steel system

Structural and micromechanical properties of ion-beam mixed tungsten layers were studied. 45 nm thick W layers deposited on HSS substrates were ion-beam mixed with $3x10^{16}$ Kr^{+}/cm^{2} at 340 keV and temperatures ranging from RT up to 450°C. A GIXRD study shows that the W layers mixed at RT are amorphous. These layers are characterised by a low friction coefficient of 0.15 and relatively low hardness. Increasing the process temperature results in the crystallisation of the layers, accompanied by an increase of their surface hardness by a factor of 1.5 and friction coefficient to 0.75. The transition from the amorphous to the crystalline state occurs at about 350°C. Wear rates of ion-beam mixed layers are always lower when compared with untreated steel substrates. The formation of soft thin layer on the surface of hard substrate can be an efficient way not only for decrease of friction coefficient but also to reduce the wear of materials.

Collaboration: *Institute of Electronic Materials Technology, Warszawa, Poland

*J. Jagielski**
*M. Kopcewicz**
W. Matz
R. Grötzschel

Thickness dependent phase transformations in nitrogen implanted iron films

Fe layers of thickness varying from 60 nm to 860 nm were deposited by rf-sputtering on oxidised silicon wafers and subsequently implanted with 100 keV N_2^{+} ions up to fluences from 1 to $4.5x10^{17}$ N/cm^{2}. The samples were analysed by CEMS, GIXRD, and RBS. The formation of iron nitrides in implanted iron depends strongly on the layer thickness. The nitrides are formed in thin (60, 130 nm) Fe layers at lower fluences and the iron is more completely nitrided than in thick layers or even bulk material. For example, for $4.5x10^{17}$ N/cm^{2} full transformation of thin (60 nm) Fe layers into Fe_2N is observed by GIXRD, whereas in thick and bulk samples CEMS and GIXRD show that about 20 % of Fe atoms in the surface layer remain in the crystalline α-Fe phase. The RBS data confirm the same amount of nitrogen in the analysed layer thickness. It is suggested that high stress in thin Fe layers formed during deposition, as revealed by GIXRD measurements, may enhance nitride formation

Collaboration: *Andrzej Soltan Institute for Nuclear Studies, Swierk/Otwock, Poland

F. Prokert
*A. Gorbunov**
N. Schell

Study of interface structure of Fe-Cr double layers by resonant X-ray reflectivity

In order to understand the physical nature of the GMR effect interface studies of the Fe-Cr system were performed. Cross-beam pulsed laser deposition (CBPLD) was used for the preparation of the double layers

Fe(20nm)/Cr(20nm) and Cr(20nm)/Fe(20nm), on an oxidised Si (100) substrate (amorphous SiO_x layer $\approx$ 500 nm). At ROBL (ESRF, Grenoble) the reflectivity was measured by specular and off-specular scans at energies near the absorption K-edges of Cr (E=5.989 keV) and Fe (E=7.111 keV). Due to the resonant scattering the weak electron density contrast between Fe and Cr is enhanced which allows to study the Cr-Fe interface structure. For the model-based simulations of the specular reflectivity as well as the diffuse scattering the REFS code package (Bede Scientific) was used. Besides the substrate and the double layer, also an oxide top layer has to be taken into account. The interface width as well as the roughness structure are very similar for both the Fe/Cr and the Cr/Fe double layer (rms-roughness $s \approx 0.8 \pm 0.1$ nm, lateral roughness correlation length $x = 1500 \pm 200$ nm, roughness exponent $h = 0.25 \pm 0.05$), and indicate that CBPLD results in an extremely large lateral correlation length of the interface roughness.

Collaboration: *Institut für Festkörper- und Werkstoffforschung Dresden

*A. Tselev**
E. Wieser
H. Reuther
F. Prokert
*D. Meyer***
*W. Pompe**

Transformation of metastable paramagnetic Fe/Cr alloys into the stable ferromagnetic bcc structure by ion implantation

Fe-Cr alloys with Cr concentrations from about 30 to 40 at.% were prepared by co-deposition of Fe and Cr using Cross Beam Pulsed Laser Deposition (CBPLD). XRD investigations reveal metastable structures from face-centered orthorhombic to the A15 (β-W) type. RT Mössbauer spectra show no indication of ferromagnetic ordering for Cr concentrations from 34.5 to 40 at.%. In contrast, at 29 at.% Cr, beside the non-magnetic central part of the spectrum also 6-line components were detected indicating ferromagnetic ordered fcc components. Samples with 29 at.% Cr and 38.5 at.% Cr (thickness 40 nm) were irradiated with 5×10^{15} Cr/cm^2 (40 keV). After implantation the XRD patterns show only reflections of the bcc lattice indicating a two-phase system consisting of bcc Fe and Cr as expected in thermal equilibrium. The Mössbauer spectra show predominantly ferromagnetically coupled Fe for the higher Cr content and nearly complete ferromagnetic Fe for the lower one. The possibility to produce metastable non-magnetic Fe/Cr by CBPLD and to transform such layers locally into the ferromagnetic state by ion implantation using masks or a writing fine focussed beam is of high interest for advanced magnetic memories.

Supported by DFG - SFB 422

Collaboration: TU Dresden: *Institut für Werkstoffwissenschaft, **Institut für Kristallographie und Festkörperphysik

Semiconductors

*N. Variam**
*U. Jeong**
*S. Falk**
*S. Mehta**
M. Posselt
*T. Feudel***
*M. Horstmann***
*C. Krüger***
*C-H. Ng****

Application of indium ion implantation for halo doping: experimental and simulation results for advanced CMOS devices

Properties of indium relevant to halo implantation were examined. Compared to conventional ions (B^+ and P^+) heavy ions show a lower range profile straggling. The channeling behavior of indium ions implanted at high tilt angles (35° and 45°) was investigated in dependence on the rotation angle, which describes the azimuthal orientation of the wafer. The results of atomistic simulations agree very well with the as-implanted indium profiles measured by SIMS. Furthermore, calculations demonstrate that the damage produced by indium implantation reduces the channeling in the subsequent arsenic extension implant. For an aggressive halo produced by low energy indium implantation, the simulated saturation threshold voltage is sensitive to small implant angle variations.

Collaboration: *Varian Semiconductor Equipment Associates, Gloucester, USA, **AMD Saxony Manufacturing, Dresden, *** AMD Sunnyvale, CA, USA

M. Posselt
*M. Behar**
R. Grötzschel

Temperature dependence of the shape of P range profiles obtained by channeling and tilted implantation

140 keV P ions were implanted into (100) Si at about 300 and 600 K and an ion dose in the order of $5x10^{15}$ cm^{-2}. At both temperatures a channeling and a tilted implant were performed. The depth profiles of phosphorus were measured by SIMS, and the implantation damage was analyzed by RBS/C. In the case of the RT implant the P depth profiles and the thickness of the amorphous layer formed could be reproduced very well by Crystal-TRIM atomistic computer simulations using the default model for damage accumulation during ion bombardment. The assumption that at 600 K the irradiation-induced defects vanish completely between subsequent implantations into the same region leads to a good agreement between SIMS data and simulation results.

Collaboration: *Instituto de Fisica, Porto Alegre, Brazil

D. Panknin
*J. Stoemenos**
*M. Eickhoff ***
V. Heera,
*N. Vouroutzis**
*G. Krötz***
W. Skorupa

Improvement of the 3C-SiC/Si interface by flash lamp annealing

The benefits of irradiation of flash lamps of 3C-SiC films epitaxially grown on Si are investigated. Energy densities in the range from 100 to 150 Jcm^{-2} were used. Due to the optical transparency of SiC the irradiation energy is mainly absorbed at the 3C-SiC/Si interface. When the energy density is sufficiently high to melt the Si at the interface, a process resembling liquid phase epitaxy occurs in SiC, which results in a substantial improvement of the SiC film eliminating also the cavities and the stress at the interface. The method is applicable only for thin SiC films of 20-40 nm, which can be used as seeds for subsequent deposition of thicker SiC films.

**Collaboration: ***Aristotle University of Thessaloniki, Physics Department, Greece, **Daimler Chrysler AG, München

V. Heera
*L. Ottaviani**
M. Voelskow
W. Skorupa

Annealing behavior of high dose Al-implanted 6H and 4H SiC

Highly Al doped ($5x10^{20}$ cm^{-3}), amorphous layers in (0001)-oriented 6H and 4H SiC with box-like profiles produced by multiple ion implantation at room temperature have been annealed in a rf-heated furnace under a pure Ar atmosphere at 1700°C for 30 min. The recrystallization process and the changes in the as-implanted Al profile were investigated by RBS/C and SIMS, respectively. For comparison, the annealing behavior of 6H-SiC implanted at 400°C has been investigated, too. The annealing of the amorphous layers is accompanied by Al loss and the formation of a very homogeneous Al profile in the region where polycrystallization dominates. However, Al diffusion into the crys-

talline bulk material is suppressed. A distinct solid phase epitaxial regrowth is obtained in the 4H-SiC samples after annealing. It is assumed that the special off-axis orientation of the standard 4H-SiC wafers used in our experiments could be the reason for the better epitaxial regrowth.

Supported by DFG

Collaboration: * INSA de Lyon, France

*B. Pécz**
V. Heera
W. Skorupa

Synthesis of epitaxial diamond grains in 3C-SiC by high temperature carbon implantation

Wide bandgap semiconductors, such as SiC and diamond, have received outstanding attention in the last couple of years. For certain purposes it would be advantageous to combine the excellent properties of both materials. Recently, it has been reported that ion beam synthesis of diamond in 6H-SiC is possible by high dose C implantation at 900°C. These studies have been extended to cubic 3C-SiC. Epitaxial 3C-SiC layers with a thickness of about 1µm grown on Si were used as substrates for the experiments. Ion implantation of carbon ions was done at 60 keV with the fluence of $1x10^{18}$ C^+/cm^2. All of the implantation experiments were carried out at elevated temperature in the range of 600-1200°C to study the phases, which are formed, when excess carbon is introduced into the SiC lattice. At 1100°C and 1200°C small diamond grains were formed, which are embedded in the SiC and form perfectly oriented grains of a few nm in size. At 600°C the textured form of graphite was detected only. At 900°C the phase formed depends on the ion current during the implantation process. At high dose rate (at this temperature) the impinging carbon ions can destroy the nucleated diamond grains.

Supported by EC (TMR-project)

Collaboration: *Research Institute for Technical Physics and Materials Science, Budapest, Hungary

V. Heera
F. Eichhorn
A. Mücklich
W. Skorupa

The nucleation of 3C-SiC nanocrystals in amorphous SiC stimulated by ion irradiation

Amorphized layers of 6H-SiC can be transformed to nanocrystalline 3C-SiC layers by ion irradiation if the nuclear deposited energy and the substrate temperature exceed threshold values of $5x10^{25}$ $eVcm^{-3}$ and 300°C, respectively. Unfortunately, in previous experiments nucleation could not be directly observed, because the transformation process was always completed. Therefore, new experiments have been performed, in order to obtain partly recrystallized layers. Isolated 3C-SiC grains within the amorphous matrix with diameters between 2 and 4 nm have been detected by XTEM in samples implanted with $3x10^{15}$ cm^{-2}, 300 keV Al^+ at a dose rate of $3x10^{13}$ $cm^{-2}s^{-1}$ and a temperature of 700°C. It turned out that, besides the temperature, the dose rate is a very important parameter of the nucleation process.

Supported by DFG

F. Eichhorn
N. Schell
A. Mücklich
W. Matz
R. Kögler

Structural relation between Si and SiC formed by carbon ion implantation

The implantation of a high fluence of C ions into Si at higher temperature induces the growth of buried 3C-SiC crystallites. The orientation relationship of SiC crystals in Si(001) wafers implanted with $3.25x10^{17}$ C/cm^2 (45 keV) or $4x10^{17}$ C/cm^2 (195 keV) at 500°C or 800°C, respectively, was studied using X-ray synchrotron radiation at ROBL and high-resolution TEM.

Three types of orientation of the SiC crystallites in Si are found: (i) random orientation like for a powder material; (ii) fibre texture with axis parallel to the surface normal with a mean orientation spread of 6°; (iii) high alignment to the Si matrix: SiC<001> || Si<001> and SiC<110> || Si<110> with orientation spread is in the range from 2° to 5° due to a coherent growth of SiC in the Si matrix. The latter dominates at high temperature.

Ion beam synthesis is an efficient method for growing SiC nanocrystals (5 nm) with a small size distribution, as the direct growth in the Si matrix also favours

a well-defined crystalline orientation. Compared to earlier experiments at RT, it appears that elevated temperature during implantation is more effective in forming an aligned crystallite distribution than post-implantation annealing even at higher temperatures.

F. Eichhorn
N. Schell
V. Heera

Formation of diamond crystals in SiC by ion beam synthesis

In the last decade increasing attention has focused on wide band gap semiconductors like SiC, GaN and diamond. In this work the formation of diamond crystals by implantation of $1x10^{18}$ C/cm^2 at an energy of 60 keV into 6H-SiC was investigated. The maximum C content of $15x10^{22}$ cm^{-3} (approximately 80 % of the atomic density in diamond) is reached at 130 nm below the surface. The implantation results in a distortion of the SiC matrix and/or in a formation of crystalline C particles depending on the implantation temperature. In order to study the real structure of these low Z materials, X-ray synchrotron radiation at ROBL at the ESRF Grenoble was used. In material implanted at 600°C, the SiC matrix has a contracted lattice with a strain in the range between $-1.6x10^{-4}$ and $-4.4x10^{-4}$ and no crystalline C phase is detected. During implantation at 900°C diamond crystals are formed. They are aligned to the 6H-SiC matrix lattice in two types: C[1 1 1] || SiC[0 0 0 1] and C[1 1 0] || SiC[1 1 -2 0]. The crystallite size estimated from the diffraction line broadening is 5 nm; the mosaic spread (corresponding to the accuracy of the alignment) is 7°.

R. Kögler
Y.M. Gueorguiev
A. Peeva
D. Panknin
A. Mücklich
W. Skorupa

Metal gettering in P-and As-implanted silicon beyond the projected ion range R_P

A deep, separated gettering layer in P- and As-implanted Si has been discovered after annealing beyond the two well-known gettering layers at $R_P/2$ and at R_P. The corresponding gettering effect is called the „trans-R_P“ effect. This effect has not been observed for Si-implanted Si. The physical mechanism leading to the formation of this gettering layer is different of that responsible for the gettering at $R_P/2$. A model has been suggested that explains the metal trapping beyond R_P by small clusters of self-interstitials, which are formed there during annealing via Ostwald ripening. The self-interstitials are moved out of the interstitial-rich R_P region by pair diffusion with the P- or As-implant. In this way self-interstitials may escape from the region of defect recombination and interstitial loop formation at R_P. The occurrence of the trans-R_P effect just for P- and As- implantation can be explained by their special diffusion mechanism in Si.

Supported by SMWK

*B. Pantchev**
*P. Danesh**
*I. Savatinova**
*E. Liarokapis***
B. Schmidt

The effect of structural disorder on mechanical stress in a-Si:H films

The effect of ion implantation on mechanical stress in a-Si:H films was studied with the aim to separate the contributions of hydrogen content and structural defects to the intrinsic compressive stress. a-Si:H films were prepared by PECVD. Si^+ ions with an energy of 160 keV were implanted and the implantation-induced damage was studied on the structural level by means of Raman backscattering spectroscopy. The stress in films was compressive and its value correlates with the short and intermediate range order. The obtained results have shown that the value of compressive stress in the material could be changed in spite of keeping constant the hydrogen content. It is suggested that the value of stress is to a high degree determined by the structural order of the silicon network.

Collaboration: *Institute of Solid State Physics, Bulgarian Academy of Sciences Sofia and **Physics Department, National Technical University, Athens

Semiconductor Spectroscopy

T. Dekorsy
M. Helm

Establishment and build-up of the new division

The aim of the new division "Semiconductor Spectroscopy" (established in July 2000) is to provide the experimental tools for the investigations of the optical properties of semiconductors and new materials. With regard to the broad and excellent background of the Institute in the area of ion-beam based material synthesis, modification and structuring, the division will aid in the exploration of new phenomena associated with these materials. Just to name a few, the linear and nonlinear optical properties of semiconductor nanoclusters and semiconductors modified on a nanometer scale by a focused ion beam should be mentioned.

Besides the establishment of standard CW spectroscopy like FTIR, photoluminescence, and Raman spectroscopy, emphasis will lie on femtosecond time-resolved investigations. These experiments performed with femtosecond pulsed lasers allow us to disentangle the time scales in the process of energy relaxation and electron-phonon dynamics in semiconductors and semiconductor nanostructures. The relevant processes and time-scales are of great interest for future devices. An example is the population inversion within the conduction band of heterostructures necessary to operate quantum cascade lasers.

Of special importance is the energy range from some meV to some 100 meV, which corresponds to THz frequencies. The possibility to generate short electromagnetic pulses at these frequencies with femtosecond lasers has opened new ways for semiconductor spectroscopy.

Finally, the operation of the free electron laser at the ELBE electron accelerator will provide a unique high intensity light source with a temporal structure of picosecond pulses, which is well suited for these kind of experiments.

Nanostructures

M. Strobel
K.-H. Heinig
W. Möller

Atomistic study of the evolution of nanoclusters in ion beam synthesis

Ion implantation is an established tool to synthesize or to modify buried low-dimensional nanostructures (e.g. nanoclusters), which have become the basis of numerous technological applications. A sound understanding of the diffusional interaction dynamics of nanoclusters have been achieved by kinetic 3D lattice Monte-Carlo simulations. In particular, the exploitation of the cluster size-concentration dependence (Gibbs-Thomson relation) under pure thermal or ion irradiation conditions provides a wealth of physical information relevant for ion beam synthesis. It was shown that for intense ion irradiation or low irradiation temperature a collisional-mixing-induced nucleation of nanoclusters occurs. This computer-simulation-based prediction goes beyond a recent theoretical prediction for nanocluster evolution under comparably weak ion irradition (or at high irradiation temperatures), namely inverse Ostwald ripening. Furthermore, this atomistic study confirms the prediction of inverse Ostwald ripening, which is the result of an analytical treatment.

K.-H. Heinig
B. Schmidt
*M. Strobel**
*H. Bernas***

Inverse Ostwald ripening and self-organization of nanoclusters due to ion irradiation

Under ion irradiation collisional mixing competes with phase separation if the irradiated solid consists of immiscible components. It was shown that, at interfaces between immiscible components, irradiation processes may lead to an unusual, far-from-equilibrium behavior. During high-fluence ion implantation the collisional mixing affects nanocluster synthesis, and ion irradiation of nanoclusters modifies their size and size distribution. The mathematical treatment of the competition between irradiation-induced detachment of atoms from clusters and their thermally activated diffusion in the surrounding matrix leads to a Gibbs-Thomson relation with modified parameters. Due to an effective interface energy, which may become negative under ion irradiation, inverse Ostwald ripening of nanoclusters may occur under ion irradiation. The theoretical predictions were confirmed by experimental studies of the evolution of Au NCs in SiO_2 irradiated by MeV ions. The negative Si/SiO_2 interface energy during ion implantation contributes critically to the self-assembling of nanoclusters in a δ-layer parallel to the Si/SiO_2, giving rise to the formation of tiny Si clusters in front of the Si/SiO_2 interface, which promotes heteronucleation of the implanted impurities during a post-implantation anneal. The self-assembled δ-layer of nanoclusters can be tailored for non-volatile memory application by a control of irradiation-induced SiO_2 damage, which was proven experimentally by a variation of ion energies.

Collaboration: *CNR-IMETEM, Catania, Italy, **CSNSM, CNRS-IN2P3, Orsay, France

B. Schmidt
K.-H. Heinig
A. Mücklich

Evolution of ion beam synthesized Au nanoclusters in SiO_2 under ion irradiation

The evolution of the mean size and the size distribution of Au nanoclusters (NCs) under high-energy ion irradiation have been studied. Au NCs were synthesized in a 480 nm thick SiO_2 layer by 330 keV Au^+ implantation and subsequent annealing at T = 1000 °C for 1h in dry O_2. XTEM images show a 70 nm thick layer of Au NCs, being centered at the projected ion range R_p(330keV) = 100 nm, having a mean NC size of 5 nm at R_p, and resembling the broad Lifshiz-Slyozov-Wagner (LSW) size distribution of diffusion controlled Ostwald ripening. Post-irradiation of the Au NCs by 4.5 MeV gold ions was used in order to tailor their size and size distribution. The high-energy Au^+ irradiations were performed at 190...210 °C with a fluence of $(0.5...1.0)x10^{16}$ cm^{-2}. As the

projected range of this irradiation is R_p (4.5 MeV Au) = 1 µm, no additional Au-atoms were incorporated in the SiO_2 film and the Au^+ ions come to rest in the (001)Si substrate. XTEM images of the post-irradiated Au NCs in the SiO_2 layer show a strong decrease of their mean size as well as the width of their size distribution. The observed NC evolution under ion irradiation agrees with recent theoretical predictions and kinetic Monte-Carlo simulations.

*G. Rizza**
M. Strobel
K.-H. Heinig
*H. Bernas**

Ion irradiation of gold inclusions in SiO_2: experimental evidence for inverse Ostwald ripening

When sub mm size gold inclusions in SiO_2 are irradiated with MeV gold ions, a ring of nanometer-size clusters is formed in their immediate vicinity. The size, density and radial distribution of these nanoclusters were determined. The observations are in agreement with the prediction that in a driven system, under appropriate ion beam and temperature conditions, the steady-state solute concentration's dependence on precipitate size may be opposite to that expected from the equilibrium Gibbs-Thomson relation. Kinetic Monte-Carlo simulations account for additional experimental results: the irradiation-induced increase in solute concentration can promote nucleation of additional precipitates around the first ring. The latter finding contradicts the usual assumption that ion beam mixing hinders nucleation.

Collaboration: *CSNSM, IN2P3, Orsay, France

L. Rebohle
*H. Fröb**
*S. Niedermeier***
W. Skorupa

Strong photoluminescence of Sn-implanted thermally grown SiO_2 layers

Light emitters, based on nanocluster containing SiO_2 films on Si, are a very promising approach for future integrated optoelectronic applications. Previous studies of Ge- and Si-implanted SiO_2 layers were extended to the case of Sn with a Sn-content of typically 1…5 at% implanted into thermally grown SiO_2 films of 500 nm thickness. The intensity of the violet photoluminescence (PL) of Sn-implanted SiO_2 layers is approximately 2 and 20 times higher than those of Ge- and Si-implanted SiO_2 layers, respectively. For optimum preparation conditions the PL efficiency (the ratio of light output to the light input power) exceeds a value of 10^{-3}. For Ge- and Sn-implanted SiO_2 layers the decay time of the violet PL was estimated to be ~100 µs and ~7 µs, respectively. The violet PL is interpreted as due to a triplet-singlet transition of the neutral oxygen vacancy typical for Si-rich SiO_2 and similar Ge- and Sn-related defects in Ge- and Sn-implanted SiO_2 films. The enhancement of the blue-violet PL and the decrease of the decay constant within the isoelectronic row of Si, Ge and Sn is explained by the increase of spin orbit coupling when substituting Si with Ge or Sn.

Supported by SMWK

Collaboration: *Institut für Angewandte Photophysik, TU Dresden, **Institut für Optik und Quantenelektronik, Friedrich-Schiller-Universität Jena

T. Gebel
L. Rebohle
J. von Borany
W. Skorupa
*B. Mrstik**

Determination of the charge storage centroid in Ge implanted SiO_2 layers

Nanocluster containing SiO_2 films exhibit trap-assisted charge storage. The localization of the trapped charge as well as the charge trapping and detrapping properties are of great interest for the understanding of the current transport and the electroluminescence mechanism in such layers. Photo-IV measurements are a suitable method to determine the charge centroid. SiO_2 layers with a thickness of 80 nm were thermally grown on (100) Si substrate. Ge implantation was performed at energies of 30...50 keV to fluences of $1.8x10^{15}$...$1.0x10^{16}$ cm^{-2}. After RTA at 1000°C for 30 s, thin transparent gold contacts have been deposited. For charging of the traps under strong UV-illumination a constant positive voltage was applied to the gate. Subsequently an IV-sweep was carried out and the centroid was determined from the observed shift of the IV-curve. The position of the centroid was found to be in strong correlation to the maxi-

mum peak concentration of the Ge implant calculated from TRIM. A shift of the centroid position towards the SiO_2/Si interface was observed at higher Ge fluences.

Supported by SMWK and SMWA

Collaboration: *Naval Research Laboratory, Washington DC, USA

T. Gebel
L. Rebohle
J. Zhao
J. von Borany
W. Skorupa

Combined IV / CV investigations of SiO_2 layers implanted with Ge

A combination of IV and CV measurements was used to investigate the amount of trapped charge at different stages of the IV characteristics. SiO_2 layers with a thickness of 80 nm were implanted with Ge - ions at energies of 30…50 keV to peak concentrations of 1..6 at.% Ge followed by an annealing treatment at 1000°C for 1...30 s. MOS devices were formed using Al as a gate contact. The IV-characteristics was measured stepwise by a voltage staircase sweep, followed by a CV scan after each step, which allows to determine the flatband voltage at the different stages of the IV curve. The flatband voltage shifts to positive values with increasing electrical field indicating electron trapping. The amount of stored charge increases only slightly with the fluence but strongly with the energy of the implant. This leads to the assumption that defects in the SiO_2/Si interface region play the key role for the trapping characteristics. At a high electrical field ($E > 8MVcm^{-1}$) a reverse shift of the CV curves was found. The reason for that is not yet fully understood. Possible processes could be hole injection, stress-induced trap modification or trap generation.

Supported by SMWK and SMWA

M. Klimenkov
J. von Borany
W. Matz
*J. Eckert**
*M. Wolf**
*K.-H. Müller**

Structure and magnetic properties of Co nanoclusters fabricated by ion beam synthesis in SiO_2 films

Co nanoparticles fabricated by ion beam synthesis in SiO_2 films were investigated with TEM, RBS and SQUID techniques. Double implantation (500 and 250 keV) into a 600 nm thick SiO_2 film with total fluence of $4x10^{16}$ Co/cm^2 leads to the formation of a 400 nm thick region with homogeneous Co concentration of about 1.5 at.%. The variation of the thermal treatment enables the formation of Co nanoclusters of different sizes ranging from 2 to 40 nm. At 800°C annealing temperature, amorphous nanoclusters with sizes of about 2-3 nm are observed in the implanted area without noticeable Co redistribution as measured with RBS. The magnetisation measurements at temperatures from 2 K to 360 K reveal their super-paramagnetic behaviour. Annealing temperatures of 900°C and 1000°C lead to the formation of crystalline Co nanoclusters with sizes above 7 nm. The Co nanocrystals are in the cubic structure. The RBS spectra show a Co diffusion towards the surface and the Si/SiO_2 interface, respectively. This redistribution is strongly enhanced with increasing temperature. The nanocrystal ensemble exhibits ferromagnetic behaviour, which is superimposed by a paramagnetic component after 1000°C annealing.

Collaboration: *Institut für Festkörper- und Werkstoffforschung Dresden

M. Klimenkov
W. Matz
*S. Nepijko**
*M. Lehmann***

Crystallisation of Ge nanoclusters in SiO_2 caused by electron irradiation in TEM

TEM is a main characterisation method of nanocluster arrangements in thin films. This study was directed to the question whether the electron irradiation during TEM analyis itself changes the morphology of the nanoclusters. Thermally grown SiO_2 layers of 20 nm thickness on Si(100) were implanted at 12 keV to a fluence of $7x10^{15}$ Ge/cm^2 and subsequently annealed at 950°C for 30 s in dry nitrogen. A band of amorphous Ge nanoclusters (mean size 3 nm) was formed in the middle of the SiO_2 layer. The irradiation was performed with a 200 keV electron beam in a TEM equipped with FEG. For low current density (3-6 A/cm^2) a dose higher than $6x10^3$ C/cm^2 induces a narrowing of the nanocluster band width together with an increase of the cluster size and a decrease of the cluster density. Irradiation with doses above $4x10^4$ C/cm^2 causes crystal-

lisation of the Ge nanoclusters. The mode depends on the current density. For values clearly below 150 A/cm^2 the Ge nanoparticles transform into single crystals. For irradiation intensities above this value the formation of single or multiply twinned particles (MTP) was observed. The reason for the formation of MTPs is the local structural instability via thermal spikes induced by high intensity electron irradiation. For current densities below 10 A/cm^2 during TEM studies, irradiation induced influence on the distribution and morphology of nanocluster assemblies can be neglected.

Collaboration: *Ukrainian Academy of Sciences, Kiev, Ukraine, **TU Dresden, Institut für Angewandte Physik

*S. Oswald**
B. Schmidt
K.-H. Heinig

Phase identification in annealed, Ge implanted SiO_2-layers by XPS depth profiling

Ge containing nanoclusters formed by Ge ion implantation and subsequent anneling in O_2 atmosphere have been identified by XPS, in combination with data evaluation by factor analysis, to consist mainly of elemental Ge and GeO_2. Among the two XPS peaks characterizing elemental Ge and GeO_2 a third spectral component was found which can be associated with the interaction between Ge containing particles and the SiO_2 matrix or, additionally, by ion beam mixing of particles during sputtering for XPS depth profiling. To decrease the influence of ion mixing during sputtering the standard sputter conditions (Ar^+, 3.5 keV) have been changed using high mass (Xe^+) low energy of (1 keV) ions. It was found that under these conditions the distribution of the three spectral components changes substantially. It has been proven that under inappropriate sputter conditions during XPS depth profiling the fraction of elemental Ge in nanoclusters embedded in SiO_2 will be underestimated.

Collaboration: *Institut für Festkörper- und Werkstofforschung Dresden

*V. Borodin**
K.-H. Heinig
B. Schmidt
*S. Oswald***

Modeling and XPS study of precipitation and oxidation of Ge in Ge^+ implanted SiO_2 layers

During annealing at 950°C in an oxidizing ambient, the redistribution of Ge in Ge^+ implanted SiO_2 layer is influenced by the Ge oxidation. Crystalline clusters precipitate immediately after sample heating. During the annealing an oxidation front proceeds into the layer, consuming crystalline clusters and leaving behind glassy precipitates barely visible by XTEM. Sputter depth profiling in conjunction with the XPS analysis was applied in order to identify the chemical state of both the precipitated Ge and that dissolved in the silicon dioxide matrix. For a reliable interpretation of the measured data, modeling of the physical processes involved in the depth profiling XPS technique was performed. It is shown that the depth profiling by ion beam sputtering causes collisional mixing of the subsurface region, which modifies the XPS signal.

Collaboration: *RRC Kurchatov Institute, Moscow, Russia, **Institut für Festkörper- und Werkstofforschung, Dresden

*S. Spiga**
*S. Ferrari**
*M. Fanciulli**
B. Schmidt
K.-H. Heinig

Kinetics of ion beam synthesis of Sn and Sb clusters in SiO_2 layers

The ion beam synthesis of Sn and Sb clusters in thin oxides by 80 keV (0.1...1.0x10^{16} cm^{-2}) Sn and Sb implantation in 85 nm thick SiO_2 and RTP annealing (800...1000°C for 30...300 s under Ar or dry N_2 ambient) leads to the formation of two nanocluster bands, the one near to the SiO_2 surface and the other close to the Si/SiO_2 interface. In addition, big isolated clusters are randomly distributed in the middle of the oxide. Cluster-size distribution and cluster-crystallinity are related to implantation dose and annealing time. Low energy (10...12 keV) Sb and Sn implantation (2...5x10^{15} cm^{-2}) leads to the formation of very uniform cluster-size distribution. Under specific process conditions, only an interface cluster band was observed. Mössbauer spectroscopy on ^{119}Sn implanted samples has been used to determine the Sn atomic local envi-

ronment.

Collaboration: *Laboratorio MDM-INFM, Agrate Brianza, Italy, **STMicroelectronics, Agrate Brianza, Italy

H. Seifarth
J.U. Schmidt
R. Grötzschel
M. Klimenkov

Phenomenological model for the prediction of SiO_X thin film stoichiometry of reactive rf-magnetron sputtering of Si in Ar/O_2 atmosphere

The process of reactive sputtering from a Si target in an Ar/O_2 gas mixture has been investigated. An optical plasma regulating circuit using the intensity of the 251.9 nm Si I plasma emission line as setpoint was employed to stabilize the sputtering process. A phenomenological model of the process has been derived that, in contrast to previous models, allows to calculate the composition of the growing SiO_x film exclusively from measurable process parameters and accounts for the non-uniform deposition at the substrate. Film compositions x predicted this way for different setpoints were verified by RBS.
As example, $SiO_2/SiO_{1.5}/SiO_2$ (5 nm/10 nm/45 nm) layer stacks were prepared on Si substrates. After annealing at 1000°C, 1 h in N_2 the sub-stoichiometric interlayer is transformed into a thin film of nanocrystalline silicon embedded in an oxide matrix. Such structures are currently investigated for application in nanocrystalline Si floating gate memory devices and Si-based light emitters.

J.U. Schmidt

Preparation of SiO_2-thin films with gate oxide quality by reactive rf-magnetron sputtering and implementation into sputtered nanocrystalline Si floating gate MOS-capacitor structures

SiO_2 thin films were deposited by reactive rf-magnetron sputtering at room temperature in an Ar/O_2 atmosphere on n-type Si wafers. The samples were annealed in N_2 at temperatures between 900 and 1050°C using either RTA or furnace processing. After Al-dot lithography and forming gas anneal at 400°C the samples were analyzed using capacitance-voltage (CV) or current-voltage (IV) measurements. The as-prepared films had interface trap densities as low as $\sim 5 \times 10^{10} cm^{-2}$ and breakdown fields of 12..13 MV/cm, which is comparable to good thermally grown oxides. Nanocrystalline Si floating gate MOS-capacitor structures were prepared using SiO_2/a-Si/SiO_2 stacks deposited in a single magnetron sputtering process. CV and IV measurements indicate the charge injection into the nc-Si layer by direct tunneling.

Supported by DFG

M. Strobel
K.-H. Heinig
W. Möller

Atomistic study of the evolution of nanoclusters in ion beam synthesis

Ion implantation is an established tool to synthesize or to modify buried low-dimensional nanostructures (e.g. nanoclusters), which have become the basis of numerous technological applications. A sound understanding of the diffusional interaction dynamics of nanoclusters has been achieved by kinetic 3D lattice Monte-Carlo simulations. In particular, the exploitation of the cluster size-concentration dependence (Gibbs-Thomson relation) under pure thermal or ion irradiation conditions provides a wealth of physical information relevant for ion beam synthesis. It was shown that for intense ion irradiation or low irradiation temperature a collisional-mixing-induced nucleation of nanoclusters occurs. This computer-simulation-based prediction goes beyond a recent theoretical prediction for nanocluster evolution under comparably weak ion irradition (or at high irradiation temperatures), namely inverse Ostwald ripening. Furthermore, this atomistic study confirms the prediction of inverse Ostwald ripening, which is the result of an analytical treatment.

Biotechnological Materials

R. Günzel
M. Maitz
*P. Chu**

Biocompatible surface layers of enhanced X-ray contrast on vascular stents

Coronary stents are seen as the most important progress in cardiology of the decade. But still problems concerning occlusion by restenosis or thrombosis have to be overcome, and X-ray contrast of the thin steel wires has to be improved. The suggested way is coating of the stents with Ta, which is known for its good biocompatibility and hemocompatibility, and its high X-ray absorption.

Ta films on flat samples of stainless steel have been deposited in an RF generated Ar plasma (p=0.4 Pa, W_{HF}= 1000 W), assisted by passive a magnetron sputter source with Ta cathode. The temperature during deposition was varied between room temperature and 500°C. PIII high voltage pulses, pulse duration 5 µs, voltages ranging from 3 to 20 kV, were applied to the samples in order to obtain an improved adhesion by intermixing of the deposited Ta layer and the substrate material. In the scratch test adhesion was quantified as 250mN, which is a promising result. The Ta layer is generally passivated by an oxide film, that inhibits corrosion in physiologic salt solutions. Potentiodynamic corrosion tests of flat samples in a physiologic salt solution (Hanks buffered salt solution) did not show any corrosion. In 0.05M H_2SO_4 there was a high positive corrosive potential (min. 225, max. 355 mV) and low corrosion currents (19 - 39 nA/cm^2). This indicates a good corrosive resistance of the coating. Coating of real stents with the same parameters caused blistering and low adhesion, which is probably due to the presence of a thick surface oxide.

Supported by DAAD

Collaboration: *City University of Hong Kong

M.T. Pham
M. Maitz
W. Matz
H. Reuther
E. Richter

Ca and P containing silicate incorporated in Ti surfaces

Ca, P, Si, and Na were consecutively implanted into polished Ti surfaces. The fluence ratios were chosen to Na:Si = 2 and Ca:P =1,5 corresponding to Bioglass. The ion energies were set to incorporate the ionic components within a surface layer of about 100 nm thickness. After ion implantation a thermal treatment at 600°C in air for 60 min has been performed. The samples were tested for their osseoinductive properties. Incubation tests in simulated body fluid (SBF) containing Ca and phosphate ions show enhanced formation of hydroxyapatite and calcium phosphate on ion implanted surfaces relative to unimplanted Ti samples. The growth of the bone forming cell line SAOS-2 was examined for ion implanted and SBF treated samples. Cell attachment and growth were retarded suggesting that the SBF treatment needs to be optimized.

W. Anwand
G. Brauer
M.T. Pham

Calcium phosphate films on titanium studied by SPIS

Thin films of calcium phosphates (acronym: CaP) are widely used as coatings on titanium-based implants for applications in orthopedics and reconstructive surgery. We have used SPIS for characterizing CaP coatings formed on titanium surfaces. By energy variation of the incident positrons it is possible to resolve depth dependent properties of coatings, reflected by a given positron parameter in a certain layer, which cannot be found by other methods. CaP films were deposited on polished pure titanium substrates by precipitating three, five, and ten days from a calcium and phosphate ions containing simulated body fluid. Two different layers were found with thickness of about 20 and 400 nm for the three-day sample, and 140 and 800 nm for the five-day sample, respectively. The ten-day sample displayed two top layers of about 90 nm and 3 µm. However, there is an indication of a third transition layer to the substrate. A control sample without CaP showed a 6 nm oxide surface layer followed by a weakly damaged layer of 250 nm.

*M.V. Vinnichenko**
M. Maitz
M.T. Pham

Corrosion testing of stainless steel under biological influences

Interactions of the body with an alloplastic material are complex, affecting the implant and the recipient. It is known that in presence of Cl^- ions, the leading anion in the serum, corrosion of stainless steel may occur. Further many proteins in the serum have complex forming properties with metal ions, and cells are able to produce high pH gradients and reactive oxygen species. These ways of corrosion are not detectable by the standard electrochemical approach.

Polished discs of stainless steel were analysed by means of optical microscopy, AFM, XPS, FTIR spectroscopy, and spectral ellipsometry to check for corrosion related changes of the discs during cell culture; Si (100) was used as a control. Detailed studies of the untreated samples allowed adequate parameterisation of their optical properties by using Lorentz multiple oscillator model. Short-term incubation in phosphate buffered saline (PBS, pH 7,4) caused changes in the ellipsometric angels (? ? ?1.5°; ? ? ?3°) in short wavelength region that could be related to additional oxidisation of the sample. In cell culture medium (Dulbecco's Modified Minimal Essential Medium DMEM with 10% fetal bovine serum) corrosive changes were higher and could be distinguished from protein adsorption.

Supported by DAAD

Collaboration: *Kyiv Taras Shevchenko University, Faculty of Physics

Ion Beam Analysis

*A.V. Dvurechenskii**
R. Grötzschel
*A.I. Yakimov**
*A.I. Nikiforov**

RBS studies of self-assembled pyramidal germanium quantum dots embedded in silicon

The formation of semiconductor quantum dots (QD) with atomic-like carrier density of states can be achieved by MBE of Ge on Si, where the strain in the Stranski-Krastanov growth mode can cause self-assembling of defect-free, uniformly sized Ge-QDs. When the Ge layer exceeds 3 monolayers (ML) pyramidal-shaped Ge islands with <100> oriented square bases and {105} sidewalls are formed on a (100) Si substrate. For further investigations such structures have to be protected by a Si cap layer. In order to identify growth temperature ranges for the successive deposition steps, which provide defect-free structures without any remarkable material interdiffusion, the crystallinity of such Ge/Si heterostructures with Ge-QD's has been studied by RBS/C. Epitaxial Ge layers with nominal thicknesses equivalent to 2, 4, 6, 8 and 10 monolayers, and subsequently epitaxial Si cap layers of 150 nm thick were deposited. Temperatures of 300°C for Ge-MBE and 500°C for Si cap growth provide a very good crystalline structure with embedded Ge films up to 10 ML equivalent thickness. At a Ge growth temperature of 400°C the Ge/Si structure remains crystalline up to 6 ML and at 500°C up to 4 ML of Ge.

Collaboration: *Institute of Semiconductor Physics, Novosibirsk, Russia.

*N.P. Barradas**
*M.F. da Silva**
*J.C. Soares**
*S. Cardoso***
*P.P. Freitas***
U. Kreissig
*W. Arnoldbik****

IBA analysis of complex ultra-thin magnetic layers for spin dependent tunnel junctions

Spin dependent tunnel junctions are of technological interest for applications in magnetic non-volatile random access memories due to their large tunnelling magnetoresistance (TMR) effect and low junction resistance-area product. Typical structures can have 10 to 20 layers with thickness between 10 and 100 Å each. This poses an extreme challenge to the analysis of the layer structure, which is important as it determines the magnetic properties. Spin valves with typical structures are Si/Al_2O_3 600Å/Ta 70Å/NiFe 70Å/CoFe 30Å/$Al_xN_yO_z$ t/CoFe 40Å/MnIr 200Å/Ta 30Å, with t=6-30 Å were analysed with He RBS, heavy ion RBS, and heavy ion ERDA after annealing at temperatures up to 500ºC. Basically, the Al_2O_3 barrier layer remains essentially unchanged on annealing, while after 400°C annealing there is diffusion between the CoFe and MnIr layers. On the contrary, the signals corresponding to the NiFe layer and to the MnIr/Ta and Al_2O_3/CoFe interfaces remain approximately the same after annealing. This explains the changes in the magnetic signal on annealing, in which the magnetic moment of the CoFe layer decreases by a factor of two due to inclusion of Mn. This is accompanied by a reduction and even disappearance of the TMR signal.

Collaboration: *Instituto Tecnologico e Nuclear, Sacavem, Portugal; **Instituto de Engenharia de Sistemas e Computadores, Lisboa, Portugal; ***Debye Institute, Utrecht University, The Netherlands

*L. S. Wielunski**
D. Grambole
U. Kreissig
R. Grötzschel
*G. Harding**

IBA analysis of hydrogen depth profiles in thin metal/hydrocarbon multilayer structures

NRA and ERDA were compared with regard to sensitivity and depth resolution for the analysis of different multilayer structures. Special multilayer samples were produced containing three identical layers of either Al, Cu, Ag, or Au separated by thin hydrocarbon layers. The samples were analyzed by NRA using the sharp resonance at 6.385 MeV of the reaction $^1H(^{15}N, \alpha\gamma)^{12}C$, by 2 MeV He RBS, and by ERDA both with 4.5 MeV He ions and 30 MeV F ions. The best depth resolution and sensitivity was achieved by NRA, however this technique is most time consuming. The He ERDA shows a good depth reso-

lution only near the surface, which is rapidly deteriorated due to multiple scattering. This reduction of depth resolution strongly depends on the sample composition. ERDA with F ions exhibits a hydrogen depth resolution similar to He ERDA, with, however, little dependence on sample composition and depth. For heavy metals multilayers and deep layers heavy ion ERDA is thus advantageous.

Collaboration: *Telecommunication and Industrial Physics Division of CSIRO, Sydney, Australia

S. Parascandola
T. Telbizova
O. Kruse
W. Möller

The influence of the oxygen partial pressure on the ion nitriding of Aluminium – an investigation by means of real-time, in-situ ERDA

Aluminium is known to be a difficult candidate for successful nitriding. It exhibits a dense native surface oxide layer that acts as a barrier for diffusional nitrogen transport. To investigate the influence of the oxygen partial pressure, samples of pure polycrystalline Al were ion nitrided at different oxygen partial pressures from a hot filament ion source. Before and during the nitriding process, depth profiling of nitrogen and oxygen has been performed by real time ERDA. The oxygen partial pressure plays a crucial role for the evolution of the surface oxide layer and thus for the nitriding result. If the surface oxide layer is removed an AlN-layer grows. The experimental evolution of the oxide thickness is in good agreement with semi-quantitative considerations assuming that the oxide thickness is controlled by the interplay of sputtering and oxidation.

*J. Weima**
J. von Borany
U. Kreissig
*W.R. Fahrner**

Surface analysis of steel plates used for polishing of diamond

Recently, ultra precise polishing of diamond with an average surface roughness of < 2 nm by a thermochemical polishing technique has been developed. During polishing at temperatures between 700-950 °C in an Ar(96%)/H_2(4%) atmosphere for several hours the diamond film is sandwiched between a rotating and ultrasonically driven steel plate and an upper steel weight. SEM, ERDA and Micro-Raman spectroscopy have been applied to characterize the surface composition and morphology of the polishing steel plates for both the virgin case and after polishing. The ERDA measurements reveal (i) an increase of the bulk carbon concentration in the steel to a value of about 10 at.%, and (ii) a significant enhancement of the carbon level in a near surface region (< 250 nm depth) ranging from 10…80 at.% depending on the polishing time (1-8 h). The latter effect is due to segregations from carbon above the solubility level. Raman spectra of the steel plates show graphite bands and C-H_n complexes at exactly the wave numbers as they appear on the diamond samples after polishing. The results agree very well with the assumption, that the thermochemical polishing is based on a catalytic conversion of diamond into non-diamond carbon at elevated temperatures and the subsequent dissolution of carbon into the polishing plates.

Supported by BMBF

Collaboration: *FernUniversität Hagen, Fakultät für Elektrotechnik

*A. Ulyashin**
J. von Borany
D. Grambole
F. Herrmann
U. Kreissig
*R. Job**
*W. R. Fahrner**

Hydrogen redistribution, nano-void and nano-cavity formation in hydrogen plasma treated Czochralski (Cz) -Silicon

The evolution of the H concentration during the post-hydrogenation annealing is one of the important parameters of H plasma treatments widely used in semiconductor technology. To investigate this evolution as well as the modification of the properties of the Cz-Si after post-hydrogenation annealing Raman spectroscopy, spreading resistance probe (SRP) analysis, SEM, ERDA and NRA studies were carried out on H plasma treated and annealed p-type Cz-Si. The samples were treated by a 110 MHz hydrogen plasma at 260°C and annealed at temperatures between 400 and 600°C. Raman spectroscopy and ERDA analysis reveal the formation of nanovoids filled with H molecules after plasma hy-

drogenation, which can not released from the voids at 400°C annealing. The H release as well as the empty nanocavities formation was observed after 600°C annealing at appropriate annealing times. Moreover, SEM analysis shows the formation of nanostructured layers in the subsurface region with a thickness of about 100 nm. ERDA and NRA investigations show a H accumulation (up to 2 at.%) in this thin layer. At 400°C annealing H diffuses into the bulk of the Cz-Si substrate and enhances the formation of thermal donors (TD). It was shown that by such a hydrogen enhanced TD formation a low-temperature doping and p-n junction formation is possible.

**Collaboration: ***Fernuniversität Hagen, Fakultät für Elektrotechnik

*P. Danesh**
*B. Pantchev**
D. Grambole
B. Schmidt

NRA study of hydrogenated amorphous silicon

Hydrogenated amorphous silicon (a-Si:H) is widely used for photovoltaic devices. The usual method for its deposition is PECVD from pure silane. Recently, the use of strong dilution of silane by hydrogen has attracted much attention due to the fact that such films exhibit an improved stability against prolonged light soaking.

Nuclear reaction analysis using the $^{1}H(^{15}N, a?)^{12}C$ resonance reaction was used to determine the H-content and its distribution in a-Si:H films prepared by PECVD (10% silane diluted in hydrogen) for various deposition temperatures (150-270°C). The H-distribution was studied in films with different thickness (100-500 nm) corresponding to growth durations of 4-20 min, respectively. The H-concentration in the films is about 15 at% with a uniform depth distribution independent of the film thickness. A slightly increased hydrogen content of about 18 at% is observed for a deposition temperature of 150°C.

**Collaboration: ***Bulgarian Academy of Sciences, Institute of Solid State Physics, Sofia, Bulgaria

*A. Golanski **
*F. Piazza **
D. Grambole
F. Herrmann

Incorporation of hydrogen into (t)a-C:H thin films deposited by a DECR plasma

The nuclear reaction $^{1}H(^{15}N,a?)^{12}C$ is used to investigate the relationship between the key parameters of the ECR plasma deposition process and the corresponding H-content in (t)a-C:H thin films. The D(istributed)ECR source operates at 2.45 GHz. Acetylene as precursor gas and a negative 13.56 MHz RF bias between -10 and -600 V at the substrate holder were applied. Under constant bias the amount of integrated hydrogen is proportional to the pressure and does not reflect the evolution of the ion current density, suggesting the hydrogen integration be controlled by chemisorption. With increasing bias the hydrogen concentration decreases. The chemisorption is now in competition with the bias-dependent desorption of hydrogen induced by atomic collisions. Under the present experimental conditions the dynamic equilibrium between chemisorption and desorption sets the minimum H content at about 20 at.%. The release of hydrogen enables more carbon to be integrated into the carbon network. Consequently hydrogen release is directly related to the growth rate. An appropriate choice of the process parameters enables the growth rate to be maximised and the hydrogen content to be reduced.

Collaboration: *Centre National de la Recherche Scientifique (CNRS), Laboratoire PHASE, Strasbourg, France

F. Herrmann
D. Grambole
R. Grötzschel

Lattice destruction during micro-channeling measurements

For extremely high dose rates up to 10^{19} $cm^{-2}s^{-1}$, which can be achieved by focused ion beams (FIB) with sub-µm beam diameters, the degree of post-implantation damage in semiconductor crystals depends on the dose rate, which can be investigated using a nuclear microprobe for RBS/C. But here, damage caused by the analysing beam must be considered, as the fluence of the light ions used for analysis is orders of magnitude higher than in ordinary RBS/C

experiments. The near-surface damage accumulation in 6H-SiC by H, He and Li ions of various energies both was studied both for channeling and random incidence. The fluence dependence of the damage accumulation, observed with beams in the MeV region, is much smaller than that at low and medium ion energies. The damage level observed by RBS/C appears to saturate at χ_{min} values far below unity. The effect of the lattice distortion by the implanted hydrogen due to swelling, bubble formation, precipitation etc. exceeds by far the ballistic disorder and is more pronounced than in the case of He or Li ions.

D. Jembrih,****
C. Neelmeijer
*M. Schreiner**
M. Mäder
*M. Ebel****
*R. Svagera****
*M. Peev***

Iridescent Art Nouveau Glass - IBA and XPS for the characterization of thin iridescent layers

Characterisation of thin iridescent layers in a non-destructive manner is an important tool to examine their manufacturing process from intact originals. The Rossendorf external proton beam was used for non-destructive and simultaneous PIXE and RBS measurements on Art Nouveau artefacts produced around 1900 by companies such as Tiffany/USA and Loetz/ Austria. PIXE identified a silver, tin and lead containing silicate glass. The characteristic surface signal of the corresponding RBS spectra could be interpreted as resulting from tin embedded in a surface layer of 20-300 nm thickness, when making use of XPS results which identified the outermost material to consists of SnO_2. In addition, the presence of a transition region between the SnO_2 layer and the glass bulk was identified by RUMP simulations. Approximately 80% of the total amount of tin was found to be located in this transition layer and only 10-20% in the top surface region.

Collaboration: *Institut für Farbenchemie, Akademie der Bildenden Künste, Wien, Österreich, **Österreichisches Forschungszentrum Seibersdorf, Österreich, ***Institut für Angewandte und Technische Physik, TU Wien, Österreich

M. Mäder
C. Neelmeijer
*H. Ricke**

Classification of glass artefacts using non-destructive ion beam analysis

Chemical composition analysis of artistic and historical objects, including glassware, assists in clarifying their authenticity and provenience. Regarding their characteristic chemical components glass objects can be classified into different glass families, which allows some rough dating of glass artefacts due to their chronology. Three glass beakers (Kunstmuseum Düsseldorf) were successfully investigated by using simultaneous PIXE, PIGE, and RBS for nondestructive composition analysis at the external proton beam. Clear distinctions between the beakers can be made not only by stylistic criterions but also by their different chemical composition. According to the analytical results, two of them, attributed to the 15^{th} century, are typical woodash-lime-silica glasses with a high amount of K_2O and CaO. In contrast to that, the third glass is characterised by a high sodium content, but the composition is not comparable with the ancient glasses. Only in this glass chromium was detected as origin of the green colour. Consequently, the beaker should have been manufactured in the 19^{th} century or later.

Supported by BMBF

Collaboration: *Kunstmuseum Düsseldorf, Bundesanstalt für Materialforschung und –prüfung Berlin, Kunstgewerbemuseum Dresden-Pillnitz

Focused Ion Beam

Ch. Akhmadaliev
L. Bischoff
J. Teichert
*K. Kazbekov**
*B. Köhler***

Ion acoustic microscopy for imaging of buried structures based on a focused ion beam system

An intensity modulated focused ion beam (FIB), which is hitting the surface of a solid, leads to a small temperature variation in the near subsurface region sufficient for thermal elastic wave generation. The measurement of these waves can be used for analysis and imaging of surface as well as subsurface structures in the material. The modified FIB equipment IMSA-100, working with 35 keV Ga^+ and Au^+ ions and an ion beam current of about 3 nA, was employed to obtain acoustic images from structures on silicon and glass targets. The acoustic signals were detected using a PZT transducer delivering an output voltage of about 50-100 nV. The beam modulation frequency was varied in the range of 60 - 170 kHz. The obtained lateral resolution of the ion acoustic images at these frequencies was about 15 µm on silicon and about 7 µm on glass. We are going to increase the modulation frequency up to the MHz range in order to reach sub-micron resolution.

Supported by DFG and DAAD

Collaboration: *Kazakh National Technical University, Almaty, Kazakhstan, **Fraunhofer-Institut für zerstörungsfreie Prüfverfahren, EADQ Dresden

Ch. Akhmadaliev
L. Bischoff
*K. Kazbekov**
*B. Köhler***

Investigation of piezoelectric detectors for the registration of ion beam induced elastic waves

The aim of this work was to develop a highly sensitive detection system for the registration of elastic waves generated by an intensity modulated focused ion beam (FIB). The maximum excitation power of the used Au^+ ion beam reached on the IMSA-100 FIB system is about 100 µW and therefore the corresponding generated acoustic signal has a very low amplitude. As a suitable sensor for such low amplitude acoustic vibration on the surface of a sample a lead-zirconium-titanium (PZT) piezoelectric transducer was chosen. Two types of PZT materials with mechanical quality factors of 100 and 1000 were tested in different geometric configurations and with different types of glue for fixing the sensor on the sample surface. The resonance behaviour was experimentally determined as well as theoretically described. Additionally a low noise integrated pre-amplifier with an amplification factor of about 10^5 was designed. As a result of this investigation a sufficient electrical signal response from the detector for ion-acoustic imaging of microstructures with micrometer resolution was obtained at blanking frequencies up to 200 kHz.

Supported by DFG and DAAD

Collaboration: *Kazakh National Technical University, Almaty, Kazakhstan, **Fraunhofer-Institut für zerstörungsfreie Prüfverfahren, EADQ Dresden

*J. Martin**
L. Bischoff
*R. Wannemacher**

Microscopy of focused ion beam generated fluorescent colour centre patterns in LiF

Colour centres have been generated on [100] surfaces of LiF crystals by irradiation with the FIB system IMSA-100 using 35 keV Ga^+ ions at room temperature and at 240 K. For this purpose a cooling target holder working with a Peltier element was constructed. By imaging microscopy as well as by laser scanning confocal microscopy (excitation wavelength: 457.9 nm) the luminescence of two centres at 655 nm and 540 nm ascribed to F_2 and F_3^+ vacancy complexes, respectively, has been detected and spatially resolved with a resolution of about 1 µm. Diffusion and pinning of colour centres have been observed directly in this way. Due to the high intensity in the focal spot of the confocal microscope, nonlinear photophysical and photochemical processes are observed. For example, an additional emission at 775 nm could be detected at high excitation density. The luminescence band is tentatively ascribed to a radiative triplet-triplet emission of F_2 centres after recombination of F_2^+ centres

with an electron.

Collaboration: *Institut für Physik, Technische Universität Chemnitz

L. Bischoff
J. Teichert

Alloy liquid metal ion sources for FIB implantation of erbium

For focused ion beam applications of Erbium as well as of several metal ions which are of interest for optical and semiconductor investigations, a LMIS operating with an Er-stainless steel alloy was developed and investigated. This alloy consists of a mixture of $Er_{70}Fe_{22}Cr_5Ni_3$ and has a melting point of about 860°C. Additionally an $Er_{69}Ni_{31}$ alloy was used for source preparation. The melting temperature at the eutectic composition amounts to 765°C. Both wetted needle type tungsten emitters showed a stable emission behaviour down to 1µA emission current. The I-V characteristics, the temperature dependence of the extraction voltage, the mass spectrum, and the energy spread of the main beam components were investigated as a function of the emission current. While in the case of the $Er_{70}Fe_{22}Cr_5Ni_3$ alloy the singly charged metal ions in the beam are not well defined due to isotope interference, i.e. m/q (Er^{3+}) = m/q (Fe^{+}), for doubly charged ions clearly separated species are available for focused ion beam applications.

Others

*T. Michely**
*M. Kalff***
*G. Comsa****
M. Strobel
K.-H. Heinig

Step edge diffusion and step atom detachment in surface evolution: Ion erosion of Pt (111)

The temperature dependent morphological evolution of Pt (111) under 1 keV Xe^+ ion bombardment has been investigated up to 600 removed monolayers. By a comparision of STM investigations and kinetic Monte Carlo simulations, a coarsening of the surface structures during erosion and a qualitative change in roughness evolution between 650 K and 700 K are found to be caused by two different atomic processes: the former by diffusion of atoms along steps, while the latter by the onset of step atom detachment.

Collaboration: *I. Physikalisches Institut, RWTH-Aachen, **Forschungszentrum Jülich, ***Universität Bonn

M. Strobel,**,****
K.-H. Heinig
*T. Michely****

Mechanisms of pit coarsening in ion erosion of fcc (111) surfaces: a kinetic 3D lattice Monte-Carlo study

Ion erosion of fcc (111) surfaces was studied by atomic computer simulations. In a fully 3D kinetic lattice Monte-Carlo model thermodynamically activated processes like adatom, step-edge or surface-vacancy diffusion were combined with ballistic effects due to single ion impacts, i.e. sputtering, adatom and surface-vacancy generation. In the course of erosion nucleation of surface vacancy islands, their growth, both laterally and vertically, and subsequent coarsening of these pits was observed. For removal of up to 6 monolayers the evolution of the surface is characterized in terms of the roughness and height-height-correlation function. The simulation results were compared with low-energy noble gas ion erosion experiments of Pt (111) surfaces. By explicitly tuning specific atomic transitions within the simulation it was demonstrated, that forbidden thermal adatom generation does hardly influence the surface evolution. Suppressed step-edge diffusion, however, considerably slows down pit coarsening and impedes pit shape relaxation, emphasizing the importance of this smoothening process in ion erosion.

Collaboration: *I. Physikalisches Institut, RWTH Aachen, **CNR-IMETEM, Catania, Italy, *** MIRIAM, University of Milano, Italy

T. Hauschild
*M. Jentschel**
*H. Börner**
K.-H. Heinig
W. Möller

Crystal-GRID: What can we learn about interatomic solid state potentials?

Crystal-GRID is a new and complementary method for studying interatomic solid-state potentials in the energy range from 1 eV to 1 keV. Systematic investigations were performed in order to specify the monocrystalline solids, which are suited for Crystal-GRID experiment due to their capture cross section for thermal neutrons, nuclear level lifetime and de-excitation cascade. The influence of the nuclear level lifetime and the interatomic potential on the γ-line-shape was re-examined. Crystal-GRID spectra of ZnS and TiO_2 were measured for the first time or with higher precision (count rates). For these two crystals it was possible to extract the nuclear level lifetime and the screening length of the Coulomb potential simultaneously from one experiment.

Collaboration: *ILL Grenoble, France

F. Prokert
*J. Piekoszewski**
*Z. Werner**

XRD study of Ti / Pd layers prepared by pulsed plasma beam in Ti substrate

The corrosion resistance of Ti windows (used in the electron-beam dry scrubber process for pollutants removal) in sulphuric acid can be improved by alloying with palladium. For this reason samples prepared by the pulsed plasma beam technique were investigated. The plasma pulses are generated by a low pressure, high-current discharge between two concentric sets of electrodes. The

pulses induce a near surface temperature near the melting point, thus enhancing rapid diffusion of alloying elements. Pd-Ti alloy surface layers in Ti formed by N- and Ar-ion pulse plasma alloying of Pd films deposited by pulse erosion of Pd electrode tips were studied by GIXRD using small incidence angles (1.5°-3.0°). The detected intensity originates mainly from the about 2 µm thick surface layer. Besides the hcp α-Ti two cubic Pd-Ti phases PdTi (PDF 23-1300, a=0.3180 nm) and Pd_3Ti (PDF 46-1036, a=0.3843 nm) were identified. From the peak broadening of the Bragg reflections one estimates that the grain size of these two phases is in the range of 20 – 30 nm in contrast to the grain size of the α-Ti, which is about one order larger.

Collaboration: *Andrzej Soltan Institute for Nuclear Studies, Otwock-Swierk, Poland

*Yu. Ivanov**
W. Matz
*V. Rotshtein**
R. Günzel
N. Shevchenko

Structural changes and improved wear resistance of high-speed steel after pulsed electron beam surface melting

By pulsed irradiation with an intense electron beam (20-30 keV, 2.5 µs, 3-18 J/cm^2) the surface of high speed steel is temporarily melted. The surface and phase structure of the steel was characterised by SEM, TEM, and XRD in dependence on the energy density. The unirradiated material is structural α-iron with carbide inclusions of M_6C type (M = W, Mo). The carbide particles are visible on the surface. With increasing electron density the carbide particles are dissolved and the surface layer changes step by step to γ-iron (austenite). At about 10 J/cm^2 both same amounts of α- and γ-iron are in a surface layer of 1 µm thickness while the surface carbide is fully dissolved. At electron densities above 12 J/cm^2 the surface layer consists of sharply defined cells of γ-iron, with very thin carbide films at their interface. A wear test with a drill showed a reduction of abrasive wear by a factor of 2 for the irradiation density of 7 J/cm^2. This is the region just before the full dissolution of the carbide particles M_6C. Thus, the formation of a strong interface region between carbide and α-iron matrix may explain the increased wear resistance.

Collaboration: *Institute of High-Current Electronics, Sibirian Branch, Russian Academy of Sciences, Tomsk

H. Reuther
*G. Behr**
*A. Teresiak**

Determination of the hyperfine parameter of α-$FeSi_2$ by angle dependent Mössbauer spectroscopy on single crystals

The hyperfine parameters of the metallic disilicide phase α-$FeSi_2$ at room temperature are determined with high accuracy by CEMS measurements on a single crystal. The single crystal was obtained by a chemical transport reaction in closed silica ampoules starting from a mixture of ^{57}Fe and Fe (5N purity) and Si (6N purity) as source materials and I_2 as the transport medium. For the CEMS measurements, the single crystal was tilted by several angles with respect to the direction of the exciting gamma radiation. Tilting in regard to the main c-axis changed the spectrum dramatically while turning around the c-axis had no effect. The best fit for all spectra was obtained by assuming exactly four single lines. Due to their intensity variations as a function of the orientation they could unambiguously be combined to quadrupole doublets, which can be ascribed to two well defined iron environments with different electron densities (isomer shifts 0.202 and 0.257 mm/s, respectively) and different electric field gradients. The environments differ by having one or none iron vacancy as next neighbour. Both quadrupole splittings are negative (-0.382 and -0.730 mm/s, respectively). The site occupation for both sites is different.

Collaboration: *Institut für Festkörper- und Werkstofforschung Dresden

F. Prokert
*I. Stephan**
A. Scholz

Determination of temperatures in the irradiation channels of the former Rheinsberg WWER-2 reactor

Temperature measurement by thermocouples fails in strong neutron fields of a reactor. Diamond powder has proved as a good temperature indicator if the neutron fluence is known. By post irradiation annealing the induced Frenkel defects recover which is projected on the lattice parameter. Thus the effective irradiation temperature can be extrapolated from the variation $a=a(T)$. For the accurate determination of the lattice parameter a the high-indexed reflections of diamond powder were measured at RT using a D5000 diffractometer. The quartz capillary with the sample was positioned along the rotation axis of the θ-θ-circles allowing a quick and reproducible change of samples during the 10 iterative tempering (from RT up to 550 °C; 2h) – measuring cycles. To reach sufficient statistical accuracy, 6 samples, comparable in temperature and radiation conditions, from channels 21 & 22 and channels 8,9 & 17, respectively, were selected into two series. The onset T_e of reduction of the lattice parameter was extrapolated to 327 °C and 325 °C, respectively, with an accuracy of about 5%. The real temperature in the reactor, T_r, follows from T_e by a correction taking into account the local neutron flux density at the irradiation position.

Collaboration: *Institut für Sicherheitsforschung, FZR

Equipment

M. Friedrich
W. Bürger
S. Turuc

Operation and development of the electrostatic accelerators

At the 2 MV VdG accelerator a Wennerlund charging belt and a belt from IPPE Obninsk/ Russia have been tested. Due to the short lifetime of the belt from IPPE the VdG has been operated since these tests with a Wennerlund belt. A mechanical valve was installed inside the terminal to stabilise the source gas inlet.

The 5 MV tandem has been applied mainly for ion beam analysis. A duoplasmatron ion source (Efremov Institute St. Petersburg) with Li charge exchange canal for generation of negative He ions was put into operation. At the duoplasmatron injector the control system and the power supplies have been modernised. For high-energy ion implantation a dedicated beam line and an irradiation chamber has been built up. The mechanical construction of the beam line from the tandem to the magnetic spectrometer for high-resolution ERDA measurements was finished. At the beginning of September the accelerator was shut down for an exchange of the original inclined field accelerating tubes (after 25 years operation!), by straight field tubes with magnetic electron suppression (HVEE) to increase the terminal voltage and to improve the acceleration of heavy ions with high charge states. Due to some production faults causing glass insulator cracks during installation, the tube exchange could not finished in 2000.

The 3 MV Tandetron has been applied mainly for high-energy implantation and ion beam analysis. No remarkable problems have appeared during its operation.

In 2000 the total operating hours of the high energy accelerators were 1147 h (VdG), 2805 h (Tandetron) and 1374 h (Tandem, up to September).

M. Friedrich
W. Pilz
*R.-D. Penzhorn**
*N. Bekris**
*V. Liechtenstein***

Tritium Detection by accelerator mass spectrometry (AMS)

The activities on tritium depth profiling by AMS have been continued routinely at the new air insulated 100 kV tandem accelerator. In collaboration with the Forschungszentrum Karlsruhe high-level samples from JET Culham/UK have been investigated. During these measurements the 100 kV tandem accelerator was equipped with a nitrogen gas stripper. In collaboration with the RRC Kurchatov Institute Moscow diamond-like carbon (DLC) stripper foils have been tested. Due to the higher stripper efficiency and the improved vacuum inside the beam line the transmission of the accelerator has been increased from 30% to 60%, and the background caused by molecular ions has been strongly reduced. The construction of a new compact 100 kV tandem accelerator equipped with a DLC stripper foil (1 $\mu g/cm^2$) and a SF_6 insulated short acceleration structure has been commenced.

Collaboration: *Tritiumlabor, Forschungszentrum Karlsruhe, **RRC Kurchatov Institute Moscow

J.R. Kaschny
R. Kögler
H. Tyrroff
W. Bürger
W. Skorupa

The Rossendorf double implantation facility

As part of the Rossendorf dual-beam facility, the double implantation chamber (DIC) allows the simultaneous implantation of materials using two ion beams. This station is located at the 45°-cross point of two beam lines, one from a single ended HVEE 500 kV ion implanter and the other from a HVEE 3 MV Tandetron accelerator. Each beam line is equipped with independent ion fluence and current measurement control. The special design of the beam sweeping system enables to scan both beams simultaneously over the target material up to 2 cm^2 in synchronous mode, i.e., both ion spots are kept at coincident positions over the target surface. At the present status, the implantation can be performed in a temperature range between room temperature and T? 500°C.

With only small modifications this experimental setup can also be used for in-situ or subsequent ion implantation and ion beam analysis (RBS). A new cooling stage will allow low-temperature implantation as well as implantation up to T . 500°C. Preliminary experiments about the formation of SiC precipitates by simultaneous high dose C- and Si-implantation into a Si-substrate are in progress.

W. Matz
*J. Bottiger**
W. Neumann
*J. Chevallier**
N. Schell

A sputter deposition chamber for in-situ observation of thin film growth by synchroton radiation scattering

A small and cheap sputter deposition chamber was designed to fit in a conventional Huber 6-circle goniometer existing at ROBL, which is also used for other experiments. In order to get as much as possible information on the growth process the chamber allows for the following types of experiments: (i) symmetric XRD in order to measure out of plane lattice constants and texture effects; (ii) GIXRD to study the crystallisation of very thin films and suppress the substrate scattering; (iii) reflectometry for the determination of film thickness and interface roughness; (iv) grazing incidence – grazing exit diffraction for the determination of lattice constants, stress and preferred orientation perpendicular to the surface; (v) crystal truncation rod (CTR) scattering. The chamber is equipped with 2 magnetrons located in 100 mm distance from the substrate under an inclination angle of 30° each. The substrate can be biased and heated up to 650°C. Although the angular ranges of the radiation windows are limited, a wide variety of materials can be studied by adapting the synchrotron radiation wavelength according to the lattice parameters. First successful in-situ experiment of depositing TiN on Si has shown that all design goals have been achieved.

Collaboration: *University of Aarhus, Institute of Physics and Astronomy, Aarhus, Denmark

T. Telbizova
T. Chevolleau

Characterization of the ion beam extracted from a hot filament ion source

A hot filament ion source (Kaufman type) has been employed for ion nitriding of Al using N_2. The determination of the identity and energy distribution of ions hitting the sample is crucial for a better understanding of the nitriding process. Therefore the ion beam has been characterized by an energy selective mass spectrometer (HIDEN EQP500), known as plasma monitor, which was located in the position of the sample holder for nitriding. The analysis shows that the beam consists of 80% N_2^+ ions and 20% N^+ ions. No other ionic species have been detected, which indicates a low amount of contamiants. For each ionic species, energy distribution consists of a single narrow peak with a full width at half maximum of about 10 eV and the mean ion energy corresponds to the accelerating potential. These results show that the energy distribution can be considered as monoenergetic and no significant collisions occur between ions and neutrals in the beam.

Glossary

AES	Auger electron spectroscopy
AFM	Atomic force microscopy
CEMS	Conversion electron Mössbauer spectroscopy
CV	Capacitance-voltage-characteristics
CVD	Chemical vapour deposition
ECR	Electron-cyclotron-resonance
ERDA	Elastic recoil detection analysis
ESRF	European Synchrotron Radiation Facility, Grenoble
FEG	Field emission gun (at the TEM)
FIB	Focused ion beam
FTIR	Fourier transform infrared spectroscopy
GDOS	Glow discharge optical spectroscopy
GIXRD	Gracing incidence X-ray diffraction
GMR	Giant magnetoresistance
GRID	Gammy-ray induced Doppler-broadening
IBA	Ion beam analysis
HSS	High speed steel
IV	Current-voltage-characteristics
NRA	Nuclear reaction analysis
PDF	Powder diffraction file
PECVD	Plasma enhanced chemical vapour deposition
PIGE	Proton-induced Gamma-ray emission
PIII	Plasma immersion ion implantation
PIXE	Proton-induces X-ray emission
PVD	Physical vapour deposition
ROBL	ROssendorf BeamLine (at the ESRF)
RBS	Rutherford backscattering spectroscopy
RBS/C	Rutherford backscattering spectroscopy under channelling conditions
RTA	Rapid thermal annealing
SEM	Scanning electron microscopy
SPIS	Slow positron implantation spectroscopy
SQUID	Superconducting quantum interferometer device
STM	Scanning tunnel microscope
TEM	Transmission electron microscopy
XPS	X-ray photoelectron spectroscopy
XRD	X-ray diffraction
XTEM	Cross-section transmission electron microscopy

Publications

Abramof, E., Beloto, A.F., Ueda, M., Gomes, G.F., Berni, L.A., Reuther, H.,
Analysis of X-ray rocking curves in (001) silicon crystals implanted with nitrogen by plasma immersion ion implantation,
Nucl. Instr. Meth. B **161-163** (2000) 1054

Barradas, N.P., Khan, R.U.A., Anguita, J.V., Silva, S.R.P., Kreissig, U., Grötzschel, R., Möller, W.,
Growth and characterization of amorphous carbon films doped with nitrogen,
Nucl. Instr. Meth. B **161-163** (2000) 969

Barradas, N.P., Parascandola, S., Sealy, B.J., Grötzschel, R., Kreissig, U.,
Simultaneous and consistent analysis of NRA, RBS and ERDA data with the IBA datafurnace,
Nucl. Instr. Meth. B **161-163** (2000) 308

Barson, S.D., Skeldon, P., Thompson, G.E., Kolitsch, A., Richter, E., Wieser, E., Piekoszewski, J., Chmielewski, A.G., Werner, W.,
Investigation of ion assisted palladium treatments for improved corrosion resistance of titanium foil in the electron beam dry scrubber process,
Surf. Coat. Technol.**127** (2000) 179

Barson, S.D., Skeldon, P., Thompson, G.E., Piekoszewski, J., Chmielewski, A.G., Werner, Z., Grötzschel, R., Wieser, E.,
Corrosion protection of titanium by pulsed plasma deposition of palladium,
Corrosion Sci. **42** (2000) 1213

Behrisch, R., Mayer, M., Jacob, W., Assmann, W., Dollinger, G., Bergmaier, A., Kreissig, U., Friedrich, M., Sun, G., Hildebrandt, D., Akbi, M., Schneider, W., Schleussner, D., Knapp, W., Edelmann, C.,
Quantitative analysis of deuterium in a-C:D layers, a Round Robin experiment,
J. Nucl. Mat. **281** (2000) 42

Berberich, F., Matz, W., Richter, E., Schell, N., Kreissig, U., Möller, W.,
Structural mechanisms of the mechanical degradation of Ti-Al-V alloys: in situ study during annealing,
Surf. Coat. Technol. **128-129** (2000) 450

Berni, L. A., Ueda, M., Gomes, G. F., Beloto, A. F., Reuther, H.,
Experimental result of a DC glow discharge source with controlled plasma floating potential for plasma immersion ion implantation,
J. Phys.D: Appl.Phys. **33** (2000) 1592

Bischoff, L., Teichert, J., Hausmann, S., Ganetsos, Th., Mair, G.L.R.,
Investigation and optimization of the emission parameters of alloy liquid metal ion sources,
Nucl. Instr. Meth. B **161-163** (2000) 1128

Bischoff, L., Teichert, J., Hausmann, S., Ganetsos, Th., Mair, G.L.R.,
Temperature and energy spread investigations of alloy LMIS,
Microel. Eng. **53** (2000) 613

Bischoff, L., Ganetsos, Th., Teichert, J., Mair, G.L.R.,
Temperature dependence of emission spectra of liquid metal alloy ion sources,
Nucl. Instr. Meth. B **164-165** (2000) 999

Bischoff, L., Ganetsos, Th., Teichert, J., Mair, G.L.R.,
Temperature dependence of the electric characteristics of liquid metal alloy ion sources,
J. Phys.D: Appl. Phys. **33** (2000) 692

Bischoff, L., Teichert, J.,
Liquid metal ion source working with an $Er_{70}Fe_{22}Ni_5Cr_3$ alloy,
J. Phys. D: Appl. Phys. **33** (2000) L69

Brauer, G., Anwand, W., Nicht, E.-M., Kuriplach, J., Prochazka, I., Becvar, F., Osipowicz, A., Coleman, P.G.,
Characterization of RF-sputtered platinum films by positron annihilation spectroscopy,
Phys. Rev. B **62** (2000) 5199

Chevolleau, T., Fukarek, W.,
Ion flux, ion energy distribution and neutral density in an inductively coupled argon discharge,
Plasma Sources Sci. Technol. **9** (2000) 568

Fichtner, P.F.P., Peeva, A., Behar, M., de M. Azevedo, G., Maltez, R. L., Koegler R., Skorupa, W.,
He-induced cavity formation in silicon upon high-temperature implantation,
Nucl. Instr. Meth. B **161-163** (2000) 1038

Fichtner, P.F.P., Behar, M., Kaschny, J.R., Peeva, A., Koegler, R., Skorupa, W.,
Copper gettering at half of the projected ion range induced by low - energy channelling He implantation into silicon,
Appl. Phys. Lett. **77** (2000) 972

Fitting, H.-J., Barfels, T., Trukhin, A. N., Schmidt, B.,
Cathodoluminescence of crystalline and amorphous SiO_2 and GeO_2,
J. Non-Cryst. Sol. **279** (2000) 51

Fitz, C., Fukarek, W., Kolitsch, A., Möller, W.,
Investigation on stress evolution in boron nitride films,
Surf. Coat.Technol. **128-129** (2000) 292

Fitz, C., Fukarek, W., Kolitsch, A., Möller, W.,
An instrument for in-situ stress measurement in thin films during growth,
Surf. Coat. Technol. **128-129** (2000) 474

Friedrich, M., Pilz, W., Sun, G., Behrisch, R., Garcia-Rosales, C., Bekris, N., Penzhorn, R.-D.,
Tritium depth profiling in carbon by accelerator mass spectrometry,
Nucl. Instr. Meth. B **161-163** (2000) 216

Friedrich, M., Pilz, W., Sun, G., Behrisch, R., Garcia-Rosales, C., Bekris, N., Penzhorn, R.-D.,
Tritium depth profiling in carbon samples from fusion experiments,
Nucl. Instr. Meth. B **172** (2000) 655

Fukarek, W., Fitz, C., Kolitsch, A., Möller, W.,
In situ measurement of stress during deposition of boron nitride films,
Mat. Sci. Forum **347-349** (2000) 256

Gebel, T., Panknin, D., Riehn, R., Parascandola, S., Skorupa, W.,
Application and improvement of the spreading resistance method for p-type 6H-SiC,
Mat. Sci. Forum **338-342** (2000) 741

Grambole, D., Neelmeijer, C., Noll, K., Herrmann, F.,
$^{19}F(p,p'\gamma)^{19}F$ and $^{18}O(p, \gamma)^{19}F$ gamma-ray interferences studied on liquids,
Nucl. Instr. Meth. B **161-163** (2000) 269

Grigull, S., Parascandola, S.,
Ion-nitriding induced plastic deformation in austenitic stainless steel,
J. Appl. Phys. **88** (2000) 6925

Groß, B., Engeldinger, J., Grambole, D., Herrmann, F., Hempelmann, R.,
Dissociative water vapour absorption in $BaZr_{0.85}Y_{0.15}O_{2.925}/H_2O$: pressure-compositions isotherms in terms of Fermi-Dirac statistics,
Phys. Chem. Chem. Phys. **2** (2000) 297

Gueorguiev,Y.M., Kögler, R., Peeva, A., Panknin, D., Mücklich, A., Yankov, R.A., Skorupa, W.,
High-energy ion-implantation-induced gettering of copper insilicon beyond the projected ion range: The trans-projected-range effect,
J. Appl. Phys. **88** (2000) 5645

Gueorguiev,Y.M., Kögler, R., Peeva, A., Panknin, D., Mücklich, A., Yankov, R.A., Skorupa, W.,
Trans-projected-range gettering of copper in high-energy ion-implanted silicon,
J. Appl. Phys. **88** (2000) 6934

Hatzopoulos, N., Skorupa, W., Siapkas, D.I.,
Double SIMOX structures formed by sequential high energy oxygen implantation into silicon,
J. Electrochem. Soc. **147** (2000) 354

Hausmann, S., Bischoff, L., Teichert, J., Voelskow, M., Möller, W.,
Dwell-time related effects in focused ion beam synthesis of cobalt disilicide,
J. Appl. Phys. **87** (2000) 57

Hecker, M., Tietjen, D., Prokert, F., Schell, N., Schneider, C. M.,
Investigation of Co/Cu/NiFe-multilayers by x-ray reflectometry and diffraction,
Mikrochim. Acta **133** (2000) 239

Heera, V., Reuther, H., Stoemenos, J., Pécz, B.,
Phase formation after high dose Al implantation into SiC,
J. Appl. Phys. **87** (2000) 78

Heera, V., Skorupa, W., Pécz, B., Dobos, L.,
Ion beam synthesis of graphite and diamond in silicon carbide,
Appl. Phys. Lett. **76** (2000) 2847

Heera, V., Fontaine, F., Skorupa, W., Pécz, B., Barna, A.,
Ion-beam synthesis of epitaxial silicon carbide in nitrogen-implanted diamond,
Appl. Phys. Lett. **77** (2000) 226

Hempel, A., Saneyasu, M., Tang, Z., Hasegawa, M., Brauer, G., Plazaola, F., Yamaguchi, S., Kawai, A.
Effects of neutron irradiation on Fe-Cu model alloys and RPV steels probed by positron and hardness measurements,
in: Effects of radiation on materials. 19th Int. Symp., Seattle/WA 1998, eds. M.L. Hamilton, A.S. Kumar, S.T. Rosinski, M.L. Grossbeck, ASTM STP 1366 (American Society for Testing and Materials, West Conshohocken/PA, 2000) 560

Heß, G., Bauer, A., Kräußlich, J., Fissel, A., Schröter, B., Richter, W., Schell, N., Matz, W., Goetz, K.,
Si/Ge-nanocrystals on SiC(0001),
Thin Solid Films **380** (2000) 86-88

Höfgen, A., Heera, V., Mücklich, A., Skorupa, W.,
Ion beam induced nanocrystallization of SiC,
Mat. Sci. Forum **338** (2000) 897

Höfgen, A., Heera, V., Mücklich, A., Eichhorn, F., Skorupa, W.,
Ion beam induced crystal grain nucleation in amorphous silicon carbide,
Nucl. Instr. Meth. B **161-163** (2000) 917

Hornauer, U., Günzel, R., Reuther, H., Richter, E., Wieser, E., Möller, W., Schumacher, G., Dettenwanger, F., Schütze, M.,
Protection of gamma-based TiAl against high temperature oxidation using ion implantation of chlorine,
Surf. Coat. Technol. **125** (2000) 89

Hornauer, U., Richter, E., Matz, W., Reuther, H., Mücklich, A., Wieser, E., Möller W., Schumacher, G., Schütze, M.,
Microstructure and oxidation kinetics of intermetallic TiAl after Si- and Mo- ion-implantation,
Surf. Coat. Technol. **128-129** (2000) 418

Jäger, H. U., Albe, K.,
Molecular-dynamics simulations of steady-state growth of ion-deposited tetrahedral amorphous carbon films,
J. Appl. Phys. **88** (2000) 1129

Kachurin, G.A., Rebohle, L., Tyschenko, I.E., Volodin, V.A., Voelskow, M., Skorupa, W., Fröb, H.,
Formation of photoluminescence centers during annealing of SiO_2 layers implanted with Ge ions,
Semiconductors **34**: 1 (2000) 21

Khan, R.U.A., Grambole, D., Silva, S.R.P.,
Studies of carbon ion self-implantation into hydrogenated amorphous carbon films,
Diam. Rel. Mat. **9** (2000) 675

Klimenkov, M., Matz, W., Borany, J. von,
In situ observation of electron-beam-induced ripening of Ge clusters in thin SiO_2 layers,
Nucl. Instr. Meth. B **168** (2000) 367

Koch, T., Heinig, K.-H., Jentschel, M., Börner, H.G.,
Study of interatomic potential in ZnS - Crystal-GRID experiments versus ab-initio calculations,
J. Res. Natl. Inst. Stand. Technol. **105** (2000) 81

Kögler, R., Peeva, A., Anwand, W., Brauer, G., Skorupa, W., Werner, P., Gösele, U.,
Reply to „Comment on ‚Interstitial-type defects away of the projected ion range in high energy ion implanted and annealed silicon'" [Appl.Phys.Lett.77, 151 (2000)],
Appl. Phys. Lett. **77** (2000) 153

Kolitsch, A., Möller, W., Malkow, Th., Bull, S.J., Magula, V., Domankova, M.,
Growth and characterisation of hard and elastic carbon nitride thin films,
Surf. Coat. Technol. **128-129** (2000) 126

Mair, G.L.R , Ganetsos, Th., Bischoff, L., Teichert,J.,
Doubly-charged ions from liquid metal alloy ion sources: direct field-evaporation or post-ionization,
J. Phys. D: Appl. Phys. **33** (2000) L86

Mändl, S., Günzel, R., Richter, E., Möller, W., Rauschenbach, B.,
Annealing behaviour of nitrogen implanted stainless steel,
Surf. Coat. Technol. **128-129** (2000) 423

Markwitz, A., Grambole, D., Herrmann, F., Trompetter, W. J., Dioses, T., Gauldie, R.W.,
Reliable micro-measurement of strontium is the key to cracking the life-history code in the fish otolith,
Nucl. Instr. Meth. B **168** (2000) 109

Mattern, N., Hecker, M., Fischer, D., Wenzel, C., Schell, N., Matz, W., Engelmann, H., Zschech, E.,
X-ray structure characterization of barriers for Cu metallization,
Microel. Reliability **40** (2000) 1765

Misiuk, A., Rebohle, L., Iller A., Tyschenko, I.E., Jun, J., Panas A.,
Photoluminescence from pressure-annealed nanostructured silicon dioxide and nitride films,
Nanostruct. and Film Coatings (2000) 157

Misiuk, A., Iller, A., Rebohle, L., Lukaszewicz, M., Kudla, A.,
Photoluminescence from pressure-annealed silicon dioxide and nitride films,
Miroel. Reliability **40** (2000) 881

Müller, W., Adam, K., Neelmeijer, C., Mäder, M.,
Naturwissenschaftliche Untersuchungen zur Ursachenklärung von Schäden an Email-Kunstwerken,
Restauro **6** (2000) 414

Neelmeijer, C., Brissaud, I., Calligaro, T., Demortier, G., Hautojärvi, A., Mäder, M., Martinot, L.,
Schreiner, M., Tuurnala, T., Weber, G.,
Paintings - a challenge for XRF and PIXE analysis,
X-Ray Spectrometry **29** (2000) 101

Neelmeijer, C., Mäder, M., Pietsch, U., Ulbricht, H., Walcha, H.-M.,
Johann Georgius Höroldt fecit ?,
in: Ion Beam Study of Art and Archeological Objects, G. Demortier, A. Adriaens (eds.) European Commission, EUR 19218 (2000) 54

Neelmeijer, C., Mäder, M., Schramm, H.-P.,
Paint layers - depth resolved analysis at the particle accelerator,
in: Ion Beam Study of Art and Archeological Objects, G. Demortier, A. Adriaens (eds.) European Commission, EUR 19218 (2000) 15

Noetzel, J., Rössler, U.K., Tselev, A., Prokert, F., Eckert, D., Müller, K.-H., Wieser, E., Möller, W.,
Preparation of granular Co/Cu by ion-beam mixing of laser-deposited multilayers,
Appl. Phys. A **71** (2000) 105

Noetzel, J., Meyer, D.C., Tselev, A., Mücklich, A., Paufler, P., Prokert, F., Wieser, E., Möller, W.,
Amorphization of Fe/Al: bulk and thin-film effects,
Appl. Phys. A **71** (2000) 47

Oswald, S., Schmidt, B., Heinig, K.-H.,
XPS investigation with factor analysis for the study of Ge clustering in SiO_2,
Interface Anal. **29** (2000) 249

Panda, B.K., Brauer, G., Skorupa, W., Kuriplach, J.,
Positron energy levels in semiconductors,
Phys. Rev. B **61** (2000) 15848

Panknin, D., Wirth, H., Anwand, W., Brauer, G., Skorupa, W.,
High concentration doping of 6H-SiC by ion implantation: flash versus furnace annealing,
Mat. Sci. Forum **338-342** (2000) 877

Parascandola, S., Telbizova, T., Kruse, O., Möller, W.,
The influence of the oxygen partial pressure on the ion nitriding of Al – an investigation by means of real time in-situ elastic recoil detection analysis,
Nucl. Instr. Meth. B **161-163** (2000) 406

Parascandola, S., Möller, W., Williamson, D.L.,
The nitrogen transport in austenitic stainless steel at moderate temperatures,
Appl. Phys. Lett. **75** (2000) 2194

Peeva, A., Kögler, R., Werner, P., de Mattos, A.A., Fichtner, P.F., Behar, M., Skorupa, W.,
Evidence for interstitial-type defects in the $R_P/2$ region of MeV-self-ion-implanted silicon produced by standard ion milling procedure,
Nucl. Instr. Meth. B **161-163** (2000) 1090

Penzhorn, R.-D., Bekris, N., Coad, P., Dörr, L., Friedrich, M., Glugla, M., Haigh, A., Lässer, R., Peacock, A.,
Status and research progress at the Tritium Laboratory Karlsruhe,
Fusion Eng. Des. **49-50** (2000) 753

Pham, M.T., Reuther, H., Matz, W., Mueller, R., Steiner, G., Oswald, S., Zyganov, I.,
Surface induced reactivity for titanium by ion implantation,
J. Mat. Sci., Mat. Med. **11** (2000) 383

Pham, M.T., Matz, W., Reuther, H., Richter, E., Steiner, G., Oswald, S.,
Surface sensitivity of ion implanted titanium to hydroxyapatite formation,
J. Mat. Sci. Lett. **19** (2000) 443

Pham, M.T., Matz, W., Reuther, H., Richter, E., Steiner, G., Oswald, S.,
Ion beam sensitizing of titanium surfaces to hydroxyapatite formation,
Surf. Coat. Technol. **128-129** (2000) 313

Pham, M.T., Matz, W., Reuther, H., Richter, E., Steiner, G.,
Hydroxyapatite nucleation on Na ion implanted titanium surfaces,
J. Mat. Sci. Lett. **19** (2000) 1029

Pham, M.T., Maitz, M.F., Matz, W., Reuther, H., Richter, E., Steiner, G.,
Promoted hydroxyapatite nucleation on titanium ion implanted with sodium,
Thin Solid Films **379** (2000) 50

Piazza, F., Arnal, Y., Lacoste, A., Relihan, G., Kildemo, M., Grambole, D., Herrmann, F., Golanski, A.,
Optical properties of ta-C:H films deposited by ECR plasma using acetylene as precursor gas,
Proc. 7th Int. Symp. on Trends and Appl. of Thin Films (2000) 376

Piekoszewski, J., Grötzschel, R., Wieser, E., Stanislawski, J., Werner, Z., Szymczyk, W., Langner, J.,
Kinetics of the pulsed erosion deposition process induced by high intensity plasma beams,
Surf. Coat. Technol. **128-129** (2000) 394

Posselt, M.,
Prediction of the morphology of the as-implanted damage in silicon using a novel combination of BCA and MD simulations,
Mat. Sci. Semicond. Proc. **3** (2000) 317

Posselt, M., Schmidt, B., Feudel, T., Strecker, N.,
Atomistic simulation of ion implantation and its application in Si technology,
Mat. Sci. Eng. B **71** (2000) 128

Rebohle, L., Borany, J. von, Fröb, H., Niedermeier, S., Skorupa, W.,
Strong photoluminescence from Sn-implanted thermally grown SiO_2 layers,
Appl. Phys. Lett. **77** (2000) 969

Rebohle, L., Borany, J. von, Fröb, H., Skorupa, W.,
Blue photo- and electroluminescence of silicon dioxide layers implanted with group IV elements,
Appl. Phys. B **71** (2000) 131

Reich, T., Bernhard, G., Geipel, G., Funke, H., Hennig, C., Rossberg, A., Matz, W., Schell, N., Nitsche, H.,
The Rossendorf Beam Line ROBL - a dedicated experimental station for XAFS measurements of actinides and other radionuclides,
Radiochim. Acta **88** (2000) 633

Reiche, R., Oswald, S., Wetzig, K., Dobler, M., Reuther, H., Walterfang, M.,
The transformation of β-$FeSi_2$ under Ar ion bombardment studied by XPS, AES and Mössbauer spectroscopy,
Nucl. Instr. Meth. B **160** (2000) 397

Richter, E., Günzel, R., Parascandola, S., Telbizova, T., Kruse, O., Möller, W.,
Nitriding of stainless steel and aluminium alloys by plasma immersion ion implantation,
Surf. Coat. Technol. **128-129** (2000) 21

Romano-Rodriguez, A., Perez-Rodriguez, A., Serre, C., Morante, J.R., Esteve, J., Acero, M.C., Kögler, R., Skorupa, W., Östling, M., Nordell, N., Karlsson, S., van Landuyt, J.,
Epitaxial growth of beta-SiC on ion beam synthesized beta-SiC: Structural characterization,
Mat. Sci. Forum **338-342** (2000) 309

Romanov, S.I., Dvurechenskii, A.V., Kirienko, V.V., Grötzschel, R., Gutakovskii, A., Sokolov, L.V., Lamin, M.A.,
Homeoepitaxy on porous silicon with a buried oxide layer: full-wafer scale SOI,
in: Perspectives, Science and Technologies for Novel Silicon on Insulator Devices, Eds. P.L.F. Hemment, V.S. Lysenko, A.N. Nazarov, 2000 Kluwer Academic Publishers, NATO Science Series 3, **73** (2000) 29

Romanov, S.I., Dvurechenskii, A.V., Yakovlev, Y.I., Grötzschel, R., Kreissig, U., Kirienko, V.V., Obodnikov, V.I., Gutakovskii, A.,
Characterization of porous silicon layers containing a buried oxide layer,
in: Perspectives, Science and Technologies for Novel Silicon on Insulator Devices, Eds. P.L.F. Hemment, V.S. Lysenko, A.N. Nazarov, 2000 Kluwer Academic Publishers, NATO Science Series 3, **73** (2000) 195

Scheerschmidt, K., Conrad, D., Belov, A., Timpel, D.,
Enhanced semi-empirical potentials in molecular dynamics simulations of wafer bonding,
Mat. Sci. Semicond. Proc. **3** (2000) 129

Schreiner, M., Mäder, M., Neelmeijer, C.,
Non-destructive characterisation of degraded glass objects and enamels,
in: Ion Beam Study of Art and Archeological Objects, G. Demortier, A. Adriaens (eds.) European Commission, EUR 19218 (2000) 45

Serre, C., Perez-Rodriguez, A., Romano-Rodriguez, A., Morante, J.R., Fonseca, L., Acero, M.C., Esteve, J., Koegler, R., Skorupa, W.,
Beta-SiC on SiO_2 formed by ion implantation and bonding for micromechanics applications,
in: "Perspectives, Science and Technologies for Novel Silicon on Insulator Devices",
P.L.F. Hemment et al. (eds.), Kluwer Academic Publishers, Dordrecht, The Netherlands (2000) 121

Serre, C., Pérez-Rodríguez, A., Morante, J.R., Esteve, J., Acero, M.C., Kögler, R., Skorupa, W.,
Ion beam synthesis of polycrystalline SiC on SiO_2 structures for MEMS applications,
J. of Micromechanics and Microengineering **10** (2000) 152

Skorupa, W.,
Ion beam processing for Si-based light emission,
Proc. XIIth Int. Conf. Ion Implantation Technology (IIT´98), June 22-26, 1998, Kyoto, Japan, IEEE Conf. Proc. 98EX144 (2000)

Stenzel, O., Lebedev, A.N., Schreiber, M., Zahn, D.R.T.,
Simulation of linear optical losses of absorbing heterogeneous thin solid films,
Thin Solid Films **372** (2000) 200

Stenzel, O., Kupfer, H., Pfeifer, T., Lebedev, A.N., Schulze, S.,
Probing ultra-thin amorphous carbon films by means of nanometric silver islands,
Optical Materials **15** (2000) 159

Stoemenos, J., Pécz, B., Heera, V.,
Consequences of high dose, high temperature Al^+ implantation in 6H-SiC,
Mat. Sci. Forum **338-342** (2000) 881

Teichert, J., Bischoff, L., Hausmann, S., Voelskow, M., Hobert, H.,
Micro- Raman and ion channeling study of crystal damage in Si induced by focused Co ion beam implantation,
Appl. Phys. A **71** (2000) 175

Teichert, J., Hobert, H., Bischoff, L., Hausmann, S.,
Raman investigation of lattice defects in the $CoSi_2$ synthesis using focused ion beam implantation,
Microel. Eng. **50** (2000) 187

Telbizova, T., Parascandola, S., Prokert, F., Richter, E., Möller, W.,
Ion nitriding of aluminium - experimental investigation of the thermal transport,
Nucl. Instr. Meth. B **161-163** (2000) 690

Telbizova, T., Parascandola, S., Kreissig, U., Günzel, R., Möller, W.,
Mechanism of diffusional transport during ion nitriding of aluminum,
Appl. Phys. Lett. **76** (2000) 1404

Thees, H.-J., Wittmaack, M., Stegemann, K.-H., Borany, J. von, Heinig, K.-H., Gebel, T.,
Microstructure and electrical properties of gate SiO_2 containing Ge nanoclusters for memory applications,
Microel. Reliability **40** (2000) 867

Theodossiu, E., Baumann, H., Klimenkov, M., Matz, W., Bethge, K.,
Characterisation of crystallinity of SiC-surface layers produced by ion implantation,
Phys. Stat. Sol. (a) **182** (2000) 653

Thiele, E., Hecker, M., Schell, N.,
Change of internal strains in ultrafine-grained nickel due to cyclic plastic deformation,
Mat. Sci. Forum **321-324** (2000) 598

Thiele, E., Bretschneider, J., Hollang, L., Schell, N., Holste, C.,
Influence of thermal treatment and cyclic plastic deformation on the defect structure in ultrafine-grained nickel,
in: T. C. Lowe and R. Z. Valiev (eds.) Investigations and Applications of Severe Plastic Deformation, Proc. of NATO Adv. Res. Workshop, Moscow, Aug. 2 – 6 1999; Kluwer Academic Publ., (2000) 173

Tsyganov, I., Wieser, E., Matz, W., Mücklich, A., Reuther, H.,
Formation of the phases Ti_3Al and TiAl by high dose implantation of aluminium into titanium,
Nucl. Instr. Meth. B **161-163** (2000) 1069

Tsyganov, I., Wieser, E., Matz, W., Mücklich, A., Reuther, H., Pham, M.T., Richter, E.,
Phase formation in aluminium implanted titanium and the correlated modification of mechanical and corrrosive properties,
Thin Solid Film **376** (2000) 188

Turos, A., Gawlik, G., Jagielski, J., Stonert, A., Madi, N., Matz, W., Mücklich, A., Grötzschel, R.,
Atomic transport effects in Kr-ion bombarded ZrO_2/Fe ternary system,
Nucl. Instr. Meth. B **166-167** (2000) 128

Tzoganakou, K., Skeldon, P., Thompson, G.E., Zhou, X., Kreissig, U., Wieser, E., Habazaki, H., Shimizu, K.,
Mobility of lithium ions in anodic alumina formed on an Al-Li alloy,
Corrosion Sci. **42** (2000) 1083

Ueda, M., Gomes, G.F., Berni, L.A., Rossi, J.O., Barroso, J.J., Beloto, A.F., Abramof, E., Reuther, H.,
Plasma immersion ion implantation using a glow discharge source with controlled plasma potential,
Nucl. Instr. Meth. B **161-163** (2000) 1064

Walterfang, M., Kruijer, S., Keune, W., Dobler, M., Reuther, H.,
Depth analysis of buried iron disilicide formation by Fe ion implantation into Si,
Appl. Phys. Lett. **76** (2000) 1413

Walterfang, M., Kruijer, S., Dobler, M., Reuther, H., Keune, W.,
Phase analysis in α-Fe after high-dose Si ion implantation by depth-selective conversion-electron Mössbauer,
Hyperfine Interactions **126** (2000) 219

Wieser, E., Schreiber, J., Wenzel, C., Bartha, J.W., Bendjus, B., Melov, V., Peikert, M., Matz, W., Adolphi, B., Fischer, D.,
Modification of Ta-based thin film barriers by ion implantation of nitrogen and oxygen,
Proc. of the Advanced Metallization Conference –AMC '99, MRS, Warrendale, PA (2000) 257

Wieteska, K., Wierzchowski, W., Graeff, W., Turos, A., Grötzschel, R.,
Characterization of implanted semiconductors by means of white-beam and plane-wave synchrotron topography,
J. Synchr. Rad. **7** (2000) 318

Zappe, S., Möller, H., Krötz, G., Eickoff, M., Skorupa, W., Obermeier, E., Stoemenos, J.,
Structural characteristics of 3C-SiC films epitaxially grown on the $Si/Si3N_4/SiO_2$ system,
Mat. Sci. Forum **338-342** (2000) 529

Conference Contributions

Abramof, E., Beloto, A. F., Ueda, M., Guenzel, R., Reuther, H.,
Reciprocal space mapping of silicon implanted with nitrogen and carbon by PIII,
Conf. on Ion Beam Modification of Materials, Rio Grande do Sul, Brazil, Sept., 2000

Akhmadaliev, Ch., Bischoff, L., Teichert, J. Kazbekov, K.,
Ion acoustic microscopy for imaging of buried structures based on a focused ion beam,
Int. Conf. on Micro-and Nano Engineering (MNE`2000), Jena, Germany, Sept.18-21, 2000

Amayri, S., Geipel, G., Reich, T., Bernhard, G., Matz, W.
Synthesis, characterization and solubility of Bayleyite $Mg_2[UO_2(CO_3)_3].18H_2O$
5th Int. Conf. on Nuclear and Radiochemistry (NRC5), Pontresina, Sept., 2000

Anwand, W., Brauer, G., Hasegawa, M., Dersch, O., Rauch, F.,
A study of positron properties in quartz crystals and synthetic silica glass,
32th Polish Seminar on Positron Annihilation, Jarnoltowek, Poland, Sept.18-22, 2000

Barbiellini, B., Kuriplach, J., Anwand, W., Brauer, G.,
Calculation of positron characteristics in silicon carbide,
MRS 2000 Fall Meeting, Boston/MA, USA, Nov. 27–Dec.1, 2000

Barradas, N.P., Wei, P., da Silva, M.F., Soares, J.C., Kreissig, U., Arnoldbik, W., Cardoso, S., Freitas, P.P.,
High resolution IBA analysis of complex ultra-thin magnetic systems: potential and limitations,
IAEA Technical Committee Meeting on Comparison of Nuclear Analytical Methods with Competitive Methods for Material Characterization, Vienna, Austria, Oct. 9-13, 2000

Beloto, A. F., Ueda, M., Abramof, E., Senna, J. R., Leite, N. F., Silva, M. D., Reuther, H.,
Porous Silicon Implanted with N by PIII,
Conf. on Ion Beam Modification of Materials, Rio Grande do Sul, Brazil, Sept., 2000

Belov, A., Jäger, H.U.,
Elastic properties of diamond-like amorphous carbon films grown by computer simulation of ion-beam deposition process,
MRS 2000 Fall Meeting, Boston/MA, USA, Nov. 27–Dec.1, 2000

Berberich, F., Matz, W., Kreissig, U., Schell, N., Richter, E., Möller, W.,
Structural characterisation of hardening of Ti-Al-V alloys by nitridation with plasma immersion ion implantation,
11. Arbeitstagung Angewandte Oberflächenanalyse (AOFA11), Leipzig, Sept. 24-28, 2000

Bischoff, L., Teichert, J., Hausmann, S.,
Dose rate dependence of irradiation damage in silicon,
E-MRS 2000 Spring Meeting, Strasbourg, France, May 30 – June 2 , 2000

Bischoff, L., Akhmadaliev, Ch., Teichert, J.,
Mass separated focused ion beams using alloy liquid metal ion sources,
4th Europ. FIB Users Group Meeting (EFUG2000), Dresden, Germany, Oct. 2, 2000

Borany, J. von, Gebel, T., Heinig, K. H., Klimenkov, M., Stegemann, K. H., Thees, H. J., Wittmaack, M.
Ion beam synthesis of shallow Ge nanocluster bands in thin SiO_2 films for non-volatile memory applications,
IECON'2000, Nagoya, Japan, Oct. 23 - 27, 2000

Brauer, G., Anwand, W., Panknin, D., Skorupa, W.,
Ion implantation induced defects in 6H-SiC and their annealing behaviour,
12th Int. Conf. on Positron Annihilation (ICPA-12), München, Germany, Aug. 6-12, 2000

Brauer, G.,
Progress report on intense positron source project at ELBE,
16th Int. Conf. on the Application of Accelerators in Research and Industry (CAARI'98),
Denton/TX, USA, Nov. 1-4, 2000

Borodin, V.A., Heinig, K.-H., Schmidt, B.,Oswald, S.,
Modeling and XPS study of precipitation and oxidation of Ge in Ge^+ implanted SiO_2 layers,
E-MRS 2000 Spring Meeting, Strasbourg, France, May 30 - June 2, 2000

Chun, S.Y., Chayahara, A., Horino, Y., Posselt, M., Möller, W.,
Cathodic arc deposition of nanoscale multilayers: experiments and computer simulations,
12th Int. Conf. on Ion Beam Modification of Materials, Canela, Brazil, Sept. 3-8, 2000

Eichhorn, F., Schell, N., Mücklich, A., Matz, W., Kögler, R.,
Strain and SiC crystallite formation in carbon implantaed silicon,
5th Biennial Conf. on High-Resolution X-Ray Diffraction and Topography (XTOP-2000),
Jaszowiec, Poland, Sept. 13-15, 2000

Erlebach, A., Benistant, F., Krause, U., Matveev, D., Strecker, N., Meniailenko, V., Mickevicius, R., Simeonov, S., Al-Bayati, A., Gallo, B., Foad, M.A., Ng, B., Trowbridge, T., Posselt, M.,
Development and calibration of physical models for processes relevant to deep submicron technologies,
13th Int. Conf. on Ion Implantation Technology (IIT2000), Alpbach, Austria, Sept. 17-22, 2000

Fichtner, P.F.P., Peeva, A., Behar, M., da Silva, D.L., Koegler, R., Skorupa, W.,
The effects of the implantation temperature on the He bubble formation in silicon,
12th Int. Conf.on Ion Beam Modification of Materials, Canela, Brasil, Sept.3-8, 2000

Fitting, H.-J., Barfels, T., Trukhin A. N., Schmidt, B.,
Cathodoluminescence of SiO_2, SiO_2:Ge, and GeO_2,
E-MRS Spring Meeting, Strasbourg, France, May 30-June 2, 2000

Fitz, C., Fukarek, W., Kolitsch, A., Möller, W.,
An optical system for in situ stress measurement in thin films,
7th Int. Conf. on Plasma Surface Engineering (PSE 2000), Garmisch-Partenkirchen, Sept. 17-21, 2000

Fitz,C., Fukarek, W., Kolitsch, A., Möller, W.,
In situ measurement of stress in BN films during ion beam assisted deposition and post deposition treatments,
7th Int. Conf. on Plasma Surface Engineering (PSE 2000), Garmisch-Partenkirchen, Sept. 17-21, 2000

Fradin, J., Thome, T., Grynszpan, R.I., Thome, L., Anwand, W., Brauer, G.,
Ion implantation in zirconia,
12th Int. Conf. on Positron Annihilation (ICPA-12), München, Germany, Aug. 6-12, 2000

Fradin, J., Thome, T., Grynszpan, R.I., Thome, L., Anwand, W., Brauer, G.,
Fluence dependence of the damage fraction in argon implanted zirconia,
12th Int. Conf. on Ion Beam Modification of Materials, Canela, Brazil, Sept.3-8, 2000

Friedrich, M., Pilz, W., Penzhorn, R.-D., Bekris, N.,
A small tandem accelerator for tritium depth profiling by AMS,
5th Int. Workshop on Hydrogen Isotopes in Solids, Stockholm, Sweden, May 17-19, 2000

Friedrich, M., Pilz, W., Sung, G., Behrisch, R., Garcia-Rosales, C., Bekris, N., Penzhorn, R.-D.,
Tritium depth profiling in carbon samples from fusion experiments,
1st Europ. Workshop on the Characterisation of First Wall Materials, Karlsruhe, Germany,
Nov. 23-24, 2000

Fukarek, W., (invited)
In situ diagnostics during growth of BN films
8th International Symposium on Trends and Applications in Thin Films, TAFT 2000, Nancy, France, March 27-30, 2000

Fukarek, W., Fitz, C., (invited)
In-situ stress diagnostics
7th International Conference on Plasma Surface Engineering, PSE 2000, Garmisch-Partenkirchen, Sept. 17-21, 2000

Fukarek, W., (invited)
In-situ characterization of thin film growth: Boron nitride on silicon
47th International Conference of the American Vacuum Society, Boston/MA, USA, Oct. 2-6, 2000

Gebel, T., Borany, J. von, Klimenkov, M., Skorupa, W., Thees, H.-J., Wittmaack, M.,
Stegemann, K.-H.,
Microstructural and electrical properties of SiO_2 layers containing and Si nanoclusters,
197th Meeting Electrochemical Society Toronto, Ontario, Canada, May 14-18, 2000

Gebel, T., Borany, J. von, Rebohle, L., Skorupa, W., Thees, H.-J., Wittmaack, M., Stegemann, K.-H.,
Electrical characterization of thin SiO_2 layers containing Ge/Si nanoclusters,
NATO Advanced Study Institute "Defects in SiO_2 and related Dielectrics: Science and Technology",
Erice, Italy, April 8-20, 2000

Gebel, T., Rebohle, L., Zhao, J., Borchert, D., Fröb, H., Borany, J. von, Skorupa, W., (invited)
Ion beam synthesized based formation of Ge- rich thermally grown silicon dioxide layers: a promising approach for a silicon based light emitter,
MRS Fall Meeting, Boston/MA, USA, Nov. 27 – Dec. 1, 2000

Gebel, T., Thees, H.-J., Borany, J. von, Wittmaack, M., Stegemann, K.-H., Skorupa, W.,
Ion beam synthesis based formation of Si-and Ge-rich thermally grown silicon dioxide layers for memory applications,
MRS Fall Meeting, Boston/MA, USA, Nov. 27 – Dec. 1, 2000

Grigull, S., Kvick, Å., Parascandola, S.,
Microstrain analysis with sub-μ depth resolution in surface nitrided stainless steel,
49th Annual Denver X-ray Conference, Denver, Colorado, USA., July 31 - Aug. 4 2000

Groß, B., Beck, C., Engeldinger, J., Grambole, D., Herrmann, F., Hempelmann, R.,
Thermodynamik der Wasserstoffabsorption in $BaZr_{0.85}Y_{0.15}O_{2.925}/H_2O$,
99. Hauptversammlung der Dt. Bunsengesellschaft für Phys. Chemie, Würzburg, June 1-3, 2000

Gueorguiev, Y. M., Kögler, R., Peeva, A., Panknin, D., Mücklich, A., Yankov, R. A., Skorupa, W.,
Trans-projected-range effect in proximity gettering of impurities in silicon,
6th Int. Conf. on Electron Beam Technologies (EBT2000), Varna, Bulgaria, June 4-7, 2000

Günzel, R., Rogozin, A.I., Astrelin, V.T.,
Fast, uniform and large-scale heat treatment by plasma based electrons,
6th Int. Conf. on Electron Beam Technologies (EBT'2000), Varna, Bulgaria, June 4-7, 2000

Günzel, R., Shevchenko, N., Matz, W., Mücklich, A., Celis, J.P.,
Structural investigation and wear resistance of submicron TiN coatings obtained ba a hybride plasma immersion ion implantation process,
7th Conf. on Plasma Surface Engineering PSE, Garmisch-Partenkirchen, Sept. 17-21, 2000

Günzel, R., Matz, W., Ivanov, Yu. F., Rotshtein, V. P.,
Pulsed electron-beam treatment of high-speed steel cutting tools: structure-phase transformations and wear resistance,
1st Int.Congress on Radiation Physics and Chemistry of Condensed Matter, High Current Electronics, and Modification of Materials with Particle Beams and Plasma Flows, Tomsk, Russia,
Sept. 14-29, 2000

Hauschild, T., Jentschel, M., Börner, H. G., Heinig, K.-H., Möller, W.,
Crystal-GRID: What can we learn about interatomic solid state potentials?,
DPG-Frühjahrstagung, Regensburg, March 27-31, 2000

Heera, V., Skorupa, W., Stoemenos, J., Pécz, B.,
High dose implantation in 6H-SiC,
3rd Europ. Conf. on Silicon Carbide and Related Materials (ECSCRM-2000), Kloster Banz, Germany, Sept. 3-7, 2000

Heinig, K.-H., (invited)
Atomic modelling of Ion Implantation Processes II,
Second ENDEASD (European Network on Defect Engineering of Advanced Semiconductor Devices) Summer School, Kista-Stockholm, Sweden, June 24-26, 2000

Heinig, K.-H., Strobel, M.,
Inverse Ostwald ripening under ion irradiation,
E-MRS 2000 Spring Meeting, Strasbourg, France, May 30 - June 2, 2000

Heinig, K.-H., Strobel, M., Rizza, G., (invited)
Nanocluster evolution under ion irradiation,
12th Int. Conf. Ion Beam Modifications of Materials, Canela, Brazil, Sept. 3-8, 2000

Heinig, K.-H., Schmidt, B., Strobel, M., Bernas, H., (invited)
Inverse Ostwald ripening and self-organization of nanoclusters due to ion irradiation,
MRS 2000 Fall Meeting, Boston/MA, USA, Nov. 27–29, 2000

Helm. M., (invited)
Intersubband lasers and detectors,
29th Int. School on the Physics of Semiconducting Compounds, Jasowiec, Poland, June 2000

Helm, M., Strasser, G.,
Correlation of vertical transport and infrared absorption in GaAs/AlGaAs superlattices
25th Int. Conf. on the Physics of Semiconductors", Osaka, Japan, Sept. 18-22, 2000

Herrmann, F., Grambole, D., Grötzschel, R.,
Lattice destruction during micro-channeling measurements,
7th Int. Conf. on Nuclear Microprobe Technology and Applications, Bordeaux, France, Sept. 2000

Hornauer, U., Günzel, R., Richter, E., Wieser, E., Möller, W., Schumacher, G., Dettenwanger, F., Schütze, M.,
Improvement of the high temperature oxidation behaviour of TiAl alloys by Cl implantation using PIII,
7th Conf. on Plasma Surface Engineering PSE 2000, Garmisch-Partenkirchen, Sept. 17-21, 2000

Hu, Y.F., Shan, Y.Y., Beling, C.D., Fung, S., Xie, M.H., Cheung, S.H., Tu, J., Brauer, G., Anwand, W., Tong, S.Y.,
GaN thin films on SiC substrates studied using variable energy positron annihilation spectroscopy,
12th Int. Conf. on Positron Annihilation (ICPA-12), München, Aug. 6-12, 2000

Jäger, H. U., Albe, K.,
Molecular-dynamics simulations of steady-state growth of ion-deposited tetrahedral amorphous carbon films,
TRANSDIAM2, Amiens, France, June 5-7, 2000

Jagielski, J., Kopcewicz, M., Matz, W., Grötzschel, R., Thomé, L.,
Phase transformations in nitrogen implanted iron layers,
12th Conf. on Ion Beam Modification of Materials, Canela, Brazil, Sept., 2000

Jembrih, D., Schreiner, M., Neelmeijer, C., Mäder, M., Peev, M., Krejsa, P., Clausen, C.,
Irisierende Jugendstilgläser - mit Röntgenfluoreszenz- und Ionenstrahlmethoden auf der Spur ihrer Geheimnisse,
Jahrestagung der GDCh, Archäometrie und Denkmalpflege, Dresden, March 29-31, 2000

Jembrih, D., Schreiner, M., Neelmeijer, C., Mäder, M., Ebel, M., Svagera, R., Peev, M.,
Iridescent Art Nouveau Glass- ion beam analysis (PIXE, PIGE, RBS) and XPS for the characterization of the iridescent layers,
7th Int. Conf. on Nuclear Microprobe Technol. and Appl., Bordeaux, France, Sept. 10-15, 2000

Klimenkov, M., Borany, J. von, Matz, W., Schulze, S.,
Application of TEM energy filtered measurements to the study of Ge redistribution in ion-implanted thin SiO_2 films,
12th Europ. Congress on Electron Microscopy, Brno, CZ, July 9-14, 2000

Klimenkov, M., Nepijko, S. A., Bao, X., Matz, W.,
TEM study of Ti doped ZSM-5 zeolite,
12th Europ. Congress on Electron Microscopy, Brno, CZ, July 9-14, 2000

Köhler, B., Irmer, G., Bischoff, L., Teichert. J.,
TEM specimen preparation by focused ion beam sputtering – optimisation of the process
4th Europ.FIB Users Group Meeting (EFUG2000), Dresden, Oct. 2, 2000

Köhler, B., Schmidt, B., Trojok, L. Bischoff, L., (Poster Award)
Nanometer scale 3D-structuring by FIB Ga-implantation and wet chemical etching,
4th Europ. FIB Users Group Meeting (EFUG2000), Dresden, Oct. 2, 2000

Kögler, R., Peeva, A., Werner, P., Skorupa, W., Gösele, U.,
Gettering centres in high-energy ion-implanted silicon investigated by point defect recombination,
12th Int. Conf. on Ion Beam Modifications of Materials, Canela, Brasil, Sept. 4-9, 2000

Kolitsch, A.,
Development of a user data base system for ion implanter operation,
7th DANFYSIK User Meeting, Surrey, UK, Oct. 5-6, 2000

Kopcewicz, M., Jagielski, J., Matz, W.,
Thickness dependent phase transformations in implanted iron,
Int. Symp.on the Industrial Applications of the Mössbauer Effect (ISIAME-2000), Virginia Beach, USA, Aug. 13-18, 2000

Krause-Rehberg, R., Brauer, G.,
EPOS – A European positron source for applied research,
12th Int. Conf. on Positron Annihilation (ICPA-12), München, Germany, Aug. 6-12, 2000

Kvasov, N. T., Danilyuk, A. L., Uglov, V. V., Fedotova, J. A., Kuleshov, A. K., Günzel, R., Reuther, H., Richter, E.,
Simulation of structural stresses during plasma impulse nitrogen implantation of steel,
7th Int. Conf. On Plasma Surface Engineering, Garmisch-Partenkirchen, Sept. 17-21, 2000

Lazar, M., Ottaviani, L., Locatelli, M.L., Raynoud, C., Planson, D., Morvan, E., Godignon, P., Skorupa, W., Chante, J.P.,
High electrical activation of Al and N implanted in 6H-SiC at room temperature by RF annealing,
3rd Europ. Conf. on Silicon Carbide and Related Materials (ECSCRM-2000), Kloster Banz, Germany, Sept. 3 - 7, 2000

Lenkeit, B., Steckemetz, S., Mücklich, A., Metz, A., Hezel, R.,
High quality screen-printed and fired-through silicon nitride rear contacts for bifacial silicon solar cells,
16th Europ. Photovoltaic Solar Energy Conf., Glasgow, UK, May 1-5, 2000

Mäder, M., Neelmeijer, C.,
Zerstörungsfreie Oberflächenanalysen an historischen Gläsern,
11. Arbeitstagung Angewandte Oberflächenanalytik (AOFA11), Leipzig, Germany, Sept. 24-28, 2000

Mäder, M., Neelmeijer, C., Ricke, H.,
Glas und Glasmalfarben: Was "sehen" Ionenstrahlen?,
Herbstsitzung der Deutschen Glastechnischen Gesellschaft, Erfurt, Germany, Sept. 22-24, 2000

Martin, J., Bischoff, L., Teichert, J., Köhler, B., Wannemacher, R.,
Point light source for near-field optical microscopy,
DPG Tagungen 2000, Potsdam, March 13–16; Regensburg, March 27–31, 2000

Matz, W., Eichhorn, F., Prokert, F., Schell, N., Berberich, F.,
Structural diagnostics of near surface regions with synchrotron radiation at ROBL,
11. Arbeitstagung Angewandte Oberflächenanalytik (AOFA11), Leipzig, Sept. 24-28, 2000

Matz, W., Schell, N., Prokert, F., Eichhorn, F., Berberich, F.,
Synchrotron radiation studies of thin films and implanted layers with the Materials Research Endstation of ROBL,
Int. School and Conference on Synchrotron Radiation in Natural Sciences, Ustron-Jaszowiec, Poland, June 12-17, 2000

Mazur, K., Sass, J., Eichhorn, F., Turos, A.,
Laterally structural surfaces of GaAs (001) characterized by conventional and synchrotron X-ray methods,
19th Europ. Crystallographic Meeting (ECM19), Nancy, France, Aug. 25-31, 2000

Mazur, K., Sass, J., Eichhorn, F., Turos, A.,
The surface gratzing on GaAs (001) characterized by conventional and synchrotron X-ray methods,
XVIII Conference on Applied Crystallography, Wisla, Poland, Sept. 4 - 7, 2000

Mohsen, M., Ismail, H., Ashry, A., Brauer, G., Mohamed, S.,
Lattice defects in industrial Al probed by positrons,
12th Int. Conf. on Positron Annihilation (ICPA-12), München, Germany, Aug. 6-12, 2000

Möller, W., (invited)
Ionenstrahlen in der Materialforschung,
Tag der Deutschen Gesellschaft für Materialkunde, Dresden, June 30, 2000

Möller, W., (invited)
Nanocluster in Oberflächen,
W.E.Heraeus-Ferienkurs für Physik "Nanophysik", TU Dresden, Sept. 28, 2000

Möller, W., (invited)
Ion Implantation: New Possibilities by Highly Charged Ions?,
Annual Meeting of the European Network "Low-Energy Ion Facilities", Berlin, Oct. 21, 2000

Möller, W., (invited)
Nitrieren durch Plasma-Immersions-Ionenimplantation,
Workshop "Plasmadiffusionsverfahren – Oberflächen nach Maß", Braunschweig, Nov. 9,2000

Müller, T., Heinig, K.-H., Schmidt, B., Mücklich, A., Möller, W.,
Shape evolution of oxidized silicon V-grooves during high dose ion implantation,
E-MRS 2000 Spring Meeting, Strasbourg, France, May 30 - June 2, 2000

Müller, T., Heinig, K.-H., Schmidt, B., Möller, W.,
Formation of quantum wires in oxidized silicon V-grooves by ion beam synthesis,
12th Int. Conf. Ion Beam Modifications of Materials (IBMM2000), Canela, Brazil, Sept. 3 - 8, 2000

Müller, T., Heinig, K.-H., Schmidt, B., Mücklich, A., Möller, W.,
Synthesis of spatially controlled nanostructures by ion implantation in V-Grooves on (001) Si surfaces,
MRS 2000 Fall Meeting, Boston/MA, USA, Nov. 27–29, 2000

Müller, W., Adam, K., Neelmeijer, C., Mäder, M.,
Sind die Emailkunstwerke im Dresdner Grünen Gewölbe zu retten?,
Jahrestagung der GDCh, Archäometrie und Denkmalpflege, Dresden, Germany, March 29-31, 2000

Nancheva, N., Docheva, P., Anwand, W., Brauer, G.,
Characterization of Sn films on silicon by slow positron implantation spectroscopy,
32th Polish Seminar on Positron Annihilation, Jarnoltowek, Poland, Sept.18-22, 2000

Nicht, E.-M., Brauer, G., Tempus, G.,
Longtime aging behaviour of the alloy Al-2024 characterized by positron annihilation spectroscopy,
32th Polish Seminar on Positron Annihilation, Jarnoltowek, Poland, Sept. 18-22, 2000

Österman, J., Hallen, A., Anand, S., Linnarsson, M., Andersson, H., Aberg, D., Skorupa, W., Panknin, D.,
Active doping profile measurements of 4H-SiC,
3rd Europ. Conf. on Silicon Carbide and Related Materials (ECSCRM-2000), Kloster Banz, Germany, Sept. 3-7, 2000

Panknin, D., Stoemenos, J., Eickhoff, M., Heera, V., Nielsen, A., Vouroutzis, N., Krötz, G., Skorupa, W.,
Improvement of the 3C-SiC/Si interface by flash lamp annealing,
3rd Europ. Conf. on Silicon Carbide and Related Materials (ECSCRM-2000), Kloster Banz, Germany, Sept. 3-7, 2000

Panknin, D., Skorupa, W.,
Flash lamp annealing of implantation doped p- and n-6H-SiC,
3rd Europ. Conf. on Silicon Carbide and Related Materials (ECSCRM-2000), Kloster Banz, Germany, Sept. 3-7, 2000

Parascandola, S.;,Möller, W., Williamson, D. L.,
Successful nitriding of austenitic stainless steel: The diffusion mechanism of nitrogen and the role of the surface oxide layer,
Int. Current Status Seminar Thermochemical Surface Engineering of Stainless Steels, Osaka, Japan, Nov. 5-8, 2000

Pécz, B., Barna, A., Heera, V., Fontaine, F. , Skorupa, W.,
TEM investigations of Si implanted natural diamond,
3rd Europ. Conf. on Silicon Carbide and Related Materials (ECSCRM-2000), Kloster Banz, Germany, Sept. 3-7, 2000

Peeva, A., Koegler, R., Skorupa, W., Fichtner, P.F.P., Behar, M.,
Helium Implantation induced metal gettering in silicon at half of the projected ion range,
2nd ENDEAST (European Network on Defect Engineering of Advanced Semiconductor Devices) Workshop, Stockholm, Sweden, June 27-29, 2000

Peeva, A., Fichtner, P.F.P., Behar, M., Koegler, R., Skorupa, W.,
Helium Implantation induced metal gettering in silicon at half of the projected ion range,
12th Int. Conf. on Ion Beam Modification of Materials, Canela, Brasil, Sept. 3-8, 2000

Peeva, A., Fichtner, P.F.P., Behar, M., Koegler, R., Skorupa, W.,
Copper gettering at the $R_P/2$ induced by low energy channelling He implantation in Si,
12th Int. Conf. on Ion Beam Modification of Materials, Canela, Brasil, Sept. 3-8, 2000

Pérez-Rodríguez, A., Serre, C., Romano-Rodríguez, A., Morante, J.R., Esteve, J., Acero, M.C., Skorupa, W., Kögler, R.,
SiCOI structures: Technology and characterisation,
NATO Advanced Research Workshop “Progress in Semiconductor-On-Insulator structures and devices operating at extreme conditions”, Kyiv, Ukraine, Oct. 15-20, 2000

Persson, P.O.A., Hultman, L., Jansson, M., Hallen, A., Panknin, D., Skorupa, W.,
Structural Defects of Ion Implanted SiC,
MRS Fall Meeting, Boston/MA, USA, Nov. 27–Dec. 1, 2000

Piazza, F., Arnal,Y., Grambole,D., Herrmann, F., Kildemo, M., Lacoste, A., Relihan, G., Golanski, A.,
Influence of the process parameters on the properties of hydrogenated amorphous carbon thin films deposited using ECR plasma,
EMRS Spring Meeting, Strasbourg, France, May 30-June 2, 2000

Piazza, F., Arnal,Y., Lacoste,A., Relihan, G., Kildemo, M., Grambole, D., Herrmann, F., Golanski, A.,
Optical properties of ta C:H films deposited by ECR plasma using acetylene as precursor gas,
7th Int. Symp. on Trends and Appl. of Thin Films, Nancy, France

Posselt, M., Teichert, J., Bischoff, L., Hausmann, S.,
Dose rate and temperature dependence of Ge range profiles in Si obtained by channeling implantation,
E-MRS 2000 Spring Meeting, Strasbourg, France, May 30 - June 2, 2000

Posselt, M., (invited)
Atomic modelling of ion implantation processes (Part I),
Second ENDEASD (European Network on Defect Engineering of Advanced Semiconductor Devices) Summer School, Kista-Stockholm, Sweden, June 24-26, 2000

Posselt, M., Belko, V., Chagarov, E.,
Influence of polytypism on elementary processes of ion-beam-induced defect production in SiC,
Second ENDEASD (European Network on Defect Engineering of Advanced Semiconductor Devices) Workshop, Kista-Stockholm, Sweden, June 27-29, 2000

Posselt, M., Belko, V., Chagarov, E.,
Influence of polytypism on elementary processes of ion-beam-induced defect production in SiC,
5th Int. Conf. on Computer Simulation of Radiation Effects in Solids (COSIRES2000), Penn State University, State College, USA, July 24-28, 2000

Posselt, M.,
Defect formation and evolution in Si within the first nanosecond after ion impact (invited),
5th Int. Conf. on Computer Simulation of Radiation Effects in Solids (COSIRES2000), Penn State University, State College, USA, July 24-28, 2000

Posselt, M., (invited)
Improving the understanding of ion-beam-induced defect formation and evolution by atomistic computer simulations,
MRS 2000 Fall Meeting, Boston/MA, USA, Nov. 27-Dec.1, 2000

Rebohle, L., Gebel, T., Borany, J. von, Skorupa, W.,
Nanocluster formation for light emission by ion implantation,
13th Int. Conf. Ion Implantation Technology (IIT 2000), Alpbach, Austria, Sept. 17-22, 2000

Reuther, H., Betzl, M., Richter, E.,
Untersuchung von durch Ionenimplantation hergestellten dünnen Fe-Mg-Legierungsschichten,
11. Arbeitstagung Angewandte Oberflächenanalytik (AOFA 11), Leipzig, Sept. 24 - 28, 2000

Reuther, H.,
Winkelabhängige Mößbauerspektroskopie an Eisensilizid-Einkristallen,
X. Mößbauerkolloquium, Freiberg, Germany, Oct. 4-5, 2000

Rizza, G.C., Strobel, M., Heinig, K.-H., Bernas, H.,
Ion irradiation of gold inclusions in SiO_2: experimental evidence for inverse Ostwald ripening,
E-MRS 2000 Spring Meeting, Strasbourg, France, May 30 - June 2, 2000

Schmidt, B., Heinig, K.-H., Mücklich, A.,
Evolution of ion beam synthesized Au nanoclusters in SiO_2 under ion irradiation,
MRS 2000 Fall Meeting, Boston/MA, USA, Nov. 27 - 29, 2000

Sendezera, E.J., Davidson, A.T., Anwand, W., Brauer, G., Nicht, E.-M.,
Positron annihilation lifetime study of pure and doped LiF,
12th Int.Conf. on Positron Annihilation (ICPA-12), München, Germany, Aug. 6-12, 2000

Serre, C., Panknin, D., Perez-Rodriguez, A., Romano-Rodriguez, A., Morante, Kögler, R., Skorupa, W., Esteve, J., Acero, M.C.,
Structural and electrical characterization of ion beam synthesized and n-doped SiC layers,
3rd Europ.Conf. on Silicon Carbide and Related Materials (ECSCRM-2000), Kloster Banz, Germany, Sept. 3-7, 2000

Serre, C., Pérez-Rodríguez, A., Romano-Rodríguez, A., Morante, J.R., Esteve, J., Acero, M.C., Kögler, R., Skorupa., W.,
Structural characterisation of ion beam synthesised polycrystalline SiC on SiO_2,
3rd Int. Conf. on Materials for Microelectronics, Dublin, Ireland, Oct.10-17, 2000

Skorupa, W., (invited)
Defect engineering and gettering in and by SOI-structures,
NATO Advanced Research Workshop "Progress in Semiconductor-On-Insulator structures and devices operating at extreme conditions", Kyiv, Ukraine, Oct. 15-20, 2000

Spiga, S., Ferrari, S., Fanciulli, M., Schmidt, B., Heinig, K.-H., Grötzschel, R., Mücklich, A., Pavia, G.,
Kinetics of ion beam synthesis of Sn and Sb clusters in SiO_2 layers,
MRS 2000 Fall Meeting, Boston/MA, USA, Nov. 27–29, 2000

Stan-Sion, C., Behrisch, R., Coad, P., Kreissig, U., Kubo, F., Lazarev, V., Lingig, S., Mayer, M., Nolte, E., Peacock, A., Rohrer, L., Roth, J.,
Hydrogen isotope depth profiling in carbon samples from the erosion dominated inner vessel walls of JET,
14th Int. Conf. on Plasma Surface Interactions, Rosenheim, Germany, May 22-26, 2000

Stegemann, K.-H., Thees, H.-J., Wittmaack, M., Borany, J. von, Heinig, K.-H., Gebel, T.,
Microstructure and electrical properties of Ge- and Si-nanoclusters in implanted gate oxide for embedded memory applications,
13th Int. Conf. Ion Implantation Technology (IIT 2000), Alpbach, Austria, Sept. 17-22, 2000

Ster, A., Posselt, M., Hallen, A., Janson, M.,
Atomistic simulation of ion implantation into different polytypes of SiC,
13th Int. Conf. Ion Implantation Technology (IIT2000), Alpbach, Austria, Sept. 17-22, 2000

Strasser, G., Gianordoli, S., Schrenk, W., Gornik, E., Mücklich, A., Helm, M., (invited)
MBE-grown GaAs/AlGaAs and strained InGaAs/AlGaAs/GaAs quantum cascade lasers
11th Int. Conference on Molecular Beam Epitaxy, Beijing, China, Sept. 11-15, 2000

Strobel, M., Heinig, K.-H., Möller, W., (invited)
Atomistic modeling of ion beam synthesis of nanostructures,
E-MRS 2000 Spring Meeting, Strasbourg, France, May 30 - June 2, 2000

Strobel, M., Heinig, K.-H., Möller, W., (invited)
A kinetic 3D lattice Monte-Carlo study of nucleation, growth, and Ostwald ripening of nanoclusters under ion irradiation,
Second ENDEASD (European Network on Defect Engineering of Advanced Semiconductor Devices) Workshop, Kista-Stockholm, Sweden, June 27-29, 2000

Strobel, M., Heinig, K.-H., Michely, T.,
3D kinetic lattice Monte-Carlo simulations of ion erosion of fcc(111) surfaces,
E-MRS 2000 Spring Meeting, Strasbourg, France, May 30 - June 2, 2000

Strobel, M., Heinig, K.-H., Michely, T.,
Morphology evolution during ion erosion of fcc (111) surfaces: a 3D kinetic lattice Monte-Carlo study,
12th Int. Conf. Ion Beam Modifications of Materials (IBMM2000), Canela, Brazil, Sept. 3-8, 2000

Strobel, M., Heinig, K.-H., Michely, T.,
Modeling and simulation of ion erosion of fcc (111) surfaces,
Europ. Consortium on Mathematics in Industry (ECMI2000), Altavilla Milicia, Italy,
Sept. 26-30, 2000

Strobel, M., Heinig, K.-H., Möller, W., (invited)
Understanding ion beam synthesis of nanostructures: modelling and atomistic simulations,
MRS 2000 Fall Meeting, Boston/MA, USA, Nov. 27–29, 2000

Teichert, J., Borany, J. von,
Decel lens system for low-energy ion implantation with high dose uniformity,
13th Int. Conf. on Ion Implantation Technology (IIT 2000), Alpach, Austria, Sept. 17–22, 2000

Telbizova, T., Parascandola, S., Prokert, F., Barradas, N. P., Richter, E., Möller W.,
Ion nitriding of Al: growth kinetics and characterisation of the nitride layer,
7th Int. Conf. on Plasma Surface Engineering, Garmisch-Partenkirchen, Sept.17-21, 2000

Thome, T., Fradin, J., Grynszpan, R.I., Anwand, W., Brauer, G.,
Positron implantation profiles of He implanted 18 carat gold-silver alloy,
E-MRS Spring Meeting 2000, Strasbourg, France, May 30 – June 2, 2000

Thome, T., Fradin, J., Grynszpan, R.I., Anwand, W., Brauer, G.,
Depth dependence of defect stability in helium implanted 18 kts gold,
12th Int. Conf. on Positron Annihilation (ICPA-12), München, Germany, Aug. 6-12, 2000

Tsyganov, I. A., Wieser, E., Matz, W., Reuther, H., Oswald, S., Pham, M. T., Richter, E.
Modification of titanium by ion implantation of calcium and/or phosphorus,
1st Int. Congress on Radiation Physics and Chemistry of Cond. Matter, High Current Electronics, and Modification of Materials with Particle Beams and Plasma Flows, Tomsk, Russia, Sept. 14-29, 2000

Tsyganov, I. A., Wieser, E., Matz, W., Mücklich, A., Reuther, H.,
Formation of the phases Ti_3Al and TiAl by high dose implantation of aluminium into titanium,
1st Int. Congress on Radiation Physics and Chemistry of Cond. Matter, High Current Electronics, and Modification of Materials with Particle Beams and Plasma Flows, Tomsk, Russia, Sept. 14-29, 2000

Ueda, M., Reuther, H., Guenzel, R., Beloto, A. F., Abramof, E., Berni, L. A.,
High dose nitrogen and carbon shallow implantations in silicon by PIII,
12th Conf. on Ion Beam Modification of Materials, Canela, Brazil, Sept.3-8, 2000

Uglov, V. V., Kuleshov, A. K., Fedotova, J. A., Kvasov, N. T., Danilyuk, A. L., Günzel, R., Reuther, H., Richter, E.,
Plasma immersion N and N + C implantation into high-speed tool steel: surface morphology, phase composition and mechanical properties,
7th Int. Conf. On Plasma Surface Engineering, Garmisch-Partenkirchen, Sept. 17-21, 2000

Variam, N., Jeong, U., Falk, S., Mehta, S., Posselt, M., Feudel, T., Horstmann, M., Krüger, C., Ng, C.-H,
Application of indium ion implantation for halo doping: experimental and simulation results for advanced CMOS devices,
13th Int. Conf. on Ion Implantation Technology (IIT2000), Alpbach, Austria, Sept. 17-22, 2000

Walterfang, M., Kruijer, S., Keune, W., Dobler, M., Reuther, H.,
Tiefenselektive Phasenanalyse der Fe-Disilizid-Bildung in Fe-ionenimplantiertem Si mittels DCEMS
Frühjahrstagung der DPG, Regensburg, March 27-31, 2000

Weiß, U., Löbner, T., Geßner, T., Hoyer, W., Grambole, D.,
Application of new materials for integrated low-energy ignition elements in airbag systems - characterization and simulation,
3th Int. Conf. on Micro Materials, Berlin, Germany, April 17-19, 2000

Werner, Z., Piekoszewski, J., Barcz, A., Grötzschel, R., Prokert, F., Stanislawski, J., Szymczyk, W.,
Alloying of Pd into Ti by pulsed plasma beams,
12th Conf. on Ion Beam Modification of Materials, Canela, Brazil, Sept. 3-8, 2000

Wieser, E., Schreiber, J., Wenzel, C., Bartha, J. W., Benjus, B., Melov, V., Peikert, M., Reuther, H., Mücklich, A., Adolphi, B., Fischer, D.,
Improvement of Ta-based thin film barriers on copper by ion implantation of nitrogen and oxygen,
3rd Int. Interconnect Technology Conference IITC 2000, San Francisco, USA, June 5-7, 2000

Williamson, D. L., Wilbur, P. J., Fickett, F. R., Parascandola, S.,
Role of ion-beam processing time in the formation and growth of the high-nitrogen phase in austenitic stainless steel,
Int. Current Status Seminar Thermochemical Surface Engineering of Stainless Steels, Osaka, Japan, Nov 5-8, 2000

Lectures

Anwand, W.,
Aufklärung ionenimplantationsbedingter Schäden in SiC mit Hilfe der Positronenstrahltechnik,
Minikolloquium „Positronen in der Materialforschung“, Rossendorf, Germany, Sept. 28, 2000

Borany, J. von,
Anwendung von Ionentechniken zur Dotierung und Analyse von Diamantsubstraten,
Abschluss-Seminar BMBF-Projekt "Sensoren für extreme Umgebungsbedingungen",
Berlin, April 4, 2000

Borany, J. von,
Halbleiter-Nanocluster in dünnen dielektrischen Schichten für Speicheranwendungen,
Infineon Technologies Dresden, April 26, 2000

Borany, J. von,
Ionenerzeugte Nanocluster für die Optoelektronik und neue Speicherkonzepte,
Frühjahrssitzung AK POT, Dresden, May 10, 2000

Borany, J. von,
Ionenstrahlsynthese von Halbleiter-Nanoclustern in SiO2-Schichten: Herstellung - Mikrostruktur - Anwendungen,
FSU Jena, June 28, 2000

Borany, J. von,
Nanocluster based memories,
Dt.-Jap. Symp. "Strategies in Nanotechnology", Berlin Oct. 30-31, 2000

Brauer, G.,
Positronenannihilationsspektroskopie im FZ Rossendorf,
Minikolloquium „Positronen in der Materialforschung“, Rossendorf, Germany, Sept. 28, 2000

Brauer, G.,
Positron annihilation spectroscopy,
Karls-Universität Prag, Czech Republic, Dec. 4, 2000

Dekorsy, T.,
Femtosecond spectroscopy of semiconductors,
IIM Program Seminar, Marienthal Monastery, June 5-7, 2000

Fitz, C.,
In situ Messung mechanischer Spannungen in BN Schichten während der Abscheidung mit IBAD, unter Ionenbestrahlung und bei thermischer Behandlung,
DACH-Abschlußkolloquium 2000, Synthese von superharten Materialien, Neuhofen, Österreich

Wieser, E., Schreiber, J., Wenzel, C., Bartha, J. W., Benjus, B., Melov, V., Peikert, M., Reuther, H., Mücklich, A., Adolphi, B., Fischer, D.,
Improvement of Ta-based thin film barriers on copper by ion implantation of nitrogen and oxygen,
3rd Int. Interconnect Technology Conference IITC 2000, San Francisco, USA, June 5-7, 2000

Williamson, D. L., Wilbur, P. J., Fickett, F. R., Parascandola, S.,
Role of ion-beam processing time in the formation and growth of the high-nitrogen phase in austenitic stainless steel,
Int. Current Status Seminar Thermochemical Surface Engineering of Stainless Steels, Osaka, Japan, Nov 5-8, 2000

Lectures

Anwand, W.,
Aufklärung ionenimplantationsbedingter Schäden in SiC mit Hilfe der Positronenstrahltechnik,
Minikolloquium „Positronen in der Materialforschung“, Rossendorf, Germany, Sept. 28, 2000

Borany, J. von,
Anwendung von Ionentechniken zur Dotierung und Analyse von Diamantsubstraten,
Abschluss-Seminar BMBF-Projekt "Sensoren für extreme Umgebungsbedingungen",
Berlin, April 4, 2000

Borany, J. von,
Halbleiter-Nanocluster in dünnen dielektrischen Schichten für Speicheranwendungen,
Infineon Technologies Dresden, April 26, 2000

Borany, J. von,
Ionenerzeugte Nanocluster für die Optoelektronik und neue Speicherkonzepte,
Frühjahrssitzung AK POT, Dresden, May 10, 2000

Borany, J. von,
Ionenstrahlsynthese von Halbleiter-Nanoclustern in SiO2-Schichten: Herstellung - Mikrostruktur - Anwendungen,
FSU Jena, June 28, 2000

Borany, J. von,
Nanocluster based memories,
Dt.-Jap. Symp. "Strategies in Nanotechnology", Berlin Oct. 30-31, 2000

Brauer, G.,
Positronenannihilationsspektroskopie im FZ Rossendorf,
Minikolloquium „Positronen in der Materialforschung“, Rossendorf, Germany, Sept. 28, 2000

Brauer, G.,
Positron annihilation spectroscopy,
Karls-Universität Prag, Czech Republic, Dec. 4, 2000

Dekorsy, T.,
Femtosecond spectroscopy of semiconductors,
IIM Program Seminar, Marienthal Monastery, June 5-7, 2000

Fitz, C.,
In situ Messung mechanischer Spannungen in BN Schichten während der Abscheidung mit IBAD, unter Ionenbestrahlung und bei thermischer Behandlung,
DACH-Abschlußkolloquium 2000, Synthese von superharten Materialien, Neuhofen, Österreich

Fukarek, W.,
Analytik des Wachstums und der Modifizierung von BN Schichten mit *in-situ* Ellisometrie unter besonderer Berücksichtigung von Depositionsrate und mechanischer Spannungsmessung,
VII. Erfahrungsaustausch „Oberflächentechnologie mit Plasmaprozessen“, Mühlleiten, March 14-16, 2000

Gebel, T.,
Nanostrukturen für die Mikroelektronik,
Messe “Karrierestart 2000”, Dresden, Jan. 22, 2000

Gebel, T.,
Blaues Licht aus Silizium – integrierbare Lösungen für die optische Kommunikation,
Hannover Messe 2000, Hannover, March 22, 2000

Gebel, T.,
Memory applications of SiO_2 layers containing Ge and Si nanoclusters,
Naval Research Laboratory, Washington DC, USA, May 23, 2000

Gebel, T.,
Microstructure and electrical properties of Ge and Si - implanted SiO_2 layers,
University of Catania, Italy, Oct. 11, 2000

Gebel, T.,
Nanostrukturen in der Optoelektronik: Eigenschaften und Anwendungen,
Universität Tübingen, Dec.19, 2000

Grötzschel, R.,
Billard mit Atomen - Teilchenbeschleuniger helfen bei der Materialanalyse dünner Schichten,
NeMa-Workshop, Mönchen-Gladbach, May 11, 2000; FDS-Workshop, Chemnitz, June 8, 2000

Grötzschel, R.,
Das ERDA-Spektrometer "Little John" am Rossendorfer Tandem,
Arbeitstreffen "Forschung mit Nuklearen Sonden und Ionenstrahlen", Göttingen, Oct. 9-11, 2000

Grötzschel, R.,
Möglichkeiten, Perspektiven und Grenzen der IBA mit höchster Tiefenauflösung,
AMD Dresden, Dec. 14, 2000

Heinig, K.-H., Strobel, M., Schmidt, B.,
Nanostructure fabrication by ion implantation and phase separation,
RRC “Kurchatov Institute”, Moscow, Russia, April 6, 2000

Heinig, K.-H.,
Synthese und Bearbeitung von Nanostrukturen mit Ionenstrahlen,
FSU Jena, Nov.17, 2000

Helm, M.,
Infrarotspektroskopie von Halbleiterübergittern,
Universitsät Erlangen, Nov. 10, 2000

Helm, M.,
Miniband absorption in strongly coupled superlattices,
Paul-Drude-Institut Berlin, Nov. 13, 2000

Helm, M.
Infrarotstrahlung zur Untersuchung von Elektronen in Halbleiter-Quantenstrukturen,
ELBE-Palaver am FZR, Dec. 6, 2000

Hornauer, U.,
Ionenimplantation zur Verbesserung des Hochtemperatur-Oxidationsverhaltens von TiAl Werkstoffen,
Hannover Messe 2000, March 21, 2000

Kögler, R.,
Metal gettering in the $R_P/2$-range of ion-implanted Si,
MPI für Mikrostrukturphysik, Halle, Germany, March 15, 2000

Kögler, R.,
Cu Gettern vor-, hinter- und im $R_P/2$ Gebiet von ionen-implantiertem Silizium,
TU Dresden, Dec. 21, 2000

Maitz, M.,
Aspekte der Implantatmaterial-Organismus-Wechselwirkung,
Universität Regensburg, Dec. 8, 2000

Maitz, M.,
The MatMed database,
MatMed Workshop Brehna bei Leipzig, May 8, 2000

Maitz, M.,
Principles of biological testing of implant materials,
City University of Hong Kong, Nov. 11, 2000

Matz, W.,
Rossendorfer Beamline ROBL in Grenoble; Synchrotronstrahlung für Ökologie- und Materialforschung,
Tag der offenen Tür des FZR, Sept. 16, 2000

Möller, W.,
Plasma-Immersions-Ionenimplantation zur Behandlung metallischer Oberflächen,
TU Chemnitz, Jan. 5, 2000

Möller, W.,
Mechanismen des Ionen-Nitrierens von Edelstahl und Aluminiumlegierungen,
Werkstoffwissenschaftliches Kolloquium, MPI für Metallforschung, Stuttgart, Jan. 24, 2000

Möller, W.,
Mechanismen des Ionennitrierens von Edelstählen und Aluminium-Werkstoffen,
Institut für Oberflächenmodifizierung, Leipzig, Nov. 16, 2000

Mücklich, A.,
TEM-Untersuchungen an ionenstrahl-modifizierten Materialien,
TU BA Freiberg, May 26, 2000

Neelmeijer, C.,
Ionenstrahlen im Dienste der Kunst,
Universität Frankfurt/M., Feb. 24, 2000

Neelmeijer, C.,
Paint layers: Depth resolved analysis at the particle accelerator,
Museo Argeológico National, Madrid, Spain, June 22-23, 2000

Neelmeijer, C.,
"Vierzehn Nothelfer" (L. Cranach) - Ion beam analysis of a painting,
University of Liège, Belgium, Nov. 16-18, 2000

Nicht, E.-M.,
PAS-Untersuchungen an Al 2024-Blechen,
Minikolloquium „Positronen in der Materialforschung“, Rossendorf, Germany, Sept. 28, 2000

Peeva, A.,
Helium implantation induced metal gettering in silicon at half of the projected ion range,
University of Poitiers, France, Oct. 27, 2000

Rebohle, L.,
Blue Photo- and Electroluminescence of SiO_2 layers implanted with group IV elements,
University of Catania, Catania, Italy, Oct.3-13, 2000

Rebohle, L.,
Anwendungen von Nanostrukturen in der Mikro- und Optoelektronik,
Industriefachmesse Dresden, Oct. 20, 2000

Skorupa, W.,
Nanocluster in SiO_2-Schichten durch Ionenstrahlsynthese:Blaue Elektrolumineszenz und nichtflüchtige Halbleiterspeicher,
FZ Jülich, Jan. 26, 2000

Skorupa, W.,
Electroluminescence and microstructure studies at ion beam synthesized Ge-rich SiO_2-layers,
Univ. of Barcelona, Spain, Feb. 11, 2000

Skorupa, W.,
Silicium basierte Lichtemission durch Ionenstrahlsynthese,
Brandenburgische TU Cottbus, April 11, 2000

Skorupa, W.,
Ion beam synthesis for nanocluster formation in SiO_2-layers: Electroluminescence and applications,
Naval Research Laboratory, Washington, D.C., USA, May 23, 2000

Skorupa, W.,
Laudatio for the Jürgen-Geiger-Award Presentation to Dr. Lars Rebohle and his Dissertation „Lumineszenzeigenschaften ionenimplantierter nanokristalliner SiO_2-Schichten“,
Cellar of the Stadtsparkasse Kaiserslautern, June 30, 2000

Skorupa, W.,
Ion beam synthesis of group-IV-atom-rich SiO_2-layers:Optical and electrical properties and their relation to microstructure,
University of Catania, Italy, July 17, 2000

Skorupa, W.,
Ion beam synthesized based formation of Ge- rich thermally grown silicon dioxide layers:
A promising approach for a silicon based light emitter,
Fed. Univ. of Rio Grande dol Sul, Porto Alegre, Brasilien, Nov.24, 2000

Skorupa, W.,
Gettering techniques for silicon-on-insulator technologies,
IBIS Technology Corp., Danvers/MA, USA, Dec.1, 2000

Skorupa, W.,
Ion beam synthesized based formation of Ge- rich thermally grown silicon dioxide layers:
A promising approach for a silicon based light emitter,
TU Dresden, Dec. 14, 2000

Strobel, M., Heinig, K.-H.,
Computersimulationen zur Ionenstrahlsynthese von Nanoclustern,
RWTH Aachen, Jan. 26, 2000

Reports

Brauer, G., (Editor)
Construction and use of an intense positron source at new LINAC facilities in Germany,
- Conceptual Report -
FZR-295, July 2000

Brauer, G.,
Materialforschung mittels Positronen-Annihilationsspektroskopie,
SMWK: 4-7533-70-FZR/705, Zwischenbericht 07.02.2000, 17.07.2000; Abschlußbericht 18.12.2000

Brauer, G.,
Positron annihilation spectroscopy of metals with complex structure,
BMBF/IB: Projekt CZE 00/035, Jahresbericht 2000, 23.11.2000

Köhler, B., Teichert, J., Bischoff, L.,
Entwicklung einer neuen Technologie zur Probenpräparation für die Transmissions-Elektronenmikroskopie (TEM) auf der Basis der Ionenfeinstrahlbearbeitung,
SMWK/4-7533-70-864-98/3, Zwischenbericht 30.06.2000; Abschlußbericht 31.12.2000

Nicht, E.-M., Brauer, G., Grambole, D., Zamponi, C.,
Comparative studies of selected materials and investigation about the H^+ problem,
Daimler-Chrysler Aerospace Airbus GmbH Bremen: 3-402-230-FZR, Bericht 29.8.2000

Oehme, W., Dienel, S., Proehl, D., Matz, W., Reich, T., Schell, N., Bernhard, G., Krug, H., Reichel, P., Strauch, U., Prokert, F., Claussner, J., Funke, H., Neumann, W., Brendler, V., Hennig, C., Berberich, F.,
Beamline-Instrumentierung und Experimentautomatisierung für ROBL an der ESRF/Grenoble (F),
FZR-291, März 2000

Wieser, E.,
Einfluß einer oberflächennahen Dotierung auf die Oxidationskinetik und die Mikrostruktur der Oxidschicht von TiAl-Werkstoffen,
Abschlussbericht zum Forschungsvorhaben I/72 726 der Volkswagen-Stiftung

Patents

Gebel, T., Skorupa, W., Borany, J. von, Rebohle, L., Borchert, D., Fahrner, W.,
Integrierter Optokoppler und Verfahren zu seiner Herstellung,
Erfindungsanmeldung beim Deutschen Patentamt, AZ 100 11 258.7, 08.03.2000

Heera, V., Höfgen, A.,
Verfahren zur Herstellung Ohmscher Kontakte auf Siliziumkarbid-Halbleiterbereichen,
Erfindungsanmeldung beim Deutschen Patentamt, AZ 100 06 378.0, 12.2.2000

Skorupa, W.,
Ion beam synthesized based formation of Ge- rich thermally grown silicon dioxide layers:
A promising approach for a silicon based light emitter,
TU Dresden, Dec. 14, 2000

Strobel, M., Heinig, K.-H.,
Computersimulationen zur Ionenstrahlsynthese von Nanoclustern,
RWTH Aachen, Jan. 26, 2000

Reports

Brauer, G., (Editor)
Construction and use of an intense positron source at new LINAC facilities in Germany,
- Conceptual Report -
FZR-295, July 2000

Brauer, G.,
Materialforschung mittels Positronen-Annihilationsspektroskopie,
SMWK: 4-7533-70-FZR/705, Zwischenbericht 07.02.2000, 17.07.2000; Abschlußbericht 18.12.2000

Brauer, G.,
Positron annihilation spectroscopy of metals with complex structure,
BMBF/IB: Projekt CZE 00/035, Jahresbericht 2000, 23.11.2000

Köhler, B., Teichert, J., Bischoff, L.,
Entwicklung einer neuen Technologie zur Probenpräparation für die Transmissions-Elektronenmikroskopie (TEM) auf der Basis der Ionenfeinstrahlbearbeitung,
SMWK/4-7533-70-864-98/3, Zwischenbericht 30.06.2000; Abschlußbericht 31.12.2000

Nicht, E.-M., Brauer, G., Grambole, D., Zamponi, C.,
Comparative studies of selected materials and investigation about the H^+ problem,
Daimler-Chrysler Aerospace Airbus GmbH Bremen: 3-402-230-FZR, Bericht 29.8.2000

Oehme, W., Dienel, S., Proehl, D., Matz, W., Reich, T., Schell, N., Bernhard, G., Krug, H., Reichel, P., Strauch, U., Prokert, F., Claussner, J., Funke, H., Neumann, W., Brendler, V., Hennig, C., Berberich, F.,
Beamline-Instrumentierung und Experimentautomatisierung für ROBL an der ESRF/Grenoble (F),
FZR-291, März 2000

Wieser, E.,
Einfluß einer oberflächennahen Dotierung auf die Oxidationskinetik und die Mikrostruktur der Oxidschicht von TiAl-Werkstoffen,
Abschlussbericht zum Forschungsvorhaben I/72 726 der Volkswagen-Stiftung

Patents

Gebel, T., Skorupa, W., Borany, J. von, Rebohle, L., Borchert, D., Fahrner, W.,
Integrierter Optokoppler und Verfahren zu seiner Herstellung,
Erfindungsanmeldung beim Deutschen Patentamt, AZ 100 11 258.7, 08.03.2000

Heera, V., Höfgen, A.,
Verfahren zur Herstellung Ohmscher Kontakte auf Siliziumkarbid-Halbleiterbereichen,
Erfindungsanmeldung beim Deutschen Patentamt, AZ 100 06 378.0, 12.2.2000

Skorupa, W.,
Ion beam synthesized based formation of Ge- rich thermally grown silicon dioxide layers:
A promising approach for a silicon based light emitter,
TU Dresden, Dec. 14, 2000

Strobel, M., Heinig, K.-H.,
Computersimulationen zur Ionenstrahlsynthese von Nanoclustern,
RWTH Aachen, Jan. 26, 2000

Reports

Brauer, G., (Editor)
Construction and use of an intense positron source at new LINAC facilities in Germany,
- Conceptual Report -
FZR-295, July 2000

Brauer, G.,
Materialforschung mittels Positronen-Annihilationsspektroskopie,
SMWK: 4-7533-70-FZR/705, Zwischenbericht 07.02.2000, 17.07.2000; Abschlußbericht 18.12.2000

Brauer, G.,
Positron annihilation spectroscopy of metals with complex structure,
BMBF/IB: Projekt CZE 00/035, Jahresbericht 2000, 23.11.2000

Köhler, B., Teichert, J., Bischoff, L.,
Entwicklung einer neuen Technologie zur Probenpräparation für die Transmissions-Elektronenmikroskopie (TEM) auf der Basis der Ionenfeinstrahlbearbeitung,
SMWK/4-7533-70-864-98/3, Zwischenbericht 30.06.2000; Abschlußbericht 31.12.2000

Nicht, E.-M., Brauer, G., Grambole, D., Zamponi, C.,
Comparative studies of selected materials and investigation about the H^+ problem,
Daimler-Chrysler Aerospace Airbus GmbH Bremen: 3-402-230-FZR, Bericht 29.8.2000

Oehme, W., Dienel, S., Proehl, D., Matz, W., Reich, T., Schell, N., Bernhard, G., Krug, H., Reichel, P., Strauch, U., Prokert, F., Claussner, J., Funke, H., Neumann, W., Brendler, V., Hennig, C., Berberich, F.,
Beamline-Instrumentierung und Experimentautomatisierung für ROBL an der ESRF/Grenoble (F),
FZR-291, März 2000

Wieser, E.,
Einfluß einer oberflächennahen Dotierung auf die Oxidationskinetik und die Mikrostruktur der Oxidschicht von TiAl-Werkstoffen,
Abschlussbericht zum Forschungsvorhaben I/72 726 der Volkswagen-Stiftung

Patents

Gebel, T., Skorupa, W., Borany, J. von, Rebohle, L., Borchert, D., Fahrner, W.,
Integrierter Optokoppler und Verfahren zu seiner Herstellung,
Erfindungsanmeldung beim Deutschen Patentamt, AZ 100 11 258.7, 08.03.2000

Heera, V., Höfgen, A.,
Verfahren zur Herstellung Ohmscher Kontakte auf Siliziumkarbid-Halbleiterbereichen,
Erfindungsanmeldung beim Deutschen Patentamt, AZ 100 06 378.0, 12.2.2000

Heera, V.,
Verfahren zur Dotierung von SiC-Halbleiterbereichen,
Erfindungsanmeldung beim Deutschen Patentamt, AZ xxx (ha1182), 12.12.2000

Schmidt, B., Bischoff, L., Eng, L.,
Verfahren zur Herstellung von integrierten Abtastnadeln,
Erfindungsanmeldung beim Deutschen Patentamt, ha 1181, 21.11.2000

Teichert, J.,
Einrichtungzur Ionenimplantation mit niedrigen Energien,
Erfindungsanmeldung beim Europäischen Patentamt, EP 1 037 254 A2, 7.03.2000

PhD Theses and Examinations

Hausmann, S.,
Die Dynamik von Strahlenschäden mit fokussierten Ionenstrahlen am Beispiel der Ionenstrahlsynthese
TU Dresden, 25.10.2000

Noetzel, J.,
Nanostruktur ionenbestrahlter Fe/Al- und Co/Cu-Grenzschichten,
TU Dresden, 17.07.2000

Diploma Theses

Kentsch, U.,
Untersuchung des Ladungseintrages hochgeladener langsamer Schwerionen in Festkörpertargets
TU Dresden, Dec. 2000

Müller, T.,
Ion Beam Synthesis of Nanowires
TU Dresden, Nov. 2000

Awards

Gebel, T.,
1. Preis der Erich – Glowatzky - Stiftung,
Dresden, Oct. 2, 2000

Gebel, T., Rebohle, L., Skorupa, W.,
2. Preis im Businessplanwettbewerb “Premiere’99” des SMWA / infineon technologies,
Dresden, April 27, 2000

Rebohle, L.,
Prof. Dr. Jürgen-Geiger-Preis für die Dissertation: Lumineszenzeigenschaften ionenimplantierter nanokristalliner SiO_2-Schichten,
Kaiserslautern, June 30, 2000

Rebohle, L.,
Doktorandenpreis des FZ Rossendorf, Dec. 2000

Skorupa, W., Rebohle, L., Gebel, T.,
Forschungspreis des FZ Rossendorf, Dec. 2000

Heera, V.,
Verfahren zur Dotierung von SiC-Halbleiterbereichen,
Erfindungsanmeldung beim Deutschen Patentamt, AZ xxx (ha1182), 12.12.2000

Schmidt, B., Bischoff, L., Eng, L.,
Verfahren zur Herstellung von integrierten Abtastnadeln,
Erfindungsanmeldung beim Deutschen Patentamt, ha 1181, 21.11.2000

Teichert, J.,
Einrichtungzur Ionenimplantation mit niedrigen Energien,
Erfindungsanmeldung beim Europäischen Patentamt, EP 1 037 254 A2, 7.03.2000

PhD Theses and Examinations

Hausmann, S.,
Die Dynamik von Strahlenschäden mit fokussierten Ionenstrahlen am Beispiel der Ionenstrahlsynthese
TU Dresden, 25.10.2000

Noetzel, J.,
Nanostruktur ionenbestrahlter Fe/Al- und Co/Cu-Grenzschichten,
TU Dresden, 17.07.2000

Diploma Theses

Kentsch, U.,
Untersuchung des Ladungseintrages hochgeladener langsamer Schwerionen in Festkörpertargets
TU Dresden, Dec. 2000

Müller, T.,
Ion Beam Synthesis of Nanowires
TU Dresden, Nov. 2000

Awards

Gebel, T.,
1. Preis der Erich – Glowatzky - Stiftung,
Dresden, Oct. 2, 2000

Gebel, T., Rebohle, L., Skorupa, W.,
2. Preis im Businessplanwettbewerb “Premiere’99” des SMWA / infineon technologies,
Dresden, April 27, 2000

Rebohle, L.,
Prof. Dr. Jürgen-Geiger-Preis für die Dissertation: Lumineszenzeigenschaften ionenimplantierter nanokristalliner SiO_2-Schichten,
Kaiserslautern, June 30, 2000

Rebohle, L.,
Doktorandenpreis des FZ Rossendorf, Dec. 2000

Skorupa, W., Rebohle, L., Gebel, T.,
Forschungspreis des FZ Rossendorf, Dec. 2000

Heera, V.,
Verfahren zur Dotierung von SiC-Halbleiterbereichen,
Erfindungsanmeldung beim Deutschen Patentamt, AZ xxx (ha1182), 12.12.2000

Schmidt, B., Bischoff, L., Eng, L.,
Verfahren zur Herstellung von integrierten Abtastnadeln,
Erfindungsanmeldung beim Deutschen Patentamt, ha 1181, 21.11.2000

Teichert, J.,
Einrichtungzur Ionenimplantation mit niedrigen Energien,
Erfindungsanmeldung beim Europäischen Patentamt, EP 1 037 254 A2, 7.03.2000

PhD Theses and Examinations

Hausmann, S.,
Die Dynamik von Strahlenschäden mit fokussierten Ionenstrahlen am Beispiel der Ionenstrahlsynthese
TU Dresden, 25.10.2000

Noetzel, J.,
Nanostruktur ionenbestrahlter Fe/Al- und Co/Cu-Grenzschichten,
TU Dresden, 17.07.2000

Diploma Theses

Kentsch, U.,
Untersuchung des Ladungseintrages hochgeladener langsamer Schwerionen in Festkörpertargets
TU Dresden, Dec. 2000

Müller, T.,
Ion Beam Synthesis of Nanowires
TU Dresden, Nov. 2000

Awards

Gebel, T.,
1. Preis der Erich – Glowatzky - Stiftung,
Dresden, Oct. 2, 2000

Gebel, T., Rebohle, L., Skorupa, W.,
2. Preis im Businessplanwettbewerb “Premiere’99” des SMWA / infineon technologies,
Dresden, April 27, 2000

Rebohle, L.,
Prof. Dr. Jürgen-Geiger-Preis für die Dissertation: Lumineszenzeigenschaften ionenimplantierter nanokristalliner SiO_2-Schichten,
Kaiserslautern, June 30, 2000

Rebohle, L.,
Doktorandenpreis des FZ Rossendorf, Dec. 2000

Skorupa, W., Rebohle, L., Gebel, T.,
Forschungspreis des FZ Rossendorf, Dec. 2000

Laboratory Visits

Brauer, G.,
FH Fulda, Fachbereich Elektrotechnik, Jan. 18-19, 2000

Brauer, G.,
Daimler-Chrysler Aerospace Airbus GmbH, Bremen, March 8-9, 2000

Brauer, G.,
University of Texas at Arlington, Department of Physics, Arlington/TX, USA,
Oct. 30-31, 2000

Brauer, G.,
Texas Christian University, Department of Physics, Ft. Worth/TX, USA, Nov.1-2, 2000

Brauer, G.,
Charles University Prague, Czech Republic, Nov. 29–Dec. 6, 2000

Brauer, G.,
FH Fulda, Fachbereich Elektrotechnik, Dec. 10-12, 2000

Chevolleau, T.,
Bulgarian Academy of Sciences, Sofia, Oct. 26-27, 2000

Dekorsy, T.,
Ludwig-Maximilians-Universität Müchen, Aug. 3, 2000

Dekorsy, T.,
RWTH Aachen, Oct. 5-6; Dec. 14, 2000

Dekorsy, T.,
MPI für Mikrostrukturphysik Halle, Oct. 9, 2000

Dekorsy, T.,
Paul-Drude-Institut Berlin, Nov. 13, 2000

Dekorsy, T.,
TU Wien, Austria, Nov. 29- Dec. 1, 2000

Eichhorn, F.,
European Synchrotron Radiation Facility, Grenoble,
Jan. 26–Feb. 2, Apr. 11–16, May 30–June 6, Sept. 5–10, 2000

Eichhorn, F.,
Institute of Electronic Materials Technology, Warsaw, Sept. 12-15, 2000

Gebel, T.,
Naval Research Laboratory, Washington DC, USA, May 22–25, 2000

Gebel, T.,
University of Catania, Catania, Italy, Oct. 3-12, 2000

Gebel, T.,
Universität Hannover/FhI für Solarsysteme, Gelsenkirchen, Dec. 11-12, 2000

Gebel, T.,
Universität Tübingen, Dec. 18-19, 2000

Günzel, R.,
City University of Hong Kong, Nov. 9-14, 2000

Heinig, K.-H., Strobel, M.
RWTH Aachen, Jan. 26-27, 2000

Heinig, K.-H.,
National Center for Scientific Research "Demokritos", IMEL, Athens, Greece, March 2-5, 2000

Heinig, K.-H.,
Russian Research Center “Kurchatov Institute”, Moscow, Russia, April 6, 2000

Heinig, K.-H.,
University of Exeter, Exeter, UK, April 13-16, 2000

Kögler, R.,
Royal Institute of Technology, Kista-Stockholm, Sweden, June 24-29, 2000

Kögler, R.,
Fed. Univ. of Rio Grande do Sul, Porto Alegre, Brasilien, Sept.7-15, 2000

Kögler, R.,
Univ. of Barcelona, Spain, Dec. 8-15, 2000

Kreher, J.
European Synchrotron Radiation Facility, Grenoble, Dec. 6–14, 2000

Lebedev, A.,
ISE Integrated Systems Engineering AG, Zurich, Switzerland, Oct. 17-20, 2000

Maitz, M.,
City University of Hong Kong, Nov. 9-14, 2000

Matz, W.,
European Synchrotron Radiation Facility, Grenoble, March 7–11, July 4–14, Oct. 26–31, 2000

Matz, W.,
Hahn-Meitner-Institut, Berlin, May 11–12, 2000

Neelmeijer, C.,
Universidad Autónoma de Madrid, Spain, June 22-23, 2000

Nicht, E.-M.,
Daimler-Chrysler Aerospace Airbus GmbH, Bremen, March 8-9, 2000

Nicht, E.-M.,
Universität Bonn, Institut für Strahlen- und Kernphysik, June 5-8, July 18-20, Oct 12, 2000

Panknin, D.,
Univ. of Barcelona, Spain, Dec. 8-15, 2000

Parascandola, S.,
European Synchrotron Radiation Facility, Grenoble, France, June 9–13, 2000

Peeva, A.,
University of Linköping, Sweden, June 18-23, 2000

Peeva, A.,
Fed. Univ. of Rio Grande do Sul, Porto Alegre, Brasil, Sept. 8 – Oct. 1, 2000

Peeva, A.,
University of Poitiers, France, Oct. 22-27, 2000

Posselt, M.,
Department of Solid State Electronics, Royal Institute of Technology, Kista-Stockholm, Sweden, June 28, 2000.

Posselt, M.,
Department of Chemistry, Penn State University, USA, July 28, 2000

Prokert, F.,
European Synchrotron Radiation Facility, Grenoble, July 11–21, Oct. 4–10, Nov. 21–26, 2000

Rebohle, L.,
University of Catania, Italy, Oct. 3-13, 2000

Reichel, P.,
European Synchrotron Radiation Facility, Grenoble, May 28–June 8, Dec. 6–14, 2000

Skorupa, W.,
FZ Jülich, Jan. 26-27, 2000

Skorupa, W.,
Univ. of Barcelona, Spain, Feb. 10-13, 2000

Skorupa, W.,
Naval Research Laboratory, Washington, D.C., USA, May 22-25, 2000

Skorupa, W.,
Royal Institute of Technology, Kista-Stockholm, Sweden, June 24-29, 2000

Skorupa, W.,
University of Catania, Italy, July 15-20, 2000

Skorupa, W.,
Institute of Semiconductor Physics, Ukrainian Academy of Science, Kyiv, Oct.19-20, 2000

Skorupa, W.,
Fed. Univ. of Rio Grande dol Sul, Porto Alegre, Brasilien, Nov. 19-24, 2000

Skorupa, W.,
Universität Hannover/FhI für Solarsysteme, Gelsenkirchen, Dec. 11-12, 2000

Skorupa, W.,
Universität Tübingen, Dec. 18-19, 2000

Guests

J.-P. Allart,
CNRS, Arcueil, France, Aug. 1-31, 2000

W. Assmann,
LMU München, May 4-5, 2000

P. Baving,
Ruhr-Universität Bochum, April 10-11, 2000

H. W. Becker,
Ruhr-Universität Bochum, April 10-11, 2000
C.D. Beling,
University of Hong Kong, P.R.China, Feb. 3-18, 2000

V. I. Belko,
Belorussian State University, Minsk, Belarus, Oct. 2-Nov. 20, 2000

V. Borodin,
RRC Kurchatov Institute, Moscow, Russia, April 3-June 4, 2000

H. H. Bukow,
Ruhr-Universität Bochum, April 10-11, 2000

V. I. Dimitrov,
Fatich University, Istanbul, Turkey, July 15-Aug. 15, 2000

A. V. Dvurechenskii,
Institute of Semiconductor Physics, Novosibirsk, Russia, July 2-28, 2000

J. Engeldinger,
Universität des Saarlandes, Saarbrücken, Feb. 21-25, 2000

S. Facsko,
RWTH Aachen, Oct. 2-3, 2000

A. Glotov,
IPP Obninsk, Russia

H. Geßner,
ELMA Electronic AG, Wetzikon, Schweiz, Nov. 13-14, 2000

S. Gosh,
Nuclear Science Center, New Delhi, India, Sept. 9-13, 2000

K. Grigorov,
Institute of Electronics, Sofia, Bulgaria, Nov. 13-18, 2000

B. Groß,
Universität des Saarlandes, Saarbrücken, Feb. 21-25, 2000

H. Haricharun
WITS University Johannesburg, South Africa, March 27–April 17, 2000

V. Harutyunyan,
University of Yerevan, Armenia, Dec. 15-20, 2000

D. Heyden,
Universität Heidelberg, Sept. 4-6, 2000

Y. Hu,
University of Hong Kong, P.R.China, Feb. 3-18, 2000

J. Jagielski,
Institute of Electronics Materials Technology, Warsaw, Poland, Feb. 27-March 2, 2000

D. Jembrih,
Technical University Vienna, Austria, Jan. 16-28, 2000

J. R. A. Kaschny,
Fed. Univ. of Rio Grande dol Sul, Porto Alegre, Brasilien, April 4 ec. 31, 2000

A. Kondurin,
Perm State University, Russia, Aug. 30-Sept. 6, 2000

R. Krause-Rehberg,
Martin-Luther-Universität Halle-Wittenberg, Germany, May 11-12, 2000

S. Kubsky,
Ruhr-Universität Bochum, April 10-11, 2000

V. Liechtenstein,
RRC Kurchatov Institute Moscow, Russia, May 15-27, 2000

J. Meijer,
Ruhr-Universität Bochum, April 10-11, 2000

R. Nipoti,
CNR Istituto LAMEL, Bologna, Italy, March 13-15, 2000

L. Ottaviani,
INSA Lyon, Mar. 1–Apr. 15, 2000

V. V. Ovchinnikov,
Institute of Electrophysics, Yekatarinburg, Russia, Oct. 1-24, 2000

A. Pathak,
University of Hyderabad, India, Oct. 2-30, 2000

A.Perez-Rodriguez,
Univ. of Barcelona, Spain, Nov. 8-10, 2000

P.O.A. Persson,
Univ. of Linköping, Sweden, Aug. 19-24, 2000

J. Piekoszewski,
Soltan Institute for Nuclear Studies, Otwock, Poland, May 4-12; Sept. 6-16; Nov. 22-Dec. 2, 2000

I. Pramatarova,
Institute of Solid State Physics, Sofia, Bulgaria, Oct. 27-Nov. 30, 2000

I. Prochazka,
Charles University, Prague, Czech Republic, Jun 5-30, Sep 4-29, Nov 1-29, 2000

D. Proskurovsky,
Institute of High Current Electronics, Tomsk, Russia, Nov. 3-14, 2000

V. Prozesky,
National Accelerator Center, Faure, South Africa, June 2-3, 2000

A. G. Revesz,
Revesz Associates, Bethesda, MD, USA and Naval Research Lab., Washington, D.C., USA
July 3-5, 2000

H. Ricke,
Kunstmuseum Düsseldorf, June 20-21, 2000

H. Röcken,
Ruhr-Universität Bochum, April 10-11, 2000

A.Romano-Rodriguez,
Univ. of Barcelona, Spain, Nov. 8-10, 2000

E. Sendezera,
University of Zululand, South Africa, July 17–Aug. 5, 2000

Y.Y. Shan,
University of Hong Kong, P.R.China, Feb. 10-18, 2000

A. Siejek,
FH Köln, FB Restaurierung/Konservierung, Köln, July 25; Aug. 28-29, 2000

A. Stephan,
Ruhr-Universität Bochum, April 10-11, 2000

A. Ster,
MTA-KFKI Budapest, Hungary, May 14-27; Sept. 10-16, 2000

X. Tian,
City Univ. of Hong Kong, P.R.China, Sept. 25-26, 2000

I. Tsyganov,
Lipetsk State Technical University, Lipetsk, Russia, Jan. 24-March 24; July 24-Oct. 23, 2000

A. Turos,
Institute of Electronics Materials Technology, Warsaw, Poland,
Feb. 27 - March 2; Sept. 3 - 7; Dec. 11-20, 2000

M. Vinnichenko,
University of Kiev, Ukraina, Dec. 1, 2000 - Feb. 28, 2001

E. Vlakhov,
Institute of Solid State Physics, Sofia, Bulgaria, Oct. 23-Nov. 11, 2000

T. Vogel,
Ruhr-Universität Bochum, April 10-11, 2000

T. Wang,
Institute of Modern Physics, Lanzhou, P.R. China, Oct. 22 , 2000 -

U. Weidenmüller,
Ruhr-Universität Bochum, April 10-11, 2000

H. Weng,
University of Science and Technology, Hefei, P.R.China, Aug. 14-15, 2000

L. Wielunski,
CSIRO Lindfield, Australia, Aug. 21-Sept. 8, 2000

H.-J. Woo,
Korea Institute of Geology, Mining and Materials, Korea, Sept. 25-26, 2000

J. Zhao,
Shanghai Inst. of Technology, P.R.China, May 11-Dec. 31, 2000

J. Zuk,
Univ. of Lublin, Poland, Aug. 28-Sept.1, 2000

European Large Scale Facility Visitors

C. Aidinis,
University of Athens, Greece, Aug. 2-9, 2000

N. Pessoa Barradas,
Nuclear and Technological Institute, Sacavem, Portugal, Jan. 6-14, 2000

P. Danesh,
Bulgarian Academy of Sciences, Institute of Solid State Physics, Bulgaria, July 8-29, 2000

T. van Dillen,
FOM-Institute for Atomic and Molecular Physics, Netherlands, Feb. 21- March 12, 2000

J. Fradin,
DGA/Centre Technique d'Arcueil/ LOT/L, France, Jan. 3-Feb. 3, 2000

S. Grillo,
CEMES/CNRS Toulouse, France, Sept. 23-Oct. 2, 2000

R. Grynszpan,
DGA/Centre Technique d'Arcueil/ LOT/L, France, Jan.3-12, 2000

R. Hellborg,
University of Lund, Sweden, March 27-29, 2000

H. Hidalgo,
University Limoges, France, April 8-14, 2000

M. Kokkoris,
National Technical University of Athens, Greece, Sept. 17-22, 2000

S. Kosionides,
National Technical University of Athens, Greece, Sept.17-22, 2000

Experimental Equipment

1. Accelerators, Ion Implanters and Ion-Assisted-Deposition

⇒	van de Graaf accelerator	1,8 MeV	
⇒	Tandem accelerator	5 MV	*NIIEFA, Russia*
⇒	Tandetron accelerator	3 MV	*HIGH VOLTAGE, NL*
⇒	Ion implanter	80 kV	Own construction
⇒	Ion implanter	180 kV, medium current	*SCANIBAL, FL*
⇒	High current ion implanter	200 kV, high current	*DANFYSIK, DK*
⇒	High energy ion implanter	500 kV	*HIGH VOLTAGE, NL*
⇒	Plasma-immersion ion implantation	5-60 keV	
⇒	Fine focused ion beam	50 keV, 100 nm, 10 A/cm^2	
⇒	Ion beam assisted deposition		
⇒	Plasma enhanced chemical vapour deposition		

2. Particle and Photon Based Analytical Techniques

⇒	RBS	Rutherford backscattering	p,a: 1-6 MeV	
⇒	ERDA	Elastic recoil detection analysis	35 MeV, ^{35}Cl	
⇒	PIXE	Proton induced X-ray analysis	+ PIGE-option, external beam	
⇒		Nuclear microprobe	MeV, > 2 µm	
⇒	NRA	Nuclear reaction analysis	^{1}H (^{15}N,αγ) ^{12}C	
⇒	TEM	Transmission electron microscope	300 kV + EDX	*PHILIPS, NL*
⇒	SEM	Scanning electron microscope	+ EDX-option	*ZEISS, D*
⇒	STM	Scanning tunneling microscope	+ AFM-option	*DME, DK*
⇒	AES	Auger electron spectroscopy	+ XPS-option	*FISIONS, GB*
⇒	CEMS	Mössbauer spectroscopy		
⇒	XRD	X-ray diffraction		*Siemens / axs, D*
⇒	SE	Spectroscopic ellipsometry	250 - 1700 nm	*WOOLLAM, USA*
⇒	FTIR	Fourier transform infrared spectrometry	600 - 7000 cm^{-1}	*NICOLET, USA*
⇒	FTIR	Fourier transform infrared spectrometry	50 – 15000 cm^{-1}	*BRUKER, D*
⇒		Ti:Sapphire femtosecond laser		*SPECTRA PHYSICS, USA*

3. Other Analytical and Measuring Techniques

⇒	Dektak surface profilometer	*VEECO, USA*
⇒	Micro indenter	*SHIMATSU, J*
⇒	Scratch tester	*SHIMATSU, J*
⇒	Spreading resistance profiling	*SENTECH, D*
⇒	Hall-effect equipment	*BIO-RAD, GB*
⇒	I-U and C-U- analyzer	*KEITHLEY, USA*

4. Preparation Techniques

⇒	Wet chemical etching and cleaning	including anisotropic selective KOH-etching
⇒	Photolithographic patterning	5 µm-level
⇒	Thermal treatment	Room Temperature - 2000°C Furnace, Flash lamp unit, RTP, RF-heating (vacuum)
⇒	Physical deposition	Sputtering DC / RF, Evaporation
⇒	Dry etching	Plasma and RIE mode
⇒	Bonding techniques	Anodic, Si-Si and Wire Bonding

I. Papadopoulos,
University of Athens, Greece, Oct. 5-20, 2000

B. Pecz,
Res. Inst. tech. Phys. and Materials Sci., Hungary, Nov. 6-10, 2000

F. Piazza,
CNRS Strasbourg, France, May 13-20, 2000

P. Scanlon,
Eindhoven University (TUE), The Netherlands, Oct. 3-5, 2000

S. Spiga,
University of Bologna, Italy, Feb. 21-March 21, 2000

A. M. Szekeres,
Bulgarian Academy of Sciences, Institute of Solid State Physics, Bulgaria, Aug.14-25, 2000

T. Thome,
DGA/Centre Technique d'Arcueil/ LOT/L, France, Jan. 10-Feb. 10, 2000

S. Tinchev,
Bulgarian Academy of Sciences, Institute of Electronics, Bulgaria, Nov.13-26, 2000

T. Vervoort,
Eindhoven University (TUE), the Netherlands, Oct. 3-11, 2000

R. Vlastou,
National Technical University of Athens, Greece, Sept.17-22, 2000

Z. Werner,
Andrzej Soltan Institute for Nuclear Studies, Poland

Seminar of the Institute

W. Assmann (LMU München, Sektion Physik),
May 4, 2000
Kühlen und Heizen von Ionen in Kristallen

C.D. Beling (University of Hong Kong, P.R.China),
Feb. 10, 2000
Progress in positron deep level transient spectroscopy

S. Berg (University of Uppsala, Sweden),
May 9, 2000
Process modeling to develop novel sputtering processes

R. Brenn (Universität Freiburg),
July 13, 2000
Strukturelle Defekte und Fremdelemente in CVD-Diamant und Gruppe-III-Nitriden

B. Brenner (IWS Dresden),
Dec. 14, 2000
Laserrandschichtveredlung von metallischen Werkstoffen - Mechanismen, Eigenschaften und Anwendungen

S. Facsko (RWTH Aachen),
Nov. 2, 2000
Bildung geordneter Nanostrukturen auf III-V Halbleiteroberflächen unter Ionenbeschuß

S. Graf (Paul-Scherrer-Institut, Switzerland),
June 16, 2000
Photon Drag Spectroscopy of the 2-dimensional electron gas

R.I. Grynszpan (CNRS, Arcueil, France),
Jan. 6, 2000
Pseudo-PET on quasi-pets: a study of bone implant resorption by PAS or Fick's law applied to rats

B. Holländer (FZ Jülich),
Nov. 23, 2000
Spannungsrelaxation pseudomorpher SiGe/Si(100) Heterostrukturen nach H^+ und He^+- Ionen-implantation

R. Koch (Paul-Drude-Institut Berlin),
June 22, 2000
Intrinsische Spannungen in ultradünnen epitaktischen Filmen

G. Luepke (College of William & Mary, Williamsburg, USA)
May 17, 2000
First results on Si-H spectroscopy using the Jefferson-LAB FEL

L. Ottaviani (INSA Lyon, France),
March 14, 2000
pn-junction formation in 6H-SiC by Al-implantation,

B. Pécz (Res. Inst. Techn. Phys.and Mater. Sci., Budapest),
Nov. 9, 2000
Structure of wide bandgap semiconducting layers and contacts to them - TEM studies

P.O.A. Persson (Univ. of Linköping, Sweden),
Aug. 22, 2000
Structural defects of ion-implanted SiC

A.G. Revesz (Revesz Assoc., Bethesda, MD, USA and Naval Research Lab., Washington, D.C., USA)
July 4, 2000
The mechanism of the proton memory device

H. Schmidt-Böcking (Universität Frankfurt, Institut für Kernphysik)
Jan. 1, 2000
Atmosphärenplasmen erzeugt mit Mikrostrukturelektroden

A. Uedono (University of Tsukuba, Tsukuba, Japan)
Aug. 15, 2000
Investigation of vacancy-type defects in P-implanted 6H-SiC using monoenergetic positron beams

A. Weidinger (HMI Berlin)
Nov. 30, 2000
Atom in der Falle: Stickstoff im C_{60}-Käfig

W. Wesch (Universität Jena, Institut für Festkörperphysik),
Jan 27, 2000
Modifizierung und Strukturierung von SiC mit Ionenstrahlen

K. Wittmaack (GSF Neuherberg),
June 8, 2000
Grundlagen und Anwendungen der Sekundärionen-Massenspektrometrie

J. Zuk (Univ. of Lublin, Poland),
Aug. 29, 2000
Brillouin scattering as a tool for elasticity studies of ion-bombarded porous silicon

List of Personnel

Directors: Prof. W. Möller Prof. M. Helm
Deputy Director: Prof. E. Wieser
Office: I. Heidel, S. Kirch

Scientific Staff:

Permanent:

Dr. L. Bischoff
Dr. J. von Borany
Dr. W. Bürger
Dr. T. Dekorsy
Dr. F. Eichhorn
Dr. M. Friedrich
Dr. W. Fukarek
Dr. D. Grambole
Dr. R. Grötzschel
Dr. R. Günzel
Dr. V. Heera
F. Herrmann
Dr. K.-H. Heinig
Dr. H.-U. Jäger
Dr. R. Kögler
Dr. A. Kolitsch
Dr. U. Kreißig
Dr. W. Matz
Dr. A. Mücklich
Dr. C. Neelmeijer
Dr. D. Panknin
Dr. M.T. Pham
Dr. M. Posselt
Dr. F. Prokert
Dr. H. Reuther
Dr. E. Richter
Dr. B. Schmidt
Dr. H. Seifarth
Dr. W. Skorupa
Dr. J. Teichert
Dr. H. Tyrroff
Dr. M. Voelskow

Post Docs:

Dr. T. Chevolleau
Dr. M. Klimenkov
Dr. M. Maitz

Projects:

W. Anwand
Dr. A. Belov
V. Beyer
Dr. G. Brauer
Dr. V. Ermel
Dr. J. Kaschny
Dr. A. Lebedev
M. Mäder
Dr. S. Malhouitre
E.-M. Nicht
M. Peikert
Dr. L. Rebohle
Dr. A. Rogozin
Dr. M. Seidel

PhD Students:

C. Akhmadaliev
F. Berberich
C. Fitz
B. Fritsche
T. Gebel
T. Hauschild
S. Hausmann
U. Hornauer
C. Klein
I. Mrotschek
J. Noetzel
S. Parascandola
A. Peeva
J. Schmidt
T. Telbizova

Diploma Students:

U. Kentsch
T. Müller
A. Reichel

Technical Staff:

Permanent:

J. Altmann
R. Aniol
G. Anwand
I. Beatus
W. Boede
K.-D. Butter
E. Christalle
K. Fukarek
W. Gäßner
B. Gebauer
H.-J. Grahl
P. Hartmann
G. Hofmann
M. Iseke
S. Klare
R. Kliemann
J. Kreher
A. Kunz
G. Küster
D. Maul
M. Mißbach
K. Müller
E. Quaritsch
P. Reichel
B. Richter
M. Roch
B. Scheumann
H. Schluttig
G. Schnabel
J. Schneider
A. Scholz
K. Thiemig
S. Turuc
A. Vetter
A. Weise
I. Winkler

Projects:

H. Felsmann
G. Grunert
H. W. Kaiser
R. Kliesch
F. Ludewig
W. Probst
A. Schneider
H. Seifert
G. Winkler